

Effective field in large size superconducting cables for fusion

Jose Manuel Trueba Cutillas

Supervisors: Prof. dr. ir. Jean-Marie Noterdaeme, Prof. Carlos Torre Ferrero (Universidad de Cantabria)

Counsellors: Dr. Pierluigi Bruzzone (EPFL), Dr. Sedlak Kamil (EPFL)

Master's dissertation submitted in order to obtain the academic degree of Master of Science in Industrial Engineering and Operations Research

Department of Applied Physics
Chair: Prof. dr. ir. Christophe Leys
Faculty of Engineering and Architecture
Academic year 2016-2017



Effective field in large size superconducting cables for fusion

Jose Manuel Trueba Cutillas

Supervisors: Prof. dr. ir. Jean-Marie Noterdaeme, Prof. Carlos Torre Ferrero (Universidad de Cantabria)

Counsellors: Dr. Pierluigi Bruzzone (EPFL), Dr. Sedlak Kamil (EPFL)

Master's dissertation submitted in order to obtain the academic degree of Master of Science in Industrial Engineering and Operations Research

Department of Applied Physics
Chair: Prof. dr. ir. Christophe Leys
Faculty of Engineering and Architecture
Academic year 2016-2017



Acknowledgements

This work would not have been possible without the close collaboration of Kamil Sedlak. From the first day, Kamil has been orientating me through his knowledge in superconductors for fusion, part of the credit should go to Kamil. I feel lucky for having the opportunity of working in something related with the fusion energy. I would like to thank especially Dr. Jean-Marie Noterdaeme and Dr. Pierluigi Bruzzone for giving me the opportunity of my dreams. I started to be fascinated about fusion since I was a child and one of the reasons to choose Ghent as an Erasmus destination was because its European Master in Nuclear Fusion Science and Engineering Physics. Today I am satisfied with my decision. I have enjoyed the city of Ghent and so the people, to me it was the opportunity of my life, that is the reason why I will never forget the town. I had the chance to know the PSI (Paul Scherrer Institute) and work with the team as I was there for part of the work, all their people helped me and treated me as someone close and I am grateful for it from the bottom of my heart.

This year has been hard for my family but especially for my father, José Manuel Trueba Martínez Sr., I know that wherever he is, he is proud of my work and me. He was an example to us all, he never gave up and I have learnt that lesson from him. Things not always go well; nevertheless, I will never give up. My mother, siblings and my aunt bring me their love and that helps me to go ahead in my life. My other family such as my cousins, my grandmother, aunts and uncles have a part of me in their hearts and they take part of my challenges of my life.

Finally, but not less important, I would like to say thanks to the family that I have chosen, my friends. They are always there for me every time I need them and for me are like my siblings. I know that wherever we go, we will always be able to be united as if the time had not passed.

Abstract

The magnetic field is not constant over the cross-section of cable superconductors. This work assesses different cable layouts from round to rectangular and square cross-section to define and compare their current sharing temperature and effective magnetic field. We discuss of the effective field vs cable layout parameters, the pros and cons applicable to fusion.

One of the most important challenges is to control the plasma in fusion reactors is design high performance superconducting magnets. Fusion was achieved in JET reactor but actually a self-sustained fusion is the goal to make new fusion energy plants. The project which could achieve this self-sustained fusion reaction is ITER reactor. ITER most powerful magnets are the toroidal field coil and the central solenoid coil. The magnetic fields of these coils are generated through CICC made with superconducting materials. The material treated in this work is Nb₃Sn. The TF coils and its conductors are described to have an idea about how they work and the importance of its effective magnetic field. This Master Dissertation tries to identify what are the best cross-section layout for different rectangular and square cross-section conductors, as compared to the round shape conductors employed in ITER reactor. The work is simulated through a MATLAB software. The simulations can describe the magnetic field distribution in different shaped conductors which share the same area. Once we have the magnetic field distribution we can simulate the critical current density distribution and finally the electric field distribution. With the different electric field distributions for different temperatures we found the current sharing temperature where the electric field average in the conductor is equal to the critical electric field. Finally, when we obtain the T_{cs} we can calculate the effective magnetic field for each aspect ratio of rectangular shapes and compare it with round conductors to draw conclusions.

Keywords: Superconductors, fusion, toroidal field coils, Nb₃Sn CICC, effective magnetic field.

Contents

Chapter 1 Introduction to fusion energy and superconductivity.....	1
1.1 Fusion energy.....	2
1.1.1 Fusion physics.....	3
1.1.2 Fusion reactor design.....	3
1.1.3 History of nuclear fusion reactors.....	5
1.1.4 International Thermonuclear Experimental Reactor.....	8
1.1.5 ITER magnet system.....	12
1.2 Superconductors.....	15
1.2.1 Magnetic behaviour.....	16
1.2.2 High and Low temperature superconductors.....	17
1.2.3 A15 superconductors.....	19
Chapter 2 Critical current density and current sharing temperature.....	21
2.1 Scaling law for parametrization of J_c	22
2.1.1 Critical temperature and critical magnetic field.....	23
2.1.2 Reduced temperature and field.....	25
2.1.3 Nb ₃ Sn and strain function.....	26
2.1.4 Production over the world.....	28
2.2 The current sharing temperature.....	31
Chapter 3 Conductors description.....	35
3.1 Cable-In-Conduit-Conductor (CICC)	36
3.1.1 CICC Manufacturing.....	38
3.1.2 Topical issues.....	42
3.1.3 World production.....	43
3.2 Rectangular conductors for fusion magnets.....	44
3.2.1 SPC conductors.....	44
3.2.2 ENEA conductors.....	46
3.2.3 CEA conductors.....	47
Chapter 4 Conductors assessment.....	49

4.1 Magnetic field assessment in round and rectangular conductors.....	50
4.1.1 Magnetic field in circular conductor.....	50
4.1.2 Magnetic field in rectangular conductor.....	54
4.2 Critical current density, J_c for a known magnetic field in superconductors.....	58
4.2.1 Critical current density in round conductor.....	58
4.2.2 Critical current density in rectangular conductor.....	60
4.3 Electric field distribution in round and rectangular superconductors.....	62
4.3.1 Electric field in round conductor.....	63
4.3.2 Electric field in rectangular conductor.....	64
Chapter 5 Conclusions.....	67
5.1 Electric field distribution as function of temperature.....	68
5.2 Effective magnetic field.....	70
5.3 Current share temperature and effective field for different aspect ratio in rectangular conductors.....	72
5.3.1 Current share temperature in function of geometry.....	72
5.3.2 Effective magnetic field in function of geometry.....	74
5.3.3 Conclusion.....	76
Results Table.....	77
Bibliography.....	78
Annexes.....	80

List of equations

Pinning force (1)	22
Normalised pinning force; Critical magnetic field depending on temperature; Ginzburg-Landau parameter(2)(3)(4)	22
Final pinning force(5)	23
Critical current density(6)	23
Critical temperature (7)	23
Reduced magnetic field at zero temperature (8)	24
Critical magnetic field at zero temperature (9)	24
Critical magnetic field(10)	25
Reduced temperature(11)	25
Reduced magnetic field(12)	26
Strain shift component(13)	26
Strain equation(14)	27
Current density in round conductors(15)	50
Magnetic field in round conductors (16)	50
Enclosed current in round conductors (17)	50
Corrected magnetic field in round conductors (18)	50
Final magnetic field equation in round conductors (19)	50
Vacuum permeability(20)	51
Vector potential of line current(21)	54
Corrected vector potential of line current in round conductors(22)	54
Corrected vector potential of line current in rectangular conductors (23)	54
Final vector potential of line current in round conductors (24)	54
H field component in x axis; H field component in y axis (25)(26)	55
Extended H field component in x axis (27)	55
Extended H field component in y axis (28)	55
Magnetic field in rectangular conductors (x component); Magnetic field in rectangular conductors (y component)(29)(30)	55
Electric field in superconductors(31)	62

Critical electric field in low temperature superconductors(32)	62
Final electric field in low temperature superconductors(33)	62
General current density(34)	62

List of figures

Figure 1. 1 Fusion reaction between Deuterium and Tritium.	3
Figure 1. 2 T-3 Tokamak built in Moscow (Russia).	4
Figure 1. 3 Stellarator W X-7 made in Germany.	5
Figure 1. 4 JET reactor inside view, the right window shows how it looks-like when it is working.	7
Figure 1. 5 ITER members in Elysée Palace to sign the ITER Agreement on 21 November 2006.	8
Figure 1. 6 Neutral beam injector design form ITER.	9
Figure 1. 7 ITER cryopump sketch [1].	10
Figure 1. 8 divertor cassette [2].	11
Figure 1. 9 ITER tokamak (French Nuclear Safety Authority).	13
Figure 1. 10 Thermal scattering sketch.	15
Figure 1. 11 Superconductor Type-II when a high external magnetic field is crossing through its vortices [4].	16
Figure 1. 12 Superconductor states in Type-I and Type-II in function of magnetic field and temperature.	17
Figure 1. 13 Critical aspects comparison between NbTi and Nb3Sn [4].	18
Figure 1. 14 Nb3Sn A15 lattice structure.	19
Figure 2. 1 Critical temperature at 0 background field (K) as function of intrinsic strain (%). The calculation is based on the EUTF4 scaling law parameters.	24
Figure 2. 2 critical magnetic field (T) at a defined temperature of 4.2 K in function of the intrinsic strain (%).	25
Figure 2. 3 Critical current density (A/mm ²) at defined temperature and background magnetic field in function of intrinsic strain (%).	28
Figure 2. 4 Different layouts for strands producers over the world for ITER [12].	30
Figure 3.1 coils and solenoid of a tokamak.	36
Figure 3. 2 TF conductor parts. National Fusion Research institute from Korea newsletter.	37
Figure 3. 3 CICC from ITER Newsline 278 (iter.org).	39

Figure 3. 4 final assembly for ITER TF cable [15].	40
Figure 3. 5 TF CICC composition to The Nb ₃ Sn filaments. Figure from Florida State University.	41
Figure 3. 6 ITER TF pancake from ASC (La Spezia, IT).	42
Figure 3. 7 TF coil structure in ITER. Japan Atomic Energy Agency (JAEA).	44
Figure 3. 8 SPC conductor specifications [18].	45
Figure 3. 9 ENEA DEMO conductor cross-section. ENEA.	46
Figure 3. 10 CEA conductor proposal [22].	48
Figure 4. 1 Area plot of the magnetic self-field in a portion of the conductor.	51
Figure 4. 2 Round conductor shelf-field.	52
Figure 4. 3 Magnetic field in round conductor with background field plus its self-field.	53
Figure 4. 4 Rectangular scheme about distances and angles.	55
Figure 4. 5 Self magnetic field in rectangular conductor 60mmx20.944mm and 2D perspective in x, y plane.	56
Figure 4. 6 Magnetic field distribution in a rectangular conductor with a 10 T external field pointing in the Y direction.	57
Figure 4. 7 J _c distribution in a round superconductor in magnetic self-field.	58
Figure 4. 8 J _c distribution when a background field of 10 T is present.	59
Figure 4. 9 J _c distribution in a rectangular conductor without background field.	60
Figure 4. 10 J _c distribution in rectangular conductor with a background field of +10T in Y direction.	61
Figure 4. 11 E field distribution over a round conductor without an external magnetic field.	63
Figure 4. 12 Electric field distribution over a round conductor cross-section when an external magnetic field of 10T is present.	64
Figure 4. 13 Electric field distribution in a rectangular conductor without external magnetic field.	65
Figure 4. 14 Electric field distribution when an external magnetic field is present in a rectangular conductor.	66

Figure 5. 1 Average electric field in a round conductor as function of temperature.	68
Figure 5. 2 E field average in rectangular conductor in function of temperature.	69
Figure 5. 3 J_c as function of external magnetic field B.	70
Figure 5. 4 Tcs for aspect ratio from 1/10 to 10/1. The red point indicates Tcs of a round cable with the same cross section area.	72
Figure 5. 5 Tcs for aspect ratio from 1/100 to 100/1.	73
Figure 5. 6 Tcs for aspect ratio from 1/2 to 2/1.	74
Figure 5. 7 B_{eff} for different aspect ratio in rectangular conductor.	74
Figure 5. 8 B_{eff} for aspect ratio from 1/100 to 100/1.	75
Figure 5. 9 B_{eff} for aspect ratio from 1/2 to 2/1.	76

List of tables

Table 2. 1 fitting parameters for calculation of strain function from EUTF4 [9].	27
Table 2. 2 Fitting parameters for calculation of strain function from EUTF4 [9].	29
Table 3. 1 Different ITER TF cable suppliers [12].	43
Table 3. 2 steel and superconductor section in the Double Layer 1 of DEMO designs [20].	47
Table 5. 1 Results calculated through MATLAB.	77

List of abbreviations

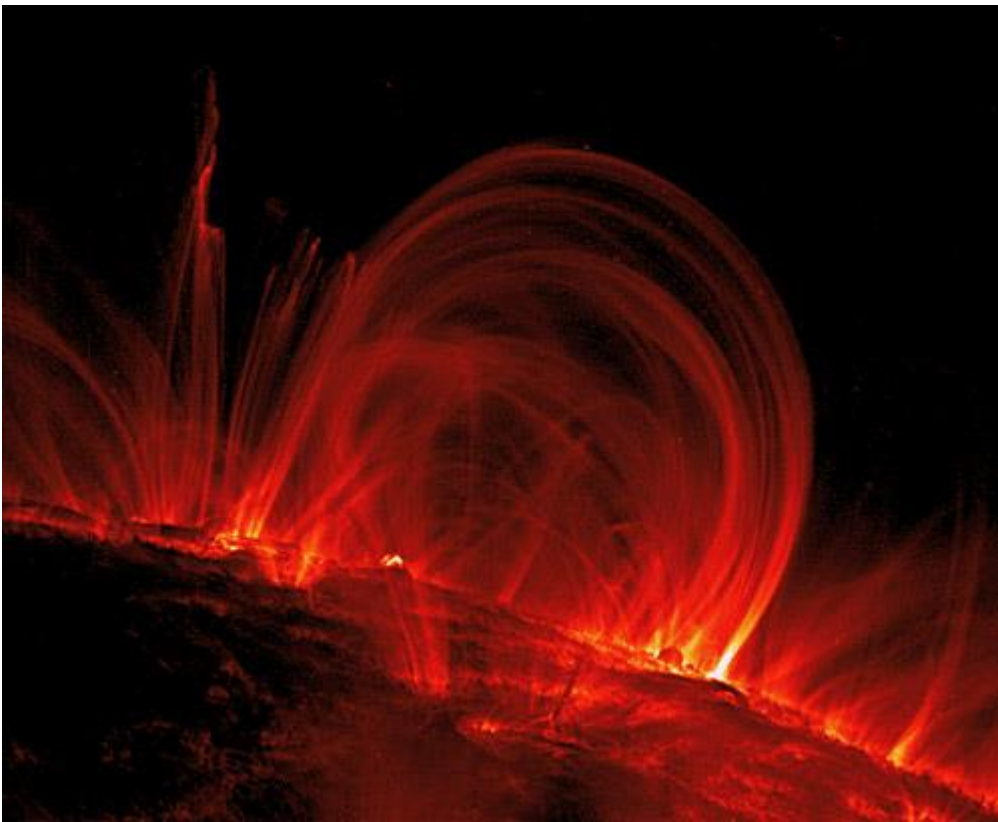
AC	Alternating Current
CC	Control Coil
CEA	Alternative Energy Commission
CICC	Cable In Conduit Conductor
CS	Central Solenoid
DEMO	DEMOstration Power Station
EAS	Energy Aquila System
ELM	Edge-Localised Modes
EUTF4	European Toroidal Field sample 4
HTS	High Temperature Superconductors
ITER	International Thermonuclear Experimental Reactor
JET	Joint European Torus
LTS	Low Temperature Superconductors
MATLAB	MATrix LABoratory
MRI	Magnetic Resonance Imaging
OST	Open System Technologies
PF	Poloidal Field
SC	SuperConductor
SPC	Swiss Plasma Center
SULTAN	SUpraLeiter Test ANgle
T-3	Tokamak 3
T-7	Tokamak 7
TF	Toroidal Field
Tokamak	TOroidal Chamber with MAgnetic Coils (from Russian)
X-7	Wendelstein Stellator

List of symbols

B_{eff}	Effective magnetic field	Tesla
BF	Background field	Tesla
Bx	Background field in x axis	Tesla
By	Background field in y axis	Tesla
E_c	Critical electric field	V/m
ϵ	strain	%
$\epsilon_{0,a}$	non-axial strain	%
ϵ_{max}	maximum strain at zero J_c	%
ϵ_{sh}	strain shift factor	%
J_c	critical current density	A/mm ²
J_{op}	operation current density	A/mm ²
μ_0	vacuum permeability	V·s/A·m
n	n-index	non-unit
T_c	current sharing temperature	Kelvin

CHAPTER 1

Introduction to fusion energy and superconductivity



Solar flare, TRACE satellite capture, Sept. 28th, 2000.

1.1 Fusion energy

As many estimations indicates, the energy consumption over the world is going to increase two or three times by the next century. The socio-technological improvement has carried the modern society to a progressive energy consumption for the last fifty years.

Nowadays some different solutions are presented and developed as the renewable energies, not only because of their low environmental impact but also because the fossil fuels constitute a limited resource.

Renewable energies are only a relatively small portion in the world electric market because this energy has not the size, quality and capacity as the large generation stations. Also in many markets, this energy need of some socio-economic facilities which are provided by the national governments.

These difficulties in the future scenario and the constant rising of energy demand, involves the necessity to find other ways for the production energy. For these purposes, a good candidate could be Fusion Energy, which is already coming true day by day in its most promising project: The International Thermonuclear Experimental Reactor (ITER), situated in Cadarache, France.

There are different types of nuclear reactions. However, the most interesting types to produce energy are the fission and fusion reactions. The fission is already employed as an electric generation commercial source. Even though there are some, already known, security problems with radioactivity and waste disposal. It is true that the electric generation by fission has been developed during the last sixty years since the earlier 50's where the first plants start to produce it. Nevertheless, fission still could lead to some risks, due mostly to unpredictable accidents.

For the time being there are over 430 commercial nuclear power reactors operating in more than thirty countries, with 372 GWe of total capacity. Nuclear fission has a solid situation in the electric market while already is not possible to produce electric power from nuclear fusion reactions. Nevertheless, the fusion reactor has three advantages in contrast with fission reactors. First of all, the fusion reaction waste, in its majority, it is not as a harmful environmental issue as the fission reaction waste. Secondly, its raw materials are relatively abundant and cheap, and finally, in case of accident or sudden switch off, the reactor has no danger of radioactive leaks or explosions, the fuel simply doesn't react.

First fusion reactions were made for military purposes, like in fission reactions origins. However, after the Second World War, the interest in the thermonuclear fusion broke out. From that time two British researchers from the university of London, Thomson and Blackman, filed a patent for a fusion reactor in 1946. The conceived idea for this device was optimistic, it was designed with a vacuum chamber in a torus shape and includes a current generation by radio-frequencies waves. These two features are fundamental aspects in the modern fusion reactors.

1.1.1 Fusion physics

The fusion reaction occurs in a very extreme scenario. The definition of the nuclear fusion consists in a process where two or more atomic nuclei of similar charge form a heavier nucleus, while an enormous quantity of energy is absorbed or released. When fusion occurs for atoms lighter than iron, commonly the energy is released and this occurs in the inverse sense of the fission reaction. The simplest case of fusion is between isotopes of hydrogen, usually deuterium and tritium, which release 17.59 MeV. When these isotopes are fusionated this reaction produces He^4 plus one free neutron. This amount of energy is released for each reaction, which means a huge quantity of energy. This Fusion reaction is illustrated in *Figure 1.1*.

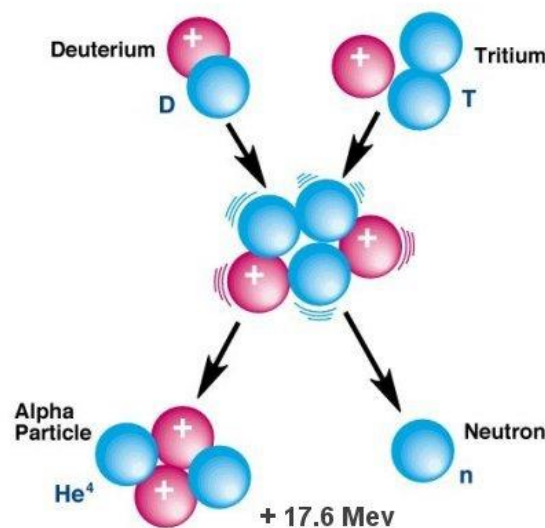


Figure 1. 1 Fusion reaction between Deuterium and Tritium.

Fusion is present in nature. The stars, due to the huge temperature (near 15,000,000 K) and pressure conditions, releases nuclear energy from the fusion of its atoms, and not only hydrogen, but some more different atoms; this type of fusion is called “*thermonuclear fusion*”. That energy is given by the sun to our planet which is able to synthetize, transform and consume it. The Nobel Prize in Physics, Doc. Hans Albrecht Bethe (1906-2005), studied the stages of the main cycle of the nuclear fusion in the stars.

1.1.2 Fusion reactor design

The challenge begins when the physicists and engineers try to reproduce the extreme scenario which allows the fusion reactions. Before fusion can be achieved a huge energy barrier of electrostatic forces must be overcome. However, today fusion is achieved, but it is not completely controlled and the main problem is that requires more energy than it provides. In view of promising progress the research continues and the ideal machine proposed for the future electric generation was the “*tokamak*”.

The tokamak word is a Russian acronym which is traduced in English as traduced as Toroidal Chamber with Magnetic Coils. It is in this device, where the plasma, as fuel, flows while it

reacts fusing its atoms and producing thermal energy. The main method to produce the fusion in a tokamak is through magnetic confinement, this method consists in maintaining the plasma contained into a magnetic bottle, which consists in a magnetic field with a determinate form. This is possible due to the Lorentz force which explains that a charged particle who moves into a magnetic field experiments a force perpendicular to the magnetic field vector and the movement vector wherewith the particle maintains inside the magnetic field. The T-3 tokamak, built in 60's, is showed at *Figure 1.2*.

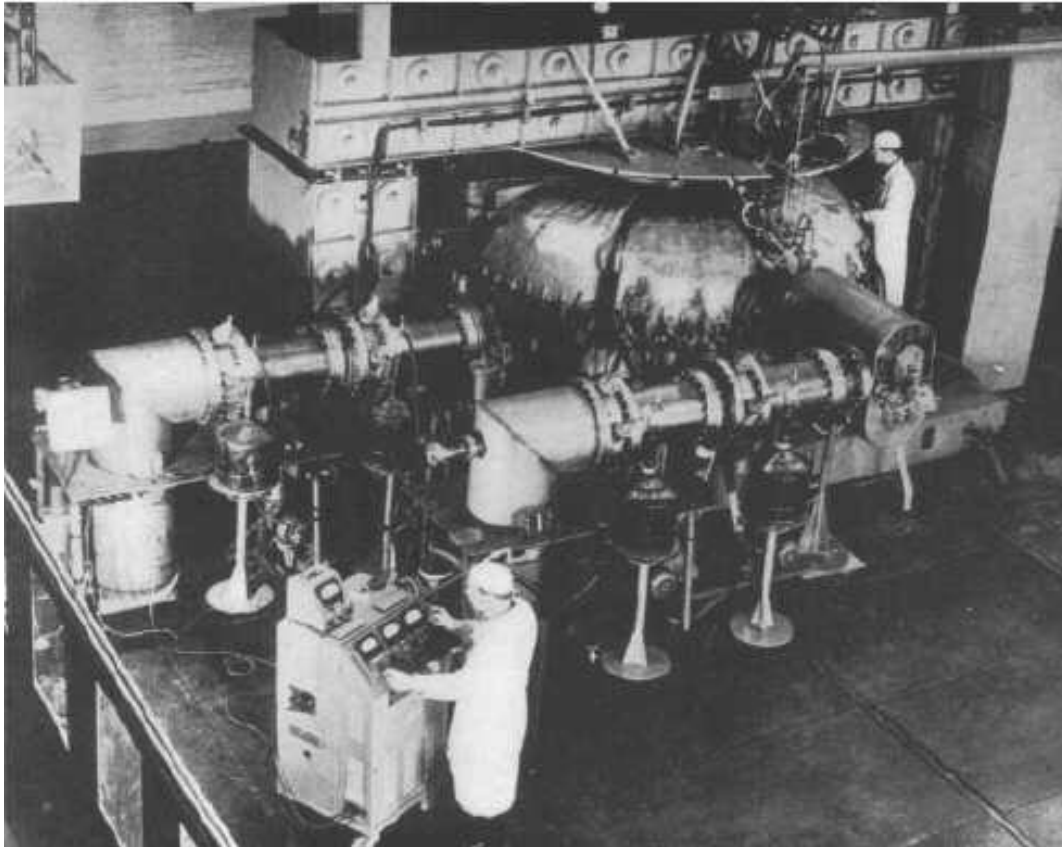


Figure 1. 2 T-3 Tokamak built in Moscow (Russia).

This kind of machines confine the plasma with a strong poloidal magnetic field producing a toroidal plasma current. With the enough strength of the current, the magnetic field pinches the plasma carrying it away from the chamber walls. As instabilities was observed for plasma current in the firsts toroidal coil machines, some auxiliary coils were added to these designs with a weak magnetic field, only to improve the stability. It was discovered that these auxiliary coils have an improvement when it has a field reversed from the toroidal direction which is called reverse field pinch. At first this field reversal appeared spontaneously, but now it is induced on purpose.

The second machine designed to confine the fusion plasmas into a magnetic field is the stellarator. The stellarator is designed to confine fusion plasmas by means of strong toroidal magnetic fields but the main difference with the tokamak is that in the stellarator the plasma stays without currents. However, as a purely toroidal field cannot balance the forces due to the plasma expansion, it is necessary to twist the magnetic field as it passes around the torus. To achieve the twisted shape in the magnetic field, each field line is wrapped around the inside

as well as the outside cross-section. Different stellarator are designed with different ways but maintaining the same basic principle with a twisted toroidal magnetic field. This layout for plasma confinement was designed in 1951 at Princeton and it would lead to the creation of the Princeton Plasma Physics Laboratory, but nowadays different new stellarators are built in Japan, Germany, Spain and recently in Costa Rica. The German stellarator, the Wendelstain 7-X is illustrated in *Figure 1.3*. In this figure, we can appreciate the twisted magnetic field as a blue tone, this is one of the most modern stellarator. However, it is designed to study the plasma flow instabilities with a few milligrams of hydrogen at different temperatures. It main constraint is the power employed to the installation cooldown, it is only a simulator project and it never will contain fuel for fusion due to the lower current performance respect to tokamaks.

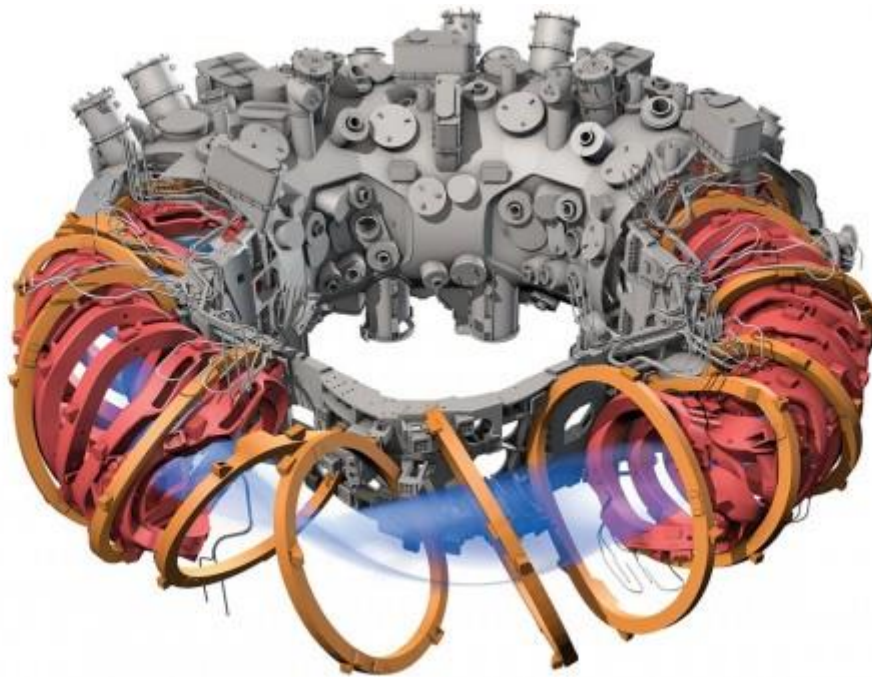


Figure 1. 3 Stellarator W X-7 made in Germany.

The theoretical work for the tokamak design was described in 1950-51 by I. E. Tamm and A. D. Sakharov in the Soviet Union. The first experiments based on the theoretical works start in 1956 in Moscow by a group of Soviet scientists. Tokamak has a very strong stabilizing toroidal field. Through the poloidal field generated by the current present in the plasma, the toroidal field is twisted and this twisted field, but without folds, plus the present current lead the tokamak to be the best candidate for a magnetically confined fusion power plant.

1.1.3 History of nuclear fusion reactors

As we comment before in the introduction, the first idea for fusion reactor had military intentions. During the Cold War, fusion researches was handled secretly and on November the 1st, 1952, U.S. of America detonated the first thermonuclear device. This device, was a bomb who obtains part of its yield from nuclear fusion. Due to the tense political situation of those times, some countries adhered to fusion research while others as U.S. of America or the URSS intensified their researches.

To achieve a powerful weapon the research was focused in the inertial confinement; this was suggested by Lawrence Livermore National Laboratory in 1962. The strategy to develop the inertial confinement was the same as the one employed in the hydrogen bomb, encapsulating, compressing and heating the fuel very fast to reach the conditions for fusion. The inertia of fuel prevents it from escape, and this is the premise to call it inertial confinement fusion. To compress one solid or liquid are in most of the cases impossible but in this case some experiments indicated that with very large pressure present in deuterium capsules, it can be compressed to densities higher than one thousand times their normal density. The best way to compressing a capsule is to heat its surface enough to evaporate very quickly. The hot gases evaporated from the surface will apply large forces to it, contributing to the inertial confinement fusion.

At the “*Atom for Peace*” conference celebrated in September 1958, 5000 scientists, government officials and observers from different countries had come to the old League of Nations building in Geneva to bear witness to the revelation of nuclear research. It was the largest international meeting ever to focus on the potential of use nuclear energy for peaceful purposes. The main attraction: the promised revelation of secret fusion research by the United States, Great Britain and the Soviet Union. The basis of the magnetic confinement was laid down by the Russian physicist Artsimovitch, but it not would be an easy way to achieve the fusion due to the complex nature inherent to the plasma and its control through magnetic fields. For this reason, the most effective way to reach the controlled fusion was to join forces. Russian scientists obtained in 1968 the most successful tokamak obtaining a performance quite advanced respect to the other researchers. This tokamak was called T-3 and opened the era of the tokamaks in other countries.

The next significantly improvement for the confinement and heat of plasma in a tokamak was obtained in the French “*Tokamak de Fontenay-aux-Roses*” being the highest-performance nuclear fusion device reaching temperatures of 2 keV between 1973 and 1976. Attracted by the growing expectations, the construction of big tokamaks was proposed in the European Community in favour of a robust fusion program and the necessary legal framework to develop a European fusion device. The result was the birth of the Joint European Tokamak (JET). In 1978 starts this project, in Oxfordshire, UK, but the first experiments started in 1983. *Figure 1.4* shows how is the inside chamber of JET. On November 1991, a preliminary deuterium-tritium experiment achieved the world’s first controlled release of fusion power, being special important that it was controlled as uncontrolled fusion exist since the hydrogen bomb exist. This fusion achieves a peak of 1.7 MW being the best performance in the fusion tokamaks race. Following experiments had better news, in 1997 another experiment in JET achieve 16 MW of energy becoming the highest energy produced by controlled thermonuclear fusion, nevertheless, the energy expended to reach this peak, during something more than one second, was 22.8 MW. The relation of generated by produced energy is known as Q and it had their maximum value around the 0.7 for the JET tokamak. Today JET is the largest tokamak in the world and the only operational fusion experiment capable of producing fusion energy. As a joint venture, JET is collectively used by more than 40 European laboratories. The European Consortium for the Development of Fusion Energy, EUROfusion for short, provides the work platform to exploit JET in an efficient and focused way. As a consequence, more than 350 scientists and engineers from all over Europe currently contribute to the JET programme.

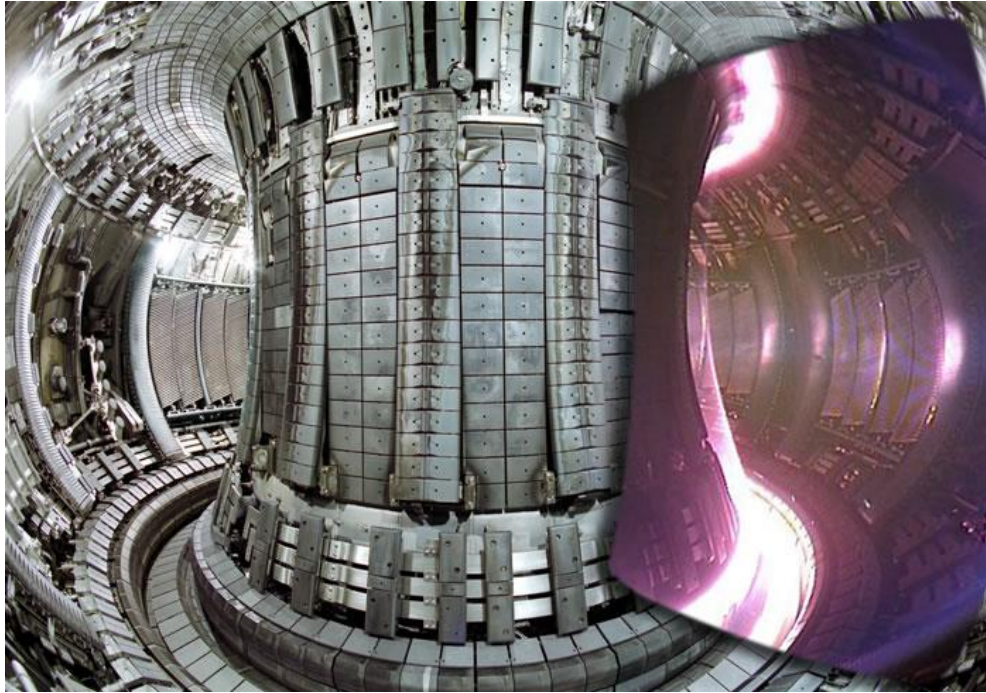


Figure 1. 4 JET reactor inside view, the right window shows how it looks-like when it is working.

After the first plasma of JET, in 1985, at the Geneva Superpower Summit, the president Mitterand of France, the prime minister Thatcher of the United Kingdom and the General Secretary Gorbachev of the former Soviet Union proposed to the U.S. president Reagan an international project aiming at developing fusion energy for peaceful purposes. The ITER project was born.

First constituents of ITER project were the European Union (Euratom), Japan, the Soviet Union and the U. S. of America. Conceptual design work began in 1988, followed by increasingly detailed engineering design phases. Until 2001, when the final design for ITER was approved by the Members. In 2003 China and Republic of Korea joined this project and in 2005 it was India who joined it. The ITER members unanimously agreed on the site proposed by the European Union for the ITER installation and it was built near Aix-en-Provence in southern France. In a ceremony hosted by French President Jacques Chirac and the President of the European Commission Mr. José Manuel Durao Barroso, this agreement was officially signed at the Elysée Palace in Paris on November 21st, 2006 by ministers from the seven countries which are present in *Figure 1.5*. The purpose of ITER is to establish the scientific and technological feasibility of fusion, delivering ten times the energy it will consume ($Q > 10$), with a power of 500 MW, the experiment will try to maintain the fusion during at least eight minutes. Today ITER is already under construction and its assembly building is ready to receive the reactor pieces which would allow the first plasma in 2025.



Figure 1. 5 ITER members in Elysée Palace to sign the ITER Agreement on 21 November 2006.

Fusion as energy production is being a very long way but thousands of people along the history feed this dream and it is bearing fruit. Step by step we are closer to fusion energy generation, and the development of the tokamaks with their different aspects could be the solution in a time not so far.

1.1.4 International Thermonuclear Experimental Reactor

The scientists working for ITER will use many different technologies to develop and analyse the biggest plasma to date. Powerful magnet systems, extreme hot and cold temperatures, sophisticated robotics, new materials and thousands of high-tech subsystems will be deployed inside the machine. This state of the fusion device will be protected by a 3.5-metre-thick wall, which will ultimately act as a safety layer between the machine and the building hosting it.

ITER will be the largest tokamak in the world, with a plasma radius of 6.2 m and a plasma volume of 840 m³. The plasma volume has a direct relation with the potential to achieve the fusion, JET is now the largest tokamak built but its radius is only 2.10 m. As more plasma is present in the reactor, more pressure and energy can be achieved, with more energy, the reaction could reach to its climax when the reaction is self-sustaining. Plasma must be at very high temperatures to react, for this reason inside ITER it is expected to be 150,000,000 °C which is ten times the Sun temperature. The changing magnetic fields that are used to control the plasma produce a heating effect. This is produced because the magnetic fields generate a high-intensity electrical current through induction, and as this current flows through the plasma, electrons and ions become energized and collide ones with others. Collisions create kind of electrical resistance that results in heat, however, as the temperature of the plasma increments, this resistance decreases with its resistance heating effect. Heat produced through high-intensity current, also called ohmic heating, is limited to a certain level. In order

to maintain the higher temperatures and reach the heat level where fusion can occur, heating techniques must be applied from external sources of the tokamak. There are two groups of external heating methods, one is the neutral beam injection and the other one is the high-frequency electromagnetic waves. It will be added to the ohmic heating to bring the ITER plasma to fusion temperature. Neutral beam injection consists in shooting high energy particles into the plasma. ITER injector is sketched in *Figure 1.6*. Outside of the tokamak, some charged deuterium particles are accelerated to a high energy level. These accelerated ions then are carried through an "ion beam neutralizer" where their electrical charge is neutralised. The high speed neutral particles can then be injected into the core of the plasma where, by means of fast collision, they transfer their energy to the plasma particles. A second external source of heat is the high frequency electromagnetic waves which is planned into the design of the ITER Tokamak to boost temperatures to the desired 150 million °C. Scientists hope that the self-sustained plasma will be achieved and in that case the external heating could be unnecessary, constituting a reduction of the invested energy and reaching Q factor.

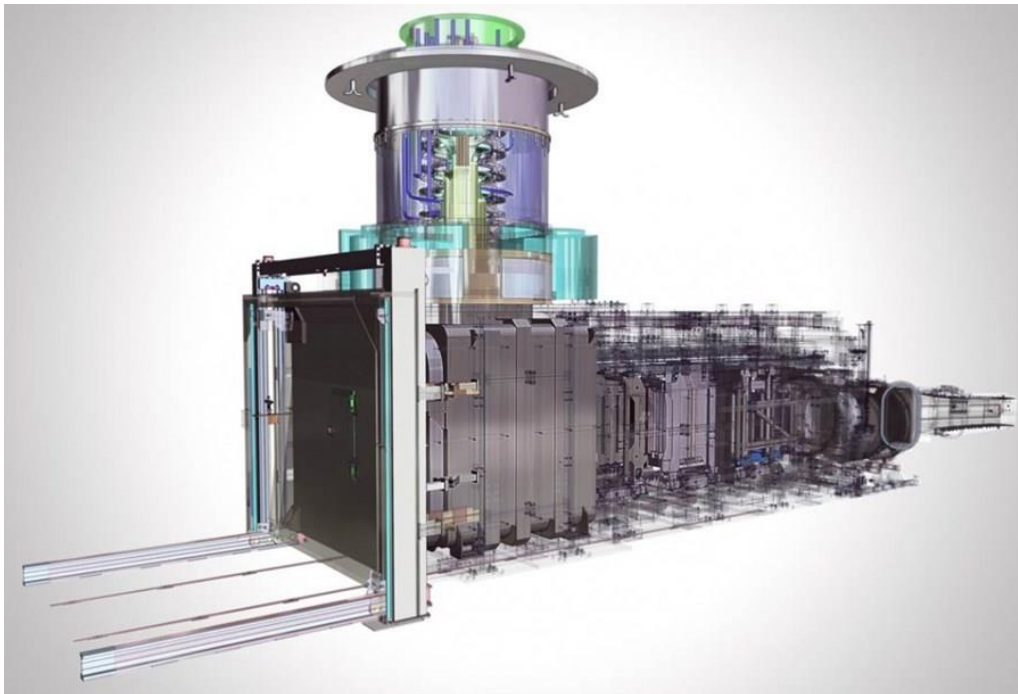


Figure 1. 6 Neutral beam injector design form ITER.

The ITER experiments will take place inside the vacuum vessel, a hermetically sealed steel container that houses the nuclear fusion reactions and acts as a first protection containment barrier. In its torus, the plasma charged particles spiral around continuously without touching the walls, in the magnetic bottle described by the superconductor magnets. Forty-four windows, or ports, in the vacuum vessel provide access for remote handling operations, analysis tasks, heating, and high vacuum systems. The blanket modules filling the walls of the vessel will provide protection from the high-energy neutrons produced by the fusion reactions.

Normally the vessel walls of fusion experiments were lined with carbon, a material that withstands extreme heat stress, nevertheless, carbon shows an affinity for hydrogen, which is an issue for future fusion devices which operate with deuterium-tritium plasmas in high-

energy state. In these machines retention tritium, due to its rare and radioactive nature, must be avoided. Metal walls made of beryllium and tungsten are the solution proposed by physicists. The 440 blanket modules that completely cover the inside walls of the vacuum vessel protect the steel structure of the reactor and the superconducting toroidal field magnets from the heat and high-energy neutrons discharged by the powerful reactions. As the neutrons are slowed in the blanket, their kinetic energy becomes into heat energy, which could be collected by the water coolant. In a future nuclear fusion power plant, this energy will be used for electrical power production, possibly through a steam turbine. The ITER blanket, which covers a total surface of 600 m², is one of the most critical and technically challenging components present in ITER project, it directly faces the hot plasma, as the divertor which has direct contact with plasma. Due to its unique physical properties as low plasma contamination or low fuel retention, beryllium has been chosen as the element to cover the first wall. The rest of the blanket modules will be made of high-strength copper and stainless-steel.

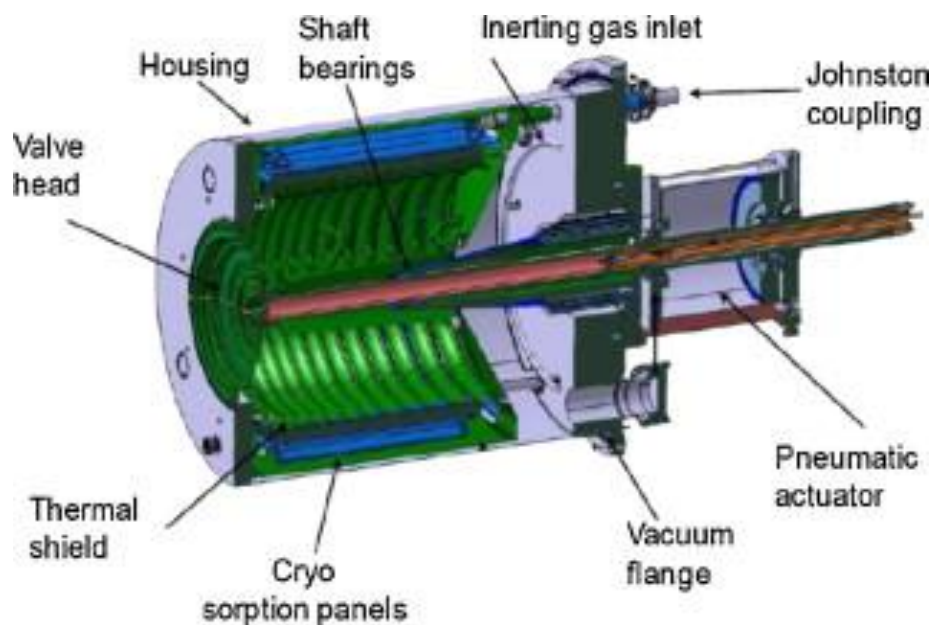


Figure 1. 7 ITER cryopump sketch [1].

Along with the magnetic coil systems, the ITER vacuum vessel is completely enclosed in a large vacuum chamber known as the cryostat. Two layers of thermal shielding are situated between the vacuum vessel and the cryostat to minimize heat impact produced by thermal radiation and conduction from warm parts to the components and structures that operate near 4.5 K, such as the superconducting magnets. Reduction of these heat input by over two orders of magnitude is compulsory to guarantee that the residual heat load can be removed by the reactor. The thermal shield is made of stainless-steel panels with a low emissivity surface that are actively cooled by helium at gas state, flowing inside of a cooling tube welded on the panel surface. During plasma operation, the temperature of the helium ranges from 80 K and 100 K. One layer of thermal shield will be installed between the vacuum vessel and the superconducting magnets, the other will be installed between the magnets and the cryostat, because magnets work at very low temperatures and heat disturbances could damage its material. The thermal shield has a surface area of approximately 10,000 m². Once assembled, it will stand 25 m at its tallest point. All these protections are fundamental issues to protect

the reactor from nuclear reactivity and the extreme heat produced by the plasma and without the development and materials research this chamber could never contained plasma in fusion state.

The cryostat which surrounds the ITER vacuum vessel is the largest stainless-steel high-vacuum pressure chamber ever built with a capacity of 16,000m³. It gives high vacuum while provides an ultra-cold environment to the vacuum vessel and the superconducting coils. It is nearly 30 m wide and its diameter is defined by the two largest poloidal field coils. The cryostat material is stainless-steel and it has a weight of 3,850 tonnes. It has large bellows between the cryostat and the vacuum vessel which allow for thermal expansion and contraction in the different structures during the operation. The vacuum pressure in this chamber could reach the 1x10⁻⁴ Pa, and to achieve this a pump is designed with 8,500 m³ volume. One ITER cryopump is sketched in *Figure 1.7*.

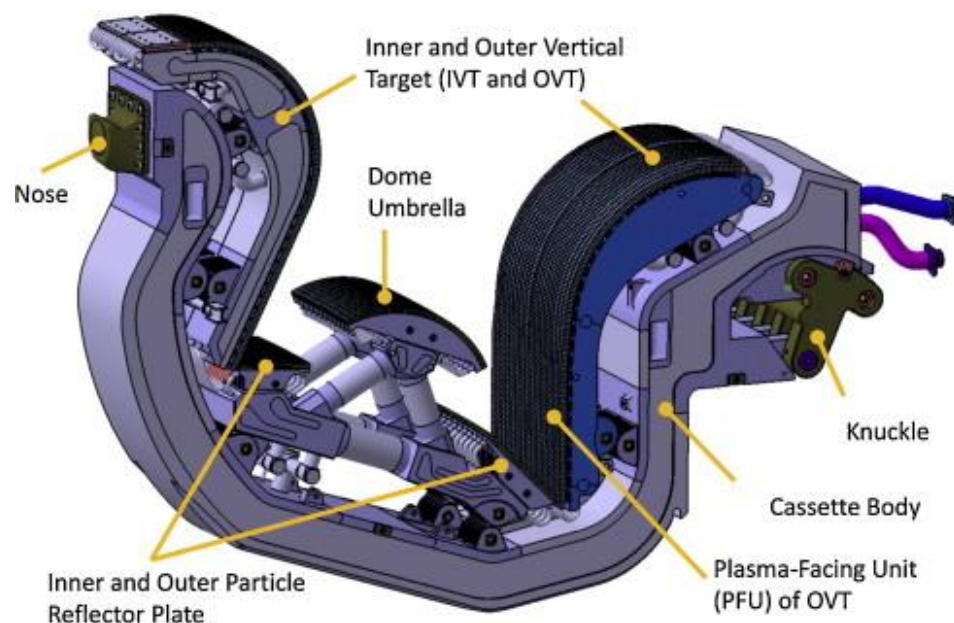


Figure 1. 8 divertor cassette [2].

In the bottom of the vacuum vessel is situated the divertor, who extracts heat and ash produced during the fusion reaction, in this way minimizes plasma contamination at the same time that protects the vessel walls from thermal and nuclear loads. The divertor is composed by 54 “cassette assemblies” as the one that is illustrated in *Figure 1.8*, and each one has their own supporting structure made of stainless-steel and three plasma-facing components, the inner and outer vertical targets and the dome target. These cassettes are provided with several diagnostic components designated for plasma control and physics analysis and optimization. Two of the three plasma-facing components, the inner and outer vertical targets, are positioned at the intersection of magnetic field lines which is a point where the particle bombardment are especially intense in the reactor. In this zone, the high-energy plasma particles are continually hitting the targets where their kinetic energy is transformed into heat which later will be removed by water cooling.

Tungsten, which has the highest melting point among all metals, has been chosen to be the armour material, after an international R&D effort, promising experimental results and

successful previous tests. This divertor should resist, in its vertical target, a heat flux estimated at 10 MWm^2 in steady state and 20 MWm^2 for slow transients. The cassettes have a weight of 10 tonnes, each one, and will be installed by remote handling [3].

1.1.5 ITER magnet system

The magnet system designed for ITER will be the largest and most integrated magnet system with superconductors ever built. This is not very strange because superconducting magnet system are not a common construction in an integrated system. However, some particular research facilities may contain these conductors. ITER magnets have a weight of 10,000 tonnes in combination with a stored magnetic energy of 51 GJ (Gigajoules) which produce the large magnetic fields necessary to start, confine, shape, and most important, control the plasma. It is made of two superconducting materials, niobium-tin (Nb_3Sn) or niobium-titanium (NbTi), but to become superconducting, the magnets need to be cooled near the 4 K ($-269 \text{ }^\circ\text{C}$) and this is achieved with supercritical Helium. Superconductor magnets have the property to carry high current and consequently generate strong magnetic fields. They also consume less power than counterparts and are cheaper to operate. These qualities make superconductors the best solution for ITER magnet system.

ITER has an enormous magnetic system which need an internally cooling system. The most technically challenging raw material is the niobium-tin (Nb_3Sn) superconducting strands used in ITER's toroidal field (TF) and central solenoid magnet systems, these strands have 500 metric tons distributed in more than 100,000 km which were produced by nine suppliers over the world in a procurement effort that lasted from 2008 to 2015. This large-scale industrial effort demanded an increase of global production capacity from 15 metric tons per year to 100 metric tons/year, as well as the introduction of three new strand suppliers. A scheme of the ITER coils and layers is sketched in *Figure 1.9*.

ITER counts with eighteen D-shaped toroidal field coils placed around the vacuum vessel to produce a magnetic field whose primary function is to confine the plasma. The TF coils are designed to generate a total magnetic energy of 41 gigajoules and a maximum magnetic field of 11.8 Tesla. TF weight 310 tonnes each one, and measuring 9 m of width and 17 m of height, they are among the largest components of the entire ITER machine. Toroidal field coils are wound in double layers of spiralled conductor inlaid in radial plates which are encased in large stainless-steel structures, these layers are called "*pancakes*". With a total weight of 3,400 tonnes, the toroidal field coils structure drives the limits of manufacturability. High-care welding techniques will be necessary to reach high quality requirements.

Six ring-shaped poloidal field coils are situated outside of the TF magnet structure to shape the plasma and contribute to its stability by pinching it away from the vessel walls. The largest coil has a radius of 12 m near the mid-plane of the TF coils. The heaviest PF coil is 400 tonnes. The poloidal field coils are designed to produce a total magnetic energy of 4 GJ and a maximum magnetic field of 6 Tesla. The four largest poloidal field coils will be produced from niobium-titanium superconductor since the magnetic field is smaller.

The central solenoid (CS) is the core of ITER's magnet system, allowing a high current to be induced in the ITER plasma and maintained during long plasma pulses. With 13 m tall, without

counting the structure, 4 m wide and 1,000 Tonnes, the central solenoid is made of six independent coil packs wound from Nb₃Sn superconducting cable. Stored magnetic energy of 6.4 GJ in the CS will initiate and sustain a plasma current of 15 MA for durations of approximately 300-500 seconds. A maximum field of 13 Tesla would be reached in the centre of the stacked modules, being the maximum magnetic field produced by of all ITER magnet systems. The independently operating coil packs will create huge electromagnetic forces that pull in different directions due to Lorentz forces. In order to maintain the structure of the central solenoid assembly in good conditions, a specially designed support structure has been performed. The support structure will have to withstand forces in the range of 60 Mega Newtons, or that is the same, 6,000 tonnes of force.

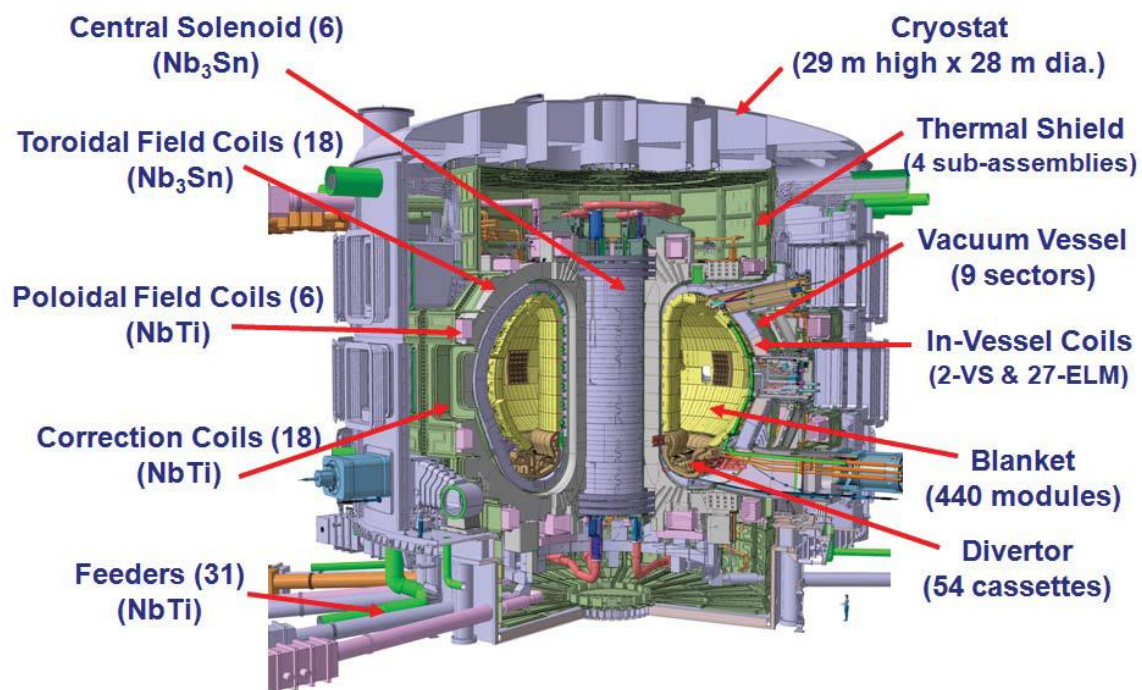


Figure 1. 9 ITER tokamak (French Nuclear Safety Authority).

To compensate the field errors caused by geometrical deviations due to manufacturing and assembly processes, eighteen superconducting correction coils (CC) will be inserted between the TF and PF coils. As these coils are only for correction, its magnetic field and running current will be smaller, around the 10kA. The correction coils are arranged in groups of six around the toroidal circumference with a width of 8 m and special challenges for assembly and installation.

Inside ITER vacuum vessel another two coil systems are situated, but they are not made of superconducting materials. These systems provide additional plasma control capabilities by means of two vertical stability coils situated above and below the vessel mid-plane, to give a fast plasma stabilization, and twenty-seven coils fixed to the vessel wall, to avoid the generated resonant magnetic perturbations in the plasma due to a kind of plasma instabilities called Edge-Localized Modes (ELM). The two types of coils are manufactured with a special type of copper conductor who has a mineral-insulation, according to the demanding conditions inside the vessel.

The magnet system which is made with superconductors need some special feeders which provide very high currents and a low temperature to maintain the superconducting state. The ITER tokamak have in total 31 superconducting feeders supplying and regulating the cryogenic materials to cool down and control the temperature of the magnets during its operation. The operating current of the magnets feeders is 68 kA while its cooler end has to be at 4.2 K. High temperature superconductors allows high-power currents from the room temperature power supplies to the cooler temperatures of the magnets with a very low heat load. The busbars designed for the current feed are made with a steel conduit filled of NbTi superconductor strands and are prepared to absorb the temperature fluctuations during the cool-down of the machine [3].

1.2 Superconductors

A superconductor is any material that conducts electricity at zero resistance below a certain temperature. Once set in motion, electrical current will flow forever in a closed loop of superconducting material. Scientist refer to “*macroscopic quantum phenomenon*”.

In a pure metal, their atoms exist as a lattice of cations immersed in flowing electrons. At room temperature, these cations have a thermal motion which scatters the electrons and this scattering is the responsible of the resistance. For this reason, when metals have lower temperatures they experiment lower resistances. In superconductors, the resistance is equal to zero when their temperature is below T_c . In *Figure 1.10* is represented the cations lattice with electrons scattering.

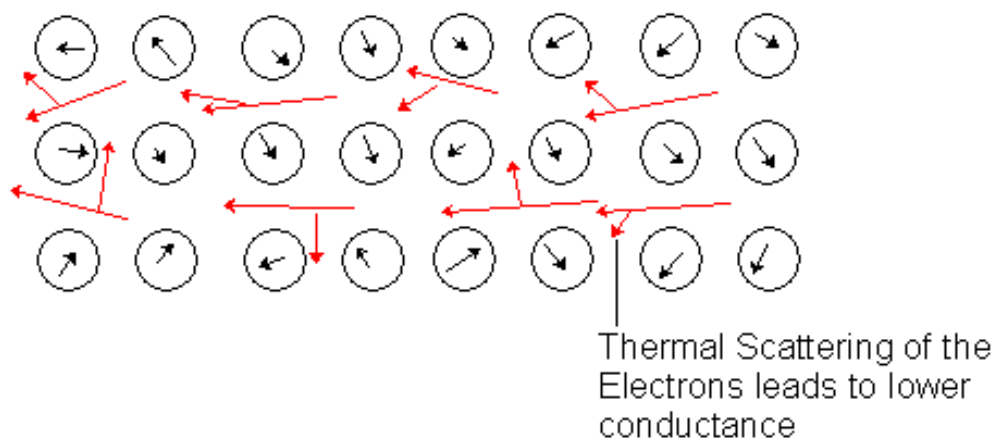


Figure 1. 10 Thermal scattering sketch.

Since superconductivity was discovered in 1913, a lot of material have been discovered with higher and higher superconductivity temperatures. Metals are the most common conductors employed but its crystal structure causes them to scatter electrons, producing a resistance. The different types of superconducting materials are: pure metals and alloys, iron based, and copper oxide based.

The first type, pure metals and alloys, need the lowest temperatures to become superconductors but they are superconductive in all three dimensions while the iron and copper oxide superconductors can work at higher temperatures but only in two dimensional planes.

The techniques to manufacture and synthesizing superconductors include reacting metal nitrates or carbonates and heat treatments under high temperatures.

Nowadays superconductors applications include magnetic field sensors, medical equipment, gyroscopes, high speed trains and recently fusion power plants. Fusion never could be controlled in a power plant scenario if superconductors had not been discovered.

1.2.1 Magnetic behaviour

Superconductor can be divided into two groups depending on the magnetic behaviour, Type-I and Type-II. The two groups distinguish themselves in their behaviour in magnetic field. When an external magnetic field is applied to a Type-I superconductor below the critical temperature it generates a current on its surface to fully shield the magnetic field. In the Type-II the magnetic field is allowed to penetrate the material.

Type-I category is composed mainly of metals and metalloids who show some conductivity at room temperatures but they need an incredible cold temperature to slow the thermal scattering enough to facilitate the unimpeded electron-flow. The inside of a bulk superconductor cannot be penetrated by a weak magnetic field, this phenomenon is called “the Meissner effect”. When the applied magnetic field becomes too large, superconductivity directly breaks down. This is a problem for the magnetic coils operation.

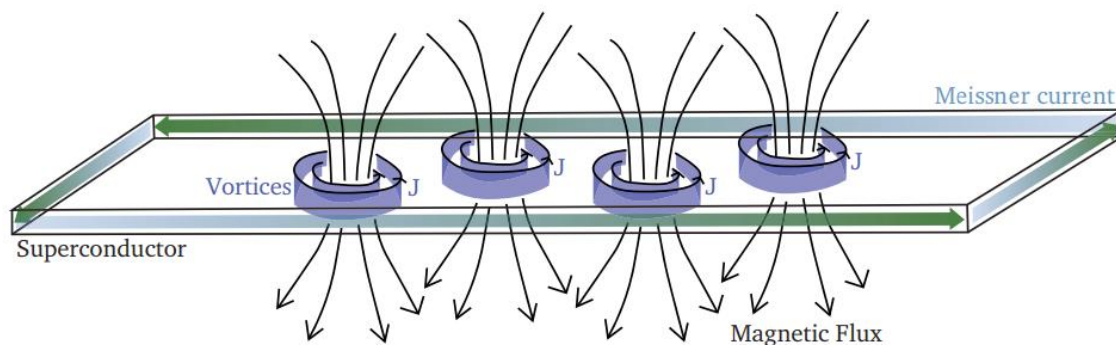


Figure 1. 11 Superconductor Type-II when a high external magnetic field is crossing through its vortices [4].

Except for the elements vanadium, technetium and niobium, the Type-II category of superconductors is composed of metallic elements and alloys. For Type-II, the materials have two critical fields, between which it allows partial penetration of the magnetic field through isolated points. These points are called vortices. The vortices composed of circulating electrical shielding currents which allow the normal state at their centres to exist as it is shown in Figure 1.11. This phenomenon is known as the Abrikosov effect. The resulting mixed state, with normal conductivity inside the vortices surrounded by material in the superconducting state, is stable and thus allows superconductivity to be maintained up to very high critical magnetic fields, making Type-II superconductors crucial for practical applications like ITER coils.

Normally these vortices are located on microstructural defects in the material because these points are energetically favourable, this effect is called flux pinning and optimizing pinning in

practical superconductors is a challenge for conductor research. The defects are artificially created to increase the number of pinning centres. The force required for separate a vortex from its pinning centre is known as pinning force. In conducting state, the current applies a Lorentz force to the vortices and when it is larger than the pinning force, the vortices start to move and there is a dissipation which cause the material to become resistive.

This places a critical limit on the superconducting current density, called critical current density (J_c). This critical current density is independent of the magnetic field and temperature. Therefore, superconductivity can only occur below the critical surface.

In magnet applications like in ITER, superconductors are provided with a good resistive conductor that can, in case of fault or quench, take over the current. Superconductors have a low free charge density which mean that they are very poor normal conductors. To allow superconductivity the electrons need to be in a low energy state [4]. A schematic comparison between both types is illustrated in *Figure 1.12*.

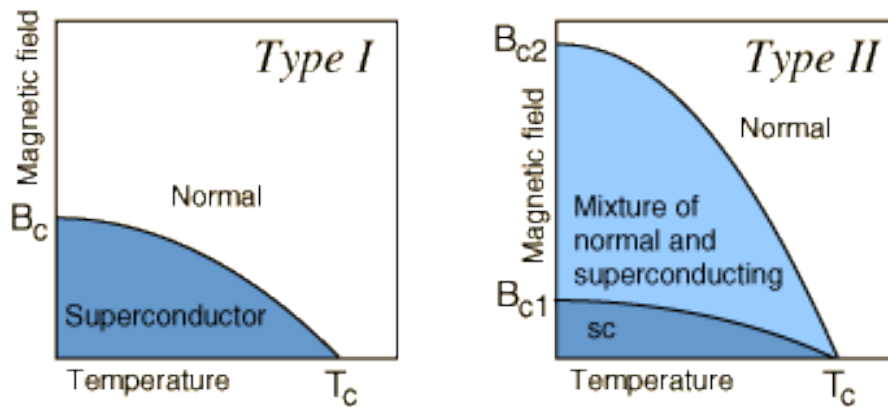


Figure 1. 12 Superconductor states in Type-I and Type-II in function of magnetic field and temperature.

1.2.2 High and Low temperature superconductors

The Type-II superconductors are divided in low temperature superconductors (LTS) and high temperature superconductors (HTS). Based on the critical temperature (T_c), when it is higher than the boiling point of liquid nitrogen temperature the superconductor is considered as HTS, otherwise it would be an LTS.

HTS are the conductors which critical temperature is higher than the liquid nitrogen (77K). These conductors have higher T_c and also higher critical magnetic field and higher critical current density.

For magnet applications, the high critical magnetic field is more important than the critical temperature. However, these materials are brittle ceramics which are expensive to manufacture, and the process to turn them in wires is difficult.

High temperature superconductors belong to the Type-II of superconductors. Some research was made for HTS applications in future fusion reactors. One interesting material which could

be used in DEMO magnet system is the ReBCO compound, which is an important candidate to substitute the Nb₃Sn. ReBCO is more resistant to mechanical stress and thermal cycling than other HTS, in addition, it does not require a heat treatment. These conditions shall improve the future tokamaks. However, HTS require significant research and development before they can be applied in a practical magnet for fusion.

The low temperature superconductors (LTS) are usually cooled with liquid helium at near 4.5 K. The most common LTS conductor for magnet applications is the alloy of niobium-titanium (NbTi), which is the only ductile Type-II superconductor that is available in long lengths of wires.

NbTi is used for almost all the applications like laboratory magnets, MRI scanners, magnetic levitation trains, particle accelerators and in the ITER magnet system. For NbTi the critical surface limits the magnetic field in a practical fusion reactor coil to about 9 T.

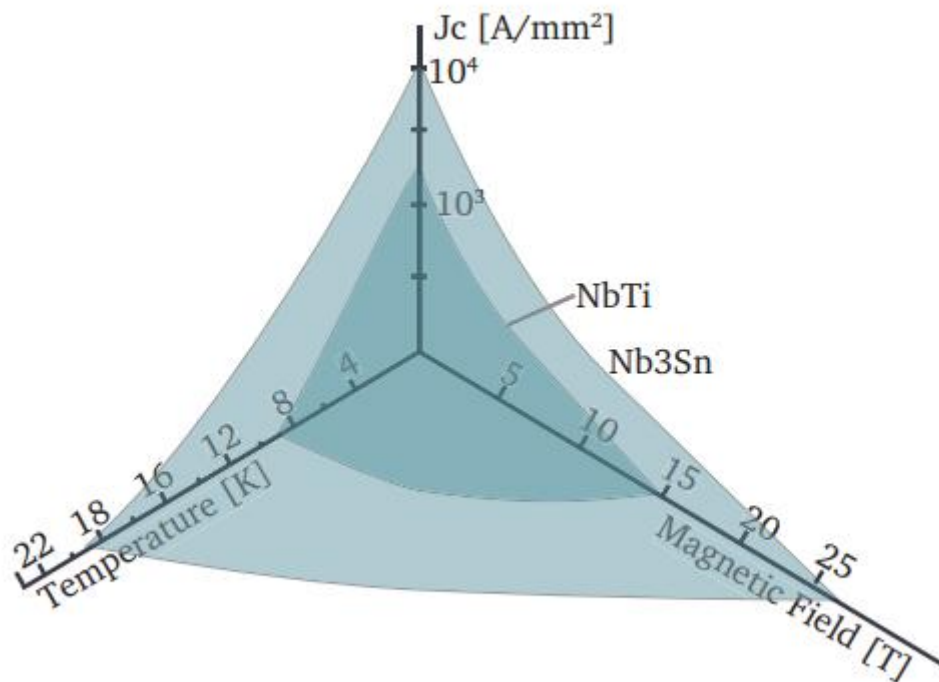


Figure 1. 13 Critical aspects comparison between NbTi and Nb₃Sn [4].

To exceed the NbTi magnetic field limit, Nb₃Sn is the solution, however, this is a brittle material which need to be protected and manufactured with care. The CS and TF coils designed for ITER are made of Nb₃Sn due to its larger effective magnetic field necessary to confine the plasma. A comparison of both LTS conductor in its independent aspects as critical current density, critical magnetic field and critical temperature is sketched in *Figure 1.13*.

As it can be observed Nb₃Sn shows a better performance than NbTi, nevertheless, NbTi is an interesting material because it is ductile and its manufacture is less expensive than the Nb₃Sn.

These characteristics make NbTi a preferred material when the magnetic field required is not very larger as in many coils of ITER like control coils CC.

1.2.3 A15 superconductors

The A15 superconductors are a good candidate for high magnetic fields generation of more than 10 T. The name is based on the beta form presented in tungsten element. Originally A15 structures was defined for tungsten but it was observed that this structure is only present for the beta phase of tungsten. The real structure was shown in an oxide but the incorrect nomenclature has persisted even after some efforts by crystallographer to rename it. The A15 structure is shown in *Figure 1.14*.

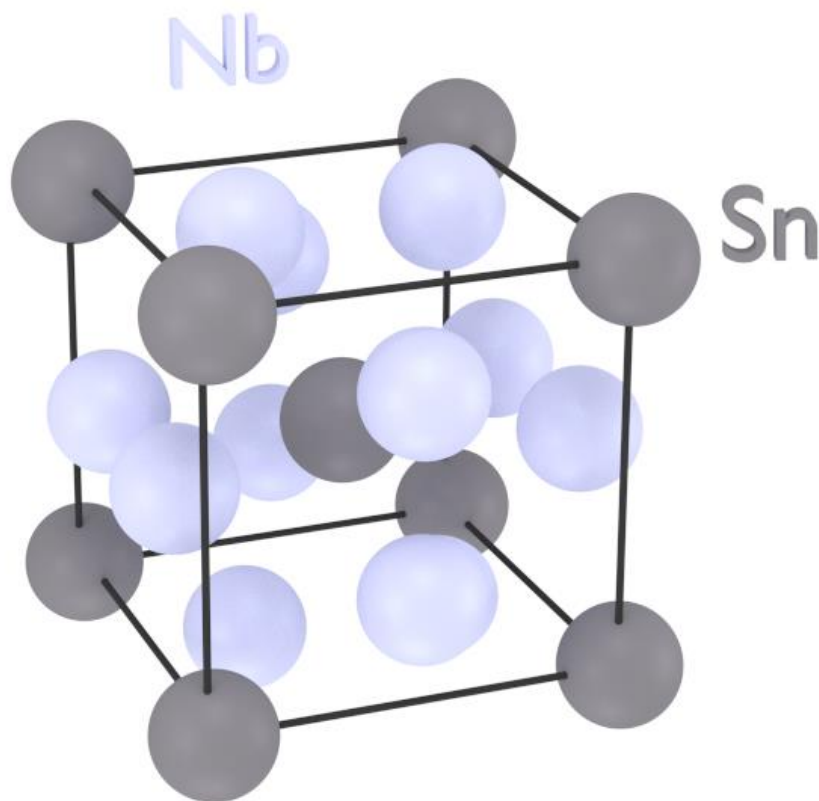


Figure 1. 14 Nb₃Sn A15 lattice structure.

The A15 lattice elements have a cubic shape below to the martensitic phase transition temperature. Above this temperature, the cube structure becomes a more tetragonal structure.

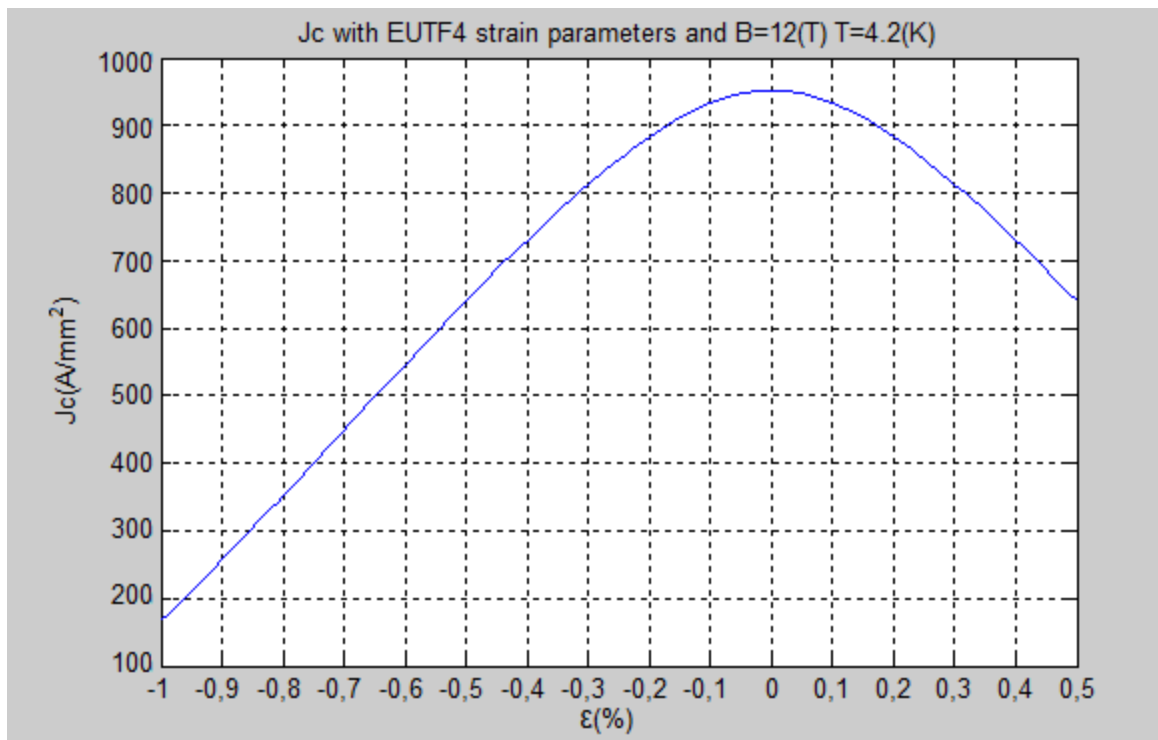
For fine filaments, the A15 compound is made through a heat treatment at approximately 700°C. Nb₃Al compound has the advantage to be less strain sensitive than Nb₃Sn but the cost and nature of Nb₃Al manufacture turns the balance in favour of Nb₃Sn.

For this work, the material considered for the conductors is the Niobium-Tin alloy Nb₃Sn used in ITER TF coils. The biggest drawback of this element is their strain sensitivity.

We conclude that a tokamak needs strong magnetic field to work and this high magnetic fields make necessary the superconducting magnets. Resistive magnets would be too large and would require a higher amount of energy while with superconducting magnets in the ITER tokamak will consume only 35 MW for the cryoplant which maintains the conductors in a cooled state. The first superconducting magnets applied for a tokamak was implemented in the T-7 tokamak at the Kurchatov institute (Moscow) who was made with NbTi as superconducting material [5].

CHAPTER 2

Critical current density and current sharing temperature



Critical current density in strain function plotted in MATLAB.

Jose Manuel Trueba Cutillas

2.1 Scaling law for parametrization of J_c

In Nb₃Sn superconductors a specific scaling law is used to calculate current density J_c . This is a function of three variables, the background magnetic field, the liquid helium temperature during the operation and the strain in this superconductor material. In this thesis, I employ the same scaling law as is used for designing the ITER and DEMO conductors. In the MATLAB software, I have implemented a function to calculate the J_c for a range of strain. The range of strain is studied for values between -1 and 0.5 in these conductors because it covers the range of strain observed in fusion conductors, and the scaling law in this range is still accurate, i.e. does not express significant deviations from measurements done on the strands [6]. It is interesting to note that the strain dependence of J_c is mainly present in Nb₃Sn conductors, while the J_c of NbTi conductors are not sensitive to strain. In the J_c function strain plays an important role, the maximum J_c is found for strain close to zero in the strain value called " ϵ_{max} ". This scaling law was developed for any Nb₃Sn conductor in fusion applications.

Scaling law consists of several related equations. In my thesis, I employ the scaling law proposed by Bottura [6]. The main equation to calculate the density current in the superconductor is obtained by combining different scaling laws from previous models. The major inspiration comes from parametrization of Durham University [7] and Godeke [8].

In this thesis, I use the scaling law parameters defined in [9]. These parameters were fitted for the EUTF4 strands. The name "EUTF4" is a label of an ITER toroidal field (TF) conductor sample tested in the SUTAN facility and produced in Europe.

To define the current density formula terms, one of the most important is the scaling constant which appears in Ampere per Tesla divided by square millimetre and is represented by C . This is a scaling constant which changes depending on the material and type of conductor. For this Thesis, we use the EUTF4 constant of 76189 AT/mm² [9].

The equation is studied starting with the pinning force, which is density current per background magnetic field B . This model of the pinning force is taken from [10]. The original equation of F_p (pinning force) is:

$$F_p = C \left[\frac{B_{C2}^*(T, \epsilon)}{B_{C20max}^*} \right]^n \frac{1}{k(T, \epsilon)^m} f_p(b) \quad (1)$$

Normalising the pinning force, critical field depending on temperature and strain and the Ginzburg-Landau parameter, the following equivalences are found:

$$f_p(b) = b^p (1 - b)^q; \quad \frac{B_{C2}^*(T, \epsilon)}{B_{C20max}^*} = s(\epsilon)(1 - t^v); \quad k(T, \epsilon) = s(\epsilon) \frac{1 - t^v}{1 - t^2} \quad (2)(3)(4)$$

Replacing and manipulating some terms in the pinning force equation, the following equation can be found:

$$Fp = C s(\varepsilon)^{n-m}(1 - t^v)^{n-m}(1 - t^2)^m b^p (1 - b)^q \quad (5)$$

This formula is similar in the $g(\varepsilon)$ and $h(t)$ found in the scaling law of Ekin [10], but the final exponent parameters are taken from Godeke [8] fitting $v=1.52$, $n=2$ and $m=1$. Dividing the pinning force by the background magnetic field with the exponents from [8], finally the Jc equation can be expressed as:

$$Jc = \frac{C}{B} s(\varepsilon)(1 - t^{1.52})(1 - t^2)b^p(1 - b)^q \quad (6)$$

The parametrization proposed is based on the accepted pinning force model of Fietz and Webb [11]. The pinning force is the root of this scaling law and is described by $Fp=Jc(B, T, \varepsilon)B$, where p and q in the final equation are the low and high field exponents of the pinning force, respectively.

Critical field scaling with strain and temperature and critical temperature scaling with strain are taken over from Ekin empirical models [10]. The advantage of these models is that the different factors as strain, temperature and field are separately accounted, which is very convenient for the experimental determination of scaling law parameters.

This scaling law is valid exclusively for Nb_3Sn conductors but it can be used for different shapes of the conductor section as rectangular or circular, and in every ITER conductor made of this material. The same parametrization is also used for designing the DEMO conductors. Though the scaling law is general, every superconducting strand (cable) is characterised by its own set of scaling law parameters, which are determined experimentally. For more information about these parameters consult the annex [A]. In ITER, there is a database of strand parameterisations for different strand manufactures and even for different strand production batches.

2.1.1 Critical temperature and critical magnetic field

Critical temperature and field depends on the strain. They are directly related to each other, so critical magnetic field depends on temperature and strain, and critical temperature is a function of magnetic field and strain. The critical temperature used in the scaling law comes from Ekin report [10] and is defined as follows:

$$Tc^*(B, \varepsilon) = Tc_{0max}^* [s(\varepsilon)]^{\frac{1}{3}} (1 - b_0)^{\frac{1}{1.52}} \quad (7)$$

Where the Tc_{0max}^* is the maximum critical temperature at zero strain and field. This temperature depends on the materials used in the strands from a given and in our own case I take this temperature of the EUTF4 from [9].

The parameter b_0 stands for reduced magnetic field at zero temperature, and is defined as:

$$b_0 = \frac{B}{Bc_2^*(0, \varepsilon)} \quad (8)$$

Here B denotes the background magnetic field acting on the superconductor as will be described in the next chapters of the thesis. $Bc_2^*(0, \varepsilon)$ is the critical field at zero temperature and applied intrinsic strain. The b_0 value is just used for calculating the T_c^* and this parameter is only employed for calculating the reduced temperature “ t ”, so in t we use the critical temperature for zero field $T_c^*(0, \varepsilon)$ which means that $B=0$, by this, b_0 is equal to zero unless $Bc_2^*(0, \varepsilon)$ would be other than zero which is mathematically indeterminate. The critical field at zero temperature can be calculated as:

$$Bc_2^*(0, \varepsilon) = Bc_{20max}^*s(\varepsilon) \quad (9)$$

where $Bc_{20max}^*(0, \varepsilon) = 32.97 \text{ T}$.

In the equation of T_c , the denominator situated in the exponent of the strain function is $1/3$, which denominator is taken as an empirical value of 3 from experiments made for ITER scaling law. It can be considered as the index of a root with the strain function as radicand. The value of the 1.52 exponent is referred with the letter ν and is recommended in [8]. Critical temperature as function of strain that I calculated for the EUTF4 scaling law parameters is presented in *Figure 2.1*:

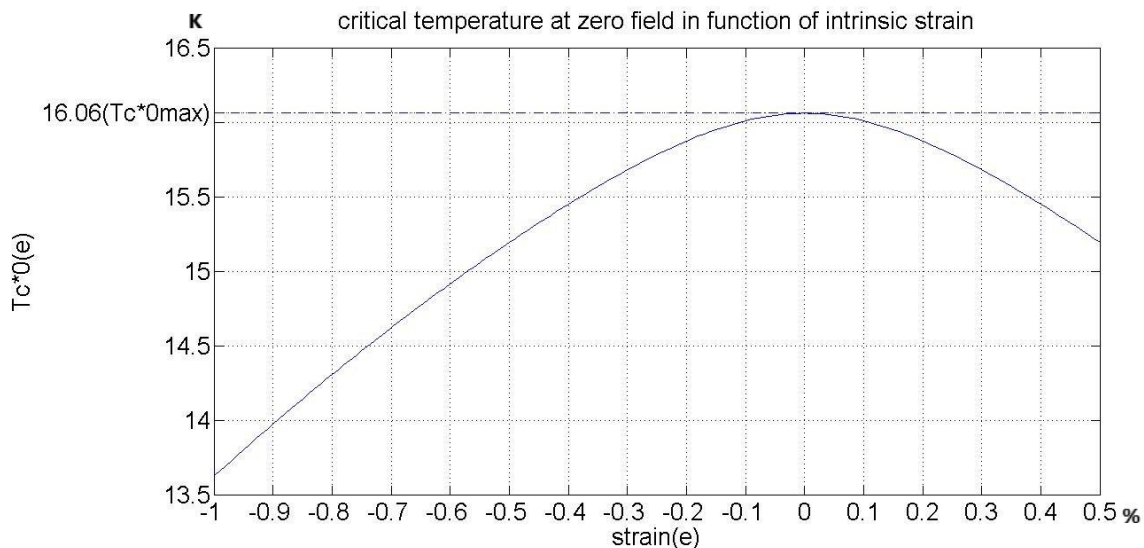


Figure 2. 1 Critical temperature at 0 background field (K) as function of intrinsic strain (%). The calculation is based on the EUTF4 scaling law parameters.

In *Figure1* the critical temperature is plotted for the case of zero background magnetic field. The units of the temperature are Kelvin. The strain has the usual unit of percentage.

It can be observed that the maximum critical temperature for 0 background field is produced when strain is equal to zero. The function of the strain used in the equation is the same as described in the previous paragraphs and has a strong influence on the Nb_3Sn conductor performance.

The critical magnetic field, opposite to the critical temperature, is in practise calculated for a defined temperature. For sake of comparisons of performance of different Nb₃Sn strands, it is usually taken at temperature of 4.2 K. This temperature corresponds to the boiling temperature of helium at atmospheric pressure. Helium is the only coolant that can be used to maintain this kind of A15 superconductors in the superconducting state with zero resistance.

This formula is composed by the maximum field for zero strain and temperature, the strain function and a factor depending on the reduced temperature. In this formula, the v value is found again to normalize the reduced temperature, and comes from Godeke [8] with the MDG relation with the pinning forces in reduced temperature function to take an approximation of all the temperature range yields, defining the relation as $MDG(t) = (1 - t^{1.52})$.

With all the parts defined, two variables are crucial in the critical magnetic field equation, the temperature and the strain in percentage:

$$Bc_2^*(T, \varepsilon) = B_{c20max}^* s(\varepsilon) (1 - t^{1.52}) \quad (10)$$

I plot the critical field at temperature of 4.2 K as function of strain in *Figure 2.2*:

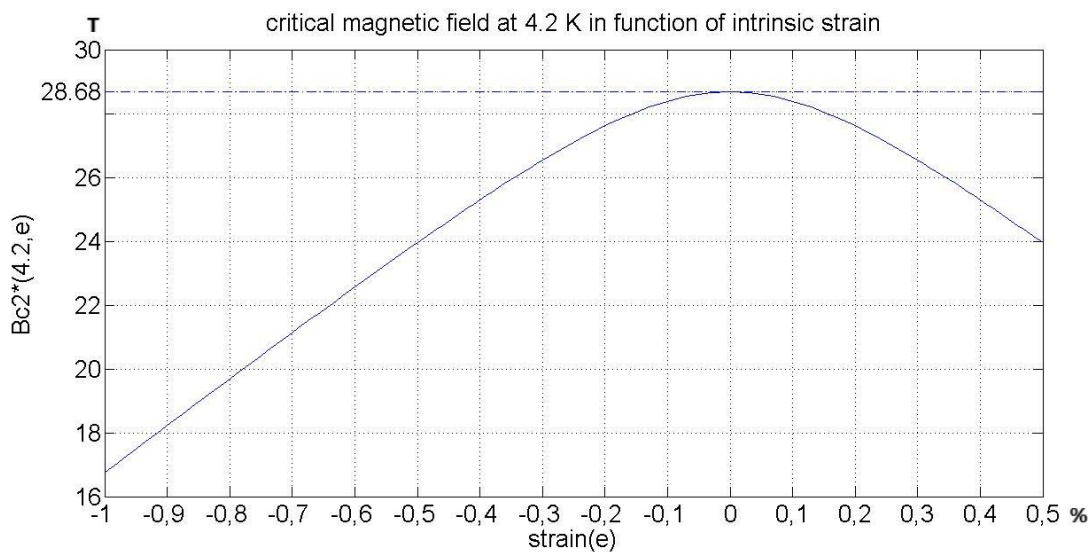


Figure 2. 2 critical magnetic field (T) at a defined temperature of 4.2 K in function of the intrinsic strain (%).

2.1.2 Reduced temperature and field

The reduced temperature has been mentioned in the previous formula as part of the critical field but this parameter has a direct implication in the final current density equation, like the reduced field. The reduced field depends on B and T, the background field and the conductor's temperature implicitly included in the reduced temperature t , which is defined as:

$$t = \frac{T}{Tc^*(0, \varepsilon)} \quad (11)$$

In this case using the critical temperature at zero field and in strain function. The temperature, the magnetic background field B and the strain are also linked at the minimal magnetic field:

$$b = \frac{B}{Bc_2^*(T, \varepsilon)} \quad (12)$$

As is showed in *Figure 1* and *2* at zero strain critical values are highest. This seems that reduced values are smaller for zero strain. That produces in the J_c equation a rise because they are normalized from MDG relation i.e. $(1 - t^{1.52})$ and E_{kin} critical temperature and field relations, described with the corrected exponent values in [8].

2.1.3 Nb₃Sn and strain function

Nb₃Sn was selected as superconducting material in ITER and DEMO toroidal field (TF) and central solenoid (CS) coils for different reasons. It is an A15 superconductor, this kind of conductors can withstand high magnetic fields above 10 T in superconducting mode. An alternative material from the A15 group, namely Nb₃Al, has also good superconducting features but it also has high costs of production and the experience with this material in practical applications is much smaller compared to Nb₃Sn. Nb₃Sn takes advantage in this aspect and this was the main reason to consider the use of Nb₃Sn in ITER superconductors. NbTi material, which is much cheaper and easier to work with, was not an option, as it cannot withstand magnetic field above ~6 T at reasonably high transport currents.

A15 conductors have a high sensitivity to strain. Nb₃Sn is a brittle material which has a limited reversible elongation, and its superconducting performance is very strain sensitive. The transverse load in a large Nb₃Sn by the Lorenz forces is the main producer of the strain. “Load protective” feature of the conductor jacket surrounding the superconducting cable serves very well as a protection for the Nb₃Sn cables in the high field, where at accumulated load above 150 MPa in the monolithic conductors come to a severe operation limit.

The hydrostatic strain components are included in the $\varepsilon_{0,a}$ term and a parameter C_{a2} which is related to the third strain invariant is added to C_a . For the final $s(\varepsilon)$ in ITER is used the Godeke equation [8] in the final Bottura scaling law [6]. The correction $C_{a2}' \varepsilon$ effectively rotates the strain dependence curve around its maximum. For more detailed information of this formula please consult annex [B]. This causes the axial position of the maximum to shift by a factor ε_{sh} :

$$\varepsilon_{sh} = \frac{C_{a2}' \varepsilon_{0,a}}{\sqrt{(C_{a1}')^2 - (C_{a2}')^2}} \quad (13)$$

The fitting parameters for the strain function are the following:

Parameter	Description	Value
Ca_1	Is a strain fitting constant representing the second strain invariant	50.06
Ca_2	Is a strain fitting constant representing the third strain invariant, in our case is equal to zero	0
$\epsilon_{0,a}$	Is the non-axial residual strain which come from remaining strain components in %.	0.00312%
ϵ_{sh}	Is a factor produced by the axial position of the maximum strain dependence curve corrected by Ca_2 and $\epsilon_{0,a}$ in %.	0%
ϵ	Is the strain applied to the conductor plus ϵ_{max} (depending of the strain), this is caused by the Lorenz forces a usually have a range from -1 to 0.5 in %.	[-1, 0.5] %

Table 2. 1 fitting parameters for calculation of strain function from EUTF4 [9].

The final strain function that is used is the same that is described in [8]. Through the MATLAB software I use the strain function in the required range of strains to calculate with this vector the definitive critical current J_c . This is the strain equation $s(\epsilon)$:

$$s(\epsilon) = 1 + \frac{C_{a1} \left(\sqrt{\epsilon_{sh}^2 + \epsilon_{0,a}^2} - \sqrt{(\epsilon - \epsilon_{sh})^2 + \epsilon_{0,a}^2} \right) - C_{a2}\epsilon}{1 - C_{a1}\epsilon_{0,a}} \quad (14)$$

The equations described are mostly empirical functions with constants coming from the experiments with the Nb₃Sn in high magnetic field experiments to analyse the deformations and physical changes in the materials. It is important to remark that these equations are for a reversible strain which can be produced by elastic deformation of the Nb₃Sn lattice. Irreversible strain can cause filament fractures or permanent changes in the strain state of the matrix which surround the filaments. The strain formula does not consider irreversible degradation. It is necessary to take care during the conductor and coil manufacturing process to fabricate and ensemble the coils such that irreversible degradation of strand properties.

As already mentioned, b and t depends on the strain function $s(\epsilon)$ and that links even more J_c results with the function of strain the dependence of the critical current density J_c on strain ϵ is shown in *Figure 2.3* It was calculated using MATLAB.

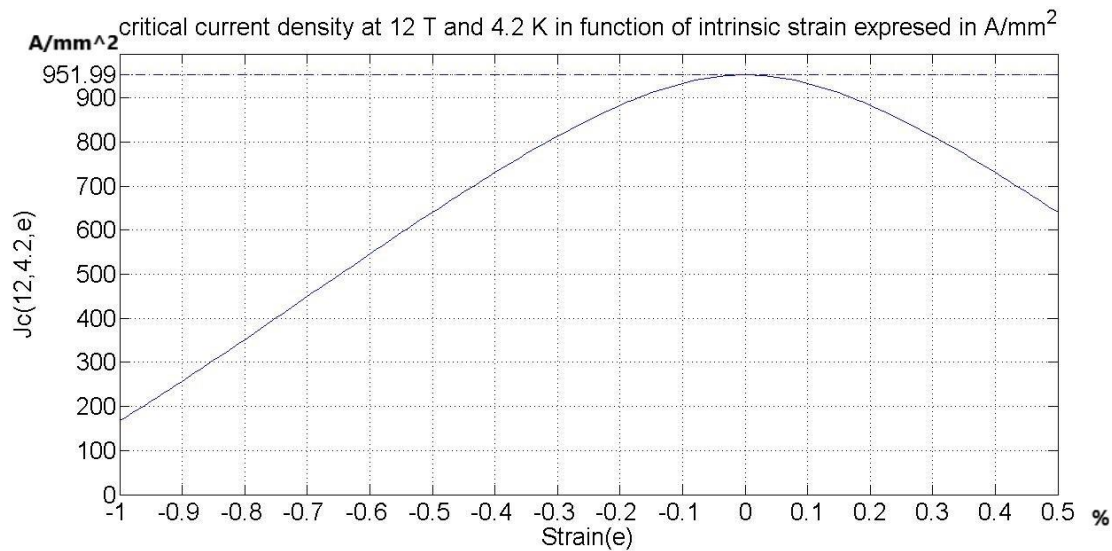


Figure 2.3 Critical current density (A/mm²) at defined temperature and background magnetic field in function of intrinsic strain (%).

Figure 2.3 illustrates the importance of the strain in the final J_c , which expresses a clear peak at zero strain. The strain may change during magnet operation, when operating current in the magnet is usually repeatedly switched on and off. During these repetitive current switches, the conductor is exposed to changing Lorenz force, the so-called load cycles. It is important to test the conductor performance during a specific number of cycles to be sure that the performance degradation of the superconductors remains within requested limits during the magnet lifetime. Also, the conductor samples of the ITER tokamak were exposed to large number of load cycles, typically 1000 cycles for the TF conductors and 10000 cycles for the CS conductors.

2.1.4 Production over the world

All Nb₃Sn conductors at ITER are described by the same scaling law formulas. However, they are produced in different countries and their properties vary from strand manufacture to manufacture, and even from strand batch to batch. Strands from different producers may have their own matrix and a different layout. Strands producers are spread between Europe, Japan, USA, South Korea, Russia and China. Every strand batch is therefore characterised by its own set of scaling law parameters. Our model parameters are taken from a European conductor sample, EUTF4, which was one of the best-performing SULTAN sample. The values from EUTF4 are described in the *Table 2.2*.

Parameter	Description	Value
Ca₁	Is a strain fitting constant representing the second strain invariant	50.06
Ca₂	Is a strain fitting constant representing the third strain invariant, in our case is equal to zero	0
ε_{0,a}	Is the non-axial residual strain which come from remaining strain components in %.	0.00312%
ε_{max}	tensile strain at which the maximum critical properties are reached	-0.110%
B_{C20max}	upper critical field at zero temperature and strain which is expressed in tesla	32.97
T_{C0max}	critical temperature at zero field and strain measured in Kelvin	16.06
C	scaling constant represented in ampere divided by square millimetre	76189
p	low field exponent of the pinning force which always is under 1 ($p < 1$, $p \approx 0.5$)	0.63
q	high field exponent of the pinning force, like p it has not units ($q \approx 2$)	2.10

Table 2. 2 Fitting parameters for calculation of strain function from EUTF4 [9].

The motivation for this choice is that strand manufacturers keep improving their products, and we expect that strands for DEMO produced in future will routinely perform as good as the best ITER strands. The differences in strands of different producers are graphically illustrated in *Figure 2.4*.

With this figure, we can appreciate important differences between the strands. Finally, the important is that the SULTAN tests of ITER samples indicated that they all satisfy the ITER acceptance criteria and can work properly in the ITER tokamak. ITER is an international project and this is the reason of the distributed production.

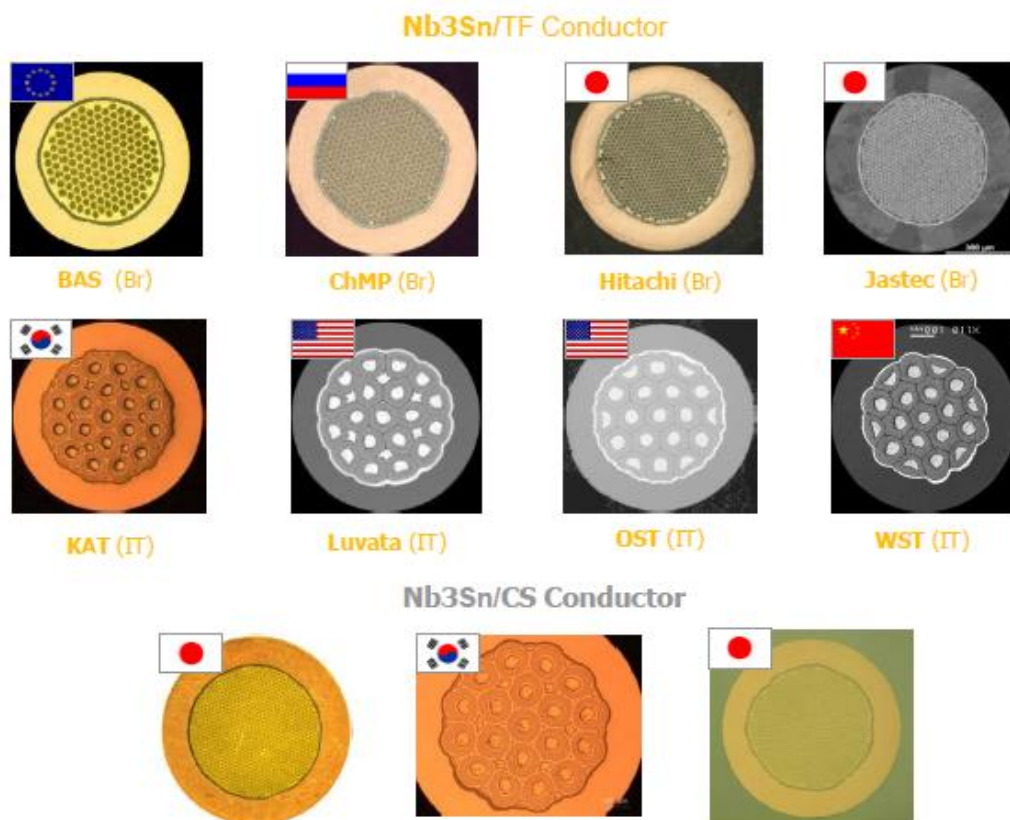


Figure 2. 4 Different layouts for strands producers over the world for ITER [12].

2.2 The current sharing temperature

The current sharing temperature T_{cs} indicates the limit where the current transported through the superconductor strands starts to flow through the stabilizer. The stabilizer is usually made of copper. The copper stabilizer under operating conditions does not conduct any current but its function is very important in the way of stabilizing the superconductor. There are three different states which are described in the next parts of this chapter based on the temperature range.

These states are defined by two temperature limits. The lower of the two limits is the current sharing temperature, T_{cs} . This limit is defined experimentally as temperature, at which a small electric field starts to develop along a section of the cable-in-conduit-conductor (CICC). When the electric field reaches a specific value known as the critical electric field E_c , typically $E_c=10\mu\text{V/m}$, part of the electricity starts to flow through the copper as an auxiliary way to carry the excess current that the superconductor material cannot transport in the superconducting state.

The strands of Nb_3Sn are produced with an external layer made of copper available to carry the excess current instantaneously when it would be necessary. The structure of a superconductor strand is shown in *Figure 2.5* where the Nb_3Sn filaments are the white dots, (the strands composition will be described in the CICC section). Copper strands are distributed over all the cable section to protect the Nb_3Sn integrity when the temperature reaches T_{cs} .

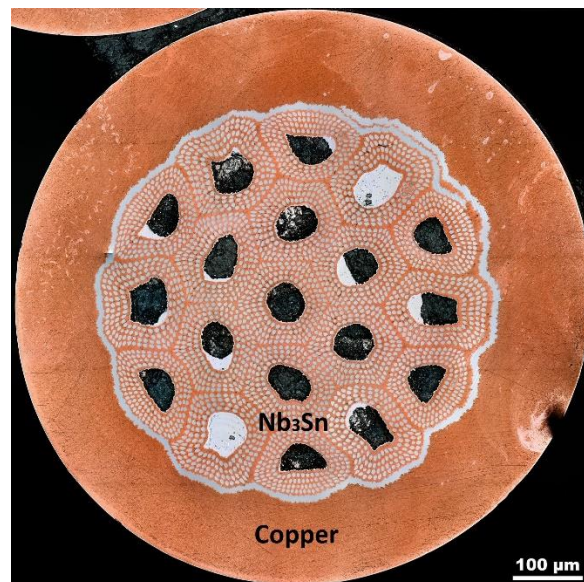


Figure 2. 5 Nb₃Sn strand courtesy of Peter Lee, Florida State University

The inconvenience of this current flowing through the copper is that the copper has a finite resistance that even at low temperatures produce some heating, and this heat can elevate the temperature of the superconductor. In some cases, the superconducting state in the superconductor may recover – for example if the source of initial heat in the strand was a

strand movement that lasted for a short time. In other cases, the Joule heating generated by the resistive current transport leads to a thermal runaway. The superconducting properties of the strand are reduced as the temperature increases, as it finally exceeds the second temperature limit, the so-called critical temperature T_c . This situation is called quench. The superconductor magnet needs to be quench-protected, i.e. the quench state has to be recognized, and current in the circuit must be damped, otherwise the fast heating could produce irreversible damages in the conductors or in other components of the coil, e.g. in the electric insulation between neighbouring turns and layers. This critical temperature of Nb_3Sn at zero magnetic field is 18.3 K.

Once the temperature limits are defined by the changes in the conductor, I will continue with the different states of the conductor and what happens in each one.

The first state, is the fully superconducting one, when the temperature T is below the T_{cs} limit, $T < T_{cs}$. In this state all the current passes through the superconducting material, and the conductor is in a cryogenic state due to the liquid helium which provides a regular temperature typically around 4.2 Kelvin. In this situation, the resistance in the conductor is absolutely zero, this means that no heat is produced by Joule losses due to electric resistance. Consequently, there is no voltage visible over some conductor length. This satisfies the Ohm equation $V = I \cdot R$. Taking in account that resistance is equal to zero, the voltage is also zero.

The temperature in the CICC is usually around 4.2 K. This temperature corresponds to the temperature of liquid helium (at atmospheric pressure), the most typical coolant used in this kind of superconductors. The helium flows in the so-called forced flow conditions often at elevated pressures, for example 5-6 bars at ITER. The helium flow is “forced” by a pressure difference at the helium inlet to the coil (e.g. 6 bars) and helium outlet at the end of the coil winding (e.g. 5 bar). The helium is then in the so-called supercritical state, and its temperature may be higher than 4.2 K, often around 4.5 K. The helium passing through the gaps between strands provides a very efficient cooling. However, in some situations in concrete zones of the conductor some disturbances could produce short-term temperature rises. It is the purpose of stabilizer in the strands, and in some cables additional stabilizer also in the form of segregated copper wires, to allow the conductor to withstand at least some of the short-term disturbances, and to enable the conductor to recover into the superconducting state.

In the second state, after the heat produces a temperature above T_{cs} , current starts to flow in both materials, Nb_3Sn and copper. This is shown in *Figure 2.2 (a)*, where Nb_3Sn is the superconductor material and copper the stabilizer.

At this state, the conductors can show their technical capabilities. To make good quality superconductors is not an easy task. Every conductor for a practical application must be tested. The last testing for very large conductors (operating current above ~40 kA) designed for large magnetic fields (of the order of 10 T or more) is often performed in the facility SULTAN installed at PSI in Villigen (Switzerland).

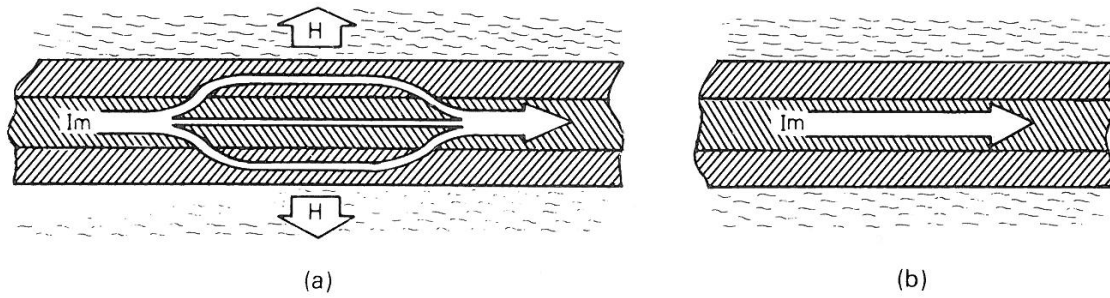


Figure 2.6 (a) The current starts to flow through the "stabilizer" and ohmic heat is transferred to the coolant. (b) The current flow again only by the superconductor and the T returns below the T_{cs} temperature. Picture from "Superconducting magnets", Martin N. Wilson.

Before being tested, a Nb_3Sn superconductor has to be heat treated in several phases, in order to produce the Nb_3Sn lattice structure inside of the strands. The heat treatment lasts around 30 days, to achieve a good quality of the conductors.

If the conductors have a good quality and the heat treatment was made with success, these should reach superconducting state after cooldown to the operating temperature. However, it is very difficult to know where the conductors could have imperfections reducing the conductor performance. For this reason, the large conductors are finally tested in SULTAN. This facility can to a large extent simulate the state of the conductor in the magnet in its operating conditions. SULTAN has high current capacity (100kA), a cryogenic pump which gets the liquid helium to a very low temperature (4.5K) and furthermore it generates a magnetic field of almost 11 Tesla. These different capabilities combined in the same facility makes it unique for the test of ITER superconductors.

The conductors are tested to find the T_{cs} at a prescribed operating current and magnetic field. This is the most representative test to determine the conductor performance [5]. During the test, the temperature is increased till the current starts to flow through the copper, which is experimentally observed as a voltage build-up on the voltage taps attached to the conductor samples. The conductors are tested after various number of load cycles, and also before and after thermal cycling, during which the conductor is warmed-up from the cryogenic temperature up to the room temperature and re-cooled back to the cryogenic temperature. This part is quite important because if the conductors would be assembled in ITER and its performance would degrade during the coil operation or maintenance, it would be serious problem. To replace a TF coil in ITER tokamak would take years.

In previous experiments it has been observed in the central solenoid coil that the T_{cs} increases when the conductors are tested with the first load cycles but after approximately 8,000 cycles the T_{cs} starts to go down [13]. In this case, it was not a big problem because the decrease in T_{cs} was in a very small rate of -4.50×10^{-6} K/cycle and it was estimated that the final T_{cs} could be enough to work in the ITER tokamak with a final T_{cs} over the acceptable limit of 6.5K.

It is estimated that the ITER CS coils must support close to 60,000 load cycles [13]. For this reason, it is very important to try to fabricate conductors whose T_{cs} does not degrade at a very high rate during tests.

The last state, that is described in this chapter occurs when the critical temperature is achieved. For this temperature, superconductor material element does not transport electric current anymore, and so all the current is conducted only through the stabilizer. Voltage corresponds to the normal state for copper and the coolant cannot recover the superconducting state.

Figure 2.7 show a Nb_3Sn filament. This material is especially fragile, and can be easily broken if exposed to mechanical stress or bending.

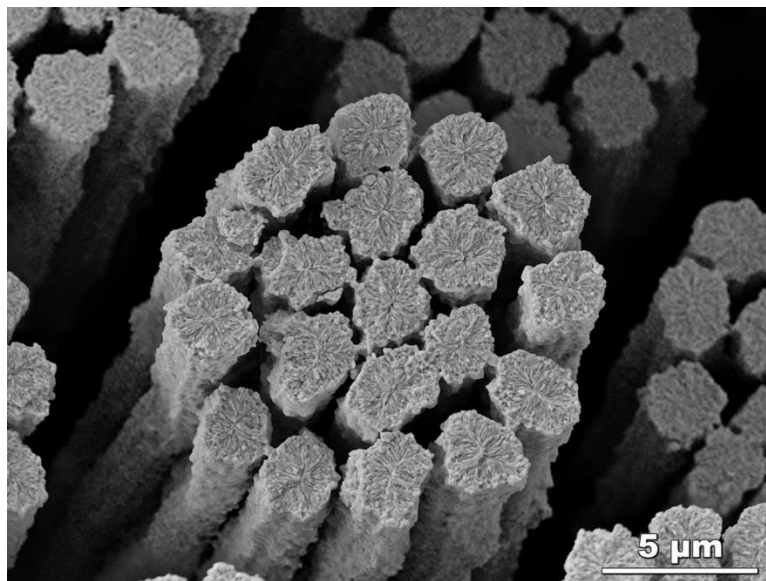


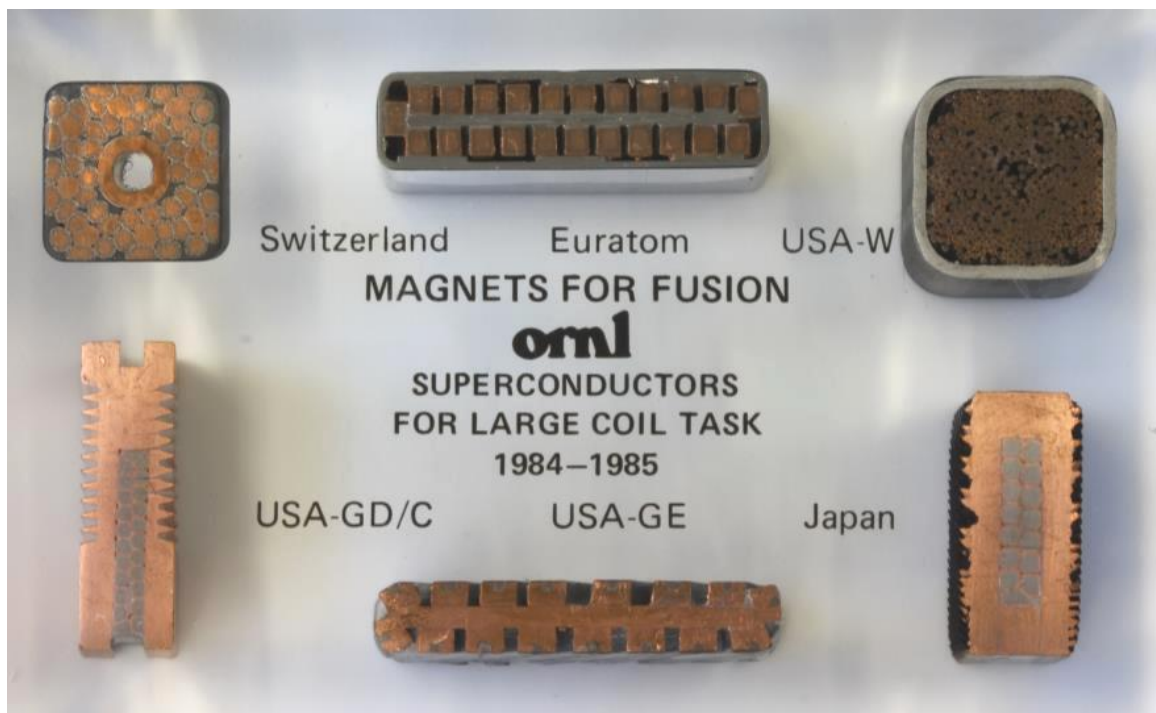
Figure 1.7 Nb_3Sn filament courtesy of Peter Lee, Florida State University.

Due to the high currents of kA the conductor must be quickly switched off because it could be seriously damaged. This is the main problem in superconductors and it is a priority to control the quenches in magnets.

A quench does not need to be understood like an accident or a failure, it is something usual in superconductors [14]. It is defined as the process of transition from superconducting state to the normal-conducting state. Previously was described how a quench is controlled to protect the magnets and technology. It is also quite important to have a very fast detection and reaction to protect the equipment and workers in a not too far future where fusion energy would be integrated in the energy market with developing and very specialized engineering.

CHAPTER 3

Conductor description



Magnets for fusion [12].

3.1 Cable-In-Conduit-Conductor (CICC)

CICC is the type of conductor used for the ITER that is designed to support high magnetic fields, while it conducts very high currents in a special cryogenic state inside the conduit. This is in order to conserve the plasma in a state of levitation sustained by the magnetic forces which give it a flow inside the tokamak and protect the walls of the toroidal chamber against the huge temperatures of the fusion reactions.

The cable is primary composed of steel, copper, and NbTi or Nb₃Sn in the case of low temperature superconductors. The CICC performance is defined by the current density J_c and by the sensitivity of its strands to the transverse load. The main objective of CICC is the mitigation of accumulated transverse electromagnetic loads, which are absorbed by the steel jacket, while the superconductor strands are protected by the jacket from the forces of neighbouring turns and layers acting on the conductor. The CICC conductor performance should ideally not degrade with electro-magnetic loading cycles. There are three main different types of coils for ITER; one is the toroidal field coil (TF) made of Nb₃Sn, second is the poloidal field coils (PF) made of NbTi and the third coil is the central solenoid (CS) made of Nb₃Sn. These coils are shown in *Figure 3.1*.

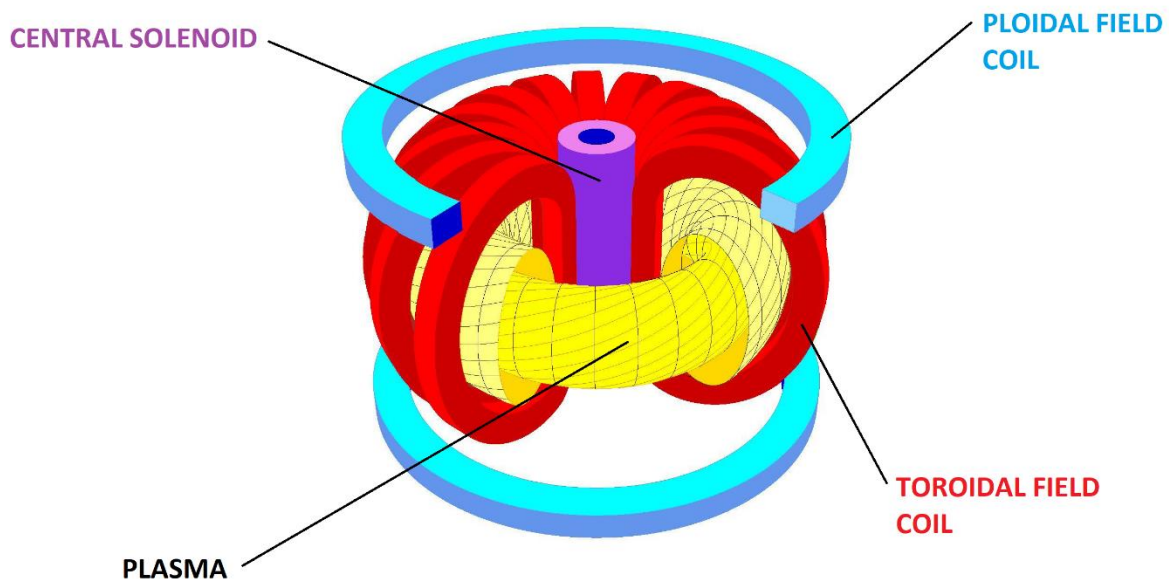


Figure 3.1 coils and solenoid of a tokamak.

A very low temperature in the CICC is maintained flowing supercritical helium as coolant through the gaps between the strands of the cable. In some conductors, there is in addition a dedicated cooling channel installed in the centre of the conductor that improves the total helium mass flow through the cable. The flow resistance (friction) in the central cooling channel is low compared to the flow resistance of helium passing in the gaps between the strands. This is useful especially in the event of quench, when temperature increase leads to pressure increase, which is released by the central cooling channel to a safe value.

The operating temperature of the helium in CICC of ITER is ~ 4.5 K at ~ 6 bar, which means that helium is in a supercritical state. A pump is used to force the helium into the CICC. Typically,

the inlet pressure is 6 bar and outlet pressure 5 bar, so the helium is forced to flow by a pressure difference of 1 bar

In this section TF CICC are going to be described. In the case of ITER, the total diameter of the TF CICC is 43.7mm including the jacket. Some advantages of the CICC for fusion magnets are described in [15]. One of these advantages is that these cables allow the design of very high currents with a lot of different layout possibilities, for example changing the number of strands and proportion of copper and superconducting strands. The possibility of a continuous flux of coolant inside the conduit as supercritical helium is an important benefit. Otherwise, e.g. in a bath-cooling case, the pressure produced during a quench could not be controlled and contained because high pressures are difficult to withstand in large volumes.

The inconvenience of the conductors is the poor relation of superconducting material with respect to the total conductor volume, because it is constituted of an important fraction of copper, helium and steel (or other jacket material), which make it a relatively low current density superconducting conductor, in comparison with other superconducting conductors. These materials are necessary to protect the superconductors in case of quench. The composition of the different parts of the CICC is schematically shown in *Figure 3.2*.

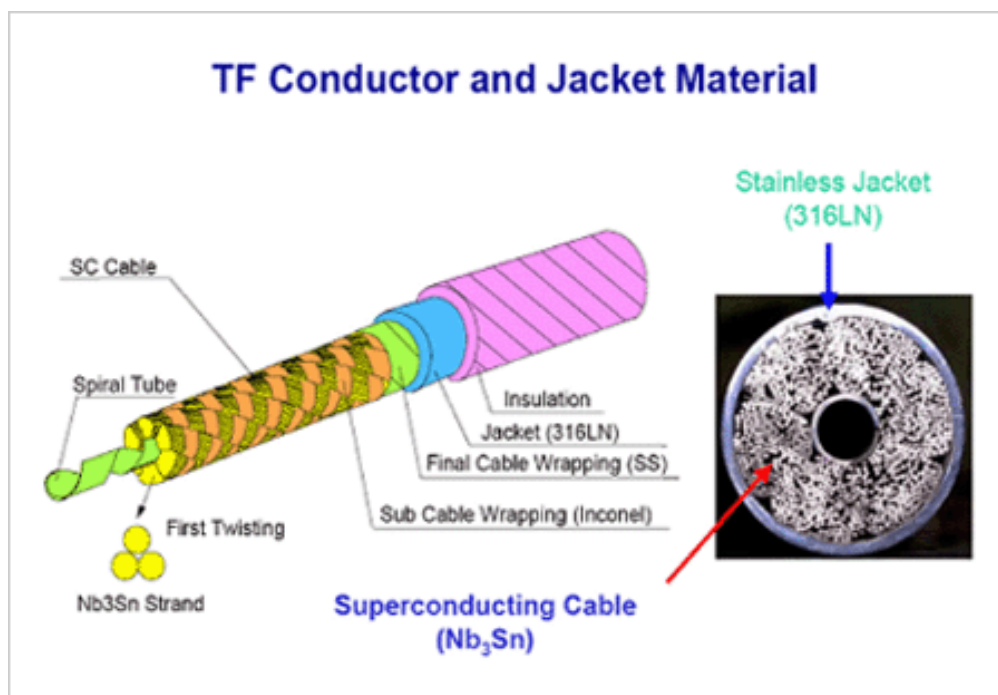


Figure 3. 2 TF conductor parts. National Fusion Research institute from Korea newsletter.

The structure of CICC in TF coils is a cylindrical shape cable with an electrical insulation layer in the most external coat of the conductor, attached on top of the so-called "jacket". The jacket is made of steel and has a strong resistance to the mechanical loads acting on the high-current conductors in the magnetic field. It is the first mechanical protection of the strands against the external forces and it mitigates the thermal strain. Usually it has a thickness of 2 mm. Inside of this mechanical protection, there is the "cable" made of 1152 strands twisted in several sub-cable stages. Each sub-cable stage is twisted and transposed in order to minimize the AC loss in the conductor resulting from current (or magnetic field) changes in

the coil. For the same reason, i.e. to minimize the AC loss, the last sub-cable stage is wrapped into a thin steel wraps. In the centre of the cable there is a spiral tube with 10 mm of hollow diameter and 1.5 mm of thickness. The Nb₃Sn strands have some copper and Nb₃Sn filaments and other materials like bronze are used, depending on the strand manufacturing process.

Nb₃Sn is subject to numerous strain components inside the CICC. One is the thermal strain, due to different thermal expansion coefficients between the steel jacket, the copper strands, and Nb₃Sn with its own copper matrix. This thermal strain is produced because the conductor is heat treated at 650 °C, which is the reaction temperature where the superconducting phase is formed, and then cooled down to 4 K, the operating temperature. Other strain component is the operating strain, which is produced due to the large Lorentz forces which appear when a magnet is electro-magnetically charged and may produce movements of the cable inside the jacket. In ITER TF conductors the forces are around 800kN m⁻¹ [15].

In the first designs for the CICC for ITER at the 90s there were many problems with the thermal strain and the conductor performance after several load cycles degraded, and was not fulfilling the ITER requirements. The conductors had to be further developed and changed. The first Incoloy 908 material for the conduit was substituted by the actual steel [12]. The J_c value increased by a 27% while the non-Cu cross section was enhanced by 7%.

In the calculations made in this thesis an effective cross-section of 2 cm radius round conductor is considered and compared with a rectangular cross-section with exactly the same area. In ITER the conductors have a circular cross section, but the new fusion reactor conductors are often designed with the rectangular cross section. One of the main design driver of a conductor for fusion is the current sharing temperature T_{cs} , which is also very important for the performance measurement and in order to analyse the current density J_c . The results of simulations are not empirical but the process is based on empirical values, which comes from real experiments.

3.1.1 CICC Manufacturing

In the strand production two manufacturing processes of Nb₃Sn strands are in use. One uses a bronze route and the other a uses a tin diffusion in the strands. Both strand types will be defined and described. The diameter of the superconductor strands is 0.82 mm and there are 900 Nb₃Sn strands for a total of 1152 strands (Nb₃Sn strands and copper wires).

For the bronze route process, one strand is chromium-plated with Ti and Ta doping in a double stacking and extrusion process. In the first phase, a pre-conductor is fabricated by inserting 55 NbTa rods into a CuSnTi matrix, after that an extrusion and drawing process is carried in the obtained stack. In the second phase, 151 hexagonally shaped pre-conductors are assembled into a copper tube with a tantalum barrier between the pre-conductors and the tube. This final billet is extruded to the final strand diameter. Afterwards the strand is electrolytically coated with a chromium layer [16].

The other strand type is manufactured with an internal Tin diffusion process. The first step is insertion of 156 Nb and NbTi rods into an oxygen-free copper billet. After the billet extrusion,

the billet is drilled in its centre and a Tin rod is inserted. In a second step, 19 sub-element rods are assembled together with a tantalum barrier into a copper tube to constitute the strand. To complete the process, the strand is drawn down to the proper diameter and plated with a chromium layer [16]. This strand is shown in the previous *Tcs* section in *Figure 2.1*.

More than 8000 low temperature tests, including critical current, Residual Resistivity Ratio (RRR), copper-to-non-copper volume ratio and hysteresis loss measurements must be performed along the strand production [16].

Each TF cable has groups of two superconductor strands with one copper strand which comes in groups of three. These are put together in groups of five and these last again in groups of five. This is known by the following structure $(2sc + 1Cu) \times 3 \times 5 \times 5$. At these wires is added a core of $(3Cu) \times 4$ in the centre of each sub-cable and there are six sub-cables which complete the whole cable structure. *Figure 3.3* shows a zoomed-in image of the CICC wires where is easy to appreciate the differences between the strands and the gaps where the helium flows and the six sub-cables in petal distribution around the central hole.



Figure 3. 3 CICC from ITER Newslines 278 (iter.org).

Each sub-cable has its own wrap to separate it from the others. These sub-cables have a specific manufacturing process which has to be followed very carefully, because the homogeneous distribution of the strands is very important at the time of operation with external magnetic forces and homogeneous current distribution. Thanks to the twisted transposed structure necessary to avoid the AC losses that was mentioned, a homogeneous cooling is carried along the conductors. The first step in the cabling manufacturing for TF is only for the torsion of the strands, and it has a high cost and takes a long in time because superconductors require extreme quality control procedures to ensure that the filaments are not broken.

Two fundamental issues must be commented on in the cabling process, the cable twist pitch sequence control and the void fraction control inside the CICC. Twist pitches are selected in the layout phase with the objective to minimize the AC losses and to have a cable design that does not degrade during electromagnetic load cycling. However, the twist pitches affect the rigidity, dimensions and regularity of each sub-cable. For this reason, all production parameters must be adapted to each specific case. For example, the parameter set introduced in the machine changes when it is operating with three copper wires as opposed to when it is operating with two superconducting strands and one copper wire, because of different mechanical properties of copper wire and superconducting strand despite the same strand/wire diameter.

Cabling is a very complex task, as it has to provide the expected shape and dimensions in a regular and compact structure while controlling the possible strand damage and excessive deformations. For these reasons cabling assembly must be carried out keeping the outer friction as low as possible by proper material choice. Large forces required for compaction should be realised by a synchronized system which carefully shapes and rolls cables while a pulling system introduces it in the conduit. It is showed in *Figure 3.4*.



Figure 3.4 final assembly for ITER TF cable [15].

A crucial step in the cable manufacturing is the compaction of the cable at the final stage. That has a strong impact in the jacketing process and requires a target void fraction of 29.7% in ITER TF coils. In this step, the strands suffer the most severe deformations due to the precision needed to set the target void fraction [15].

In ITER TF CICC it is very important that the cable steel wrapping maintain a round shape. The wrap tension should be as large as possible for the mechanical properties of the wrap. The wrap thickness is 0.1 mm for sub-cables and for the total cable wrapping. Tension is monitored by a load cell and a feedback circuit maintains it at the pre-set value through a motorized

brake. At the final step of cabling the cable is tested, including the destructive examination of a sample taken of the production length to verify all components and cable layout details. The different sub parts of the cable including billet of a Sn diffusion strand and a Nb₃Sn filament are shown in *Figure 3.5*.

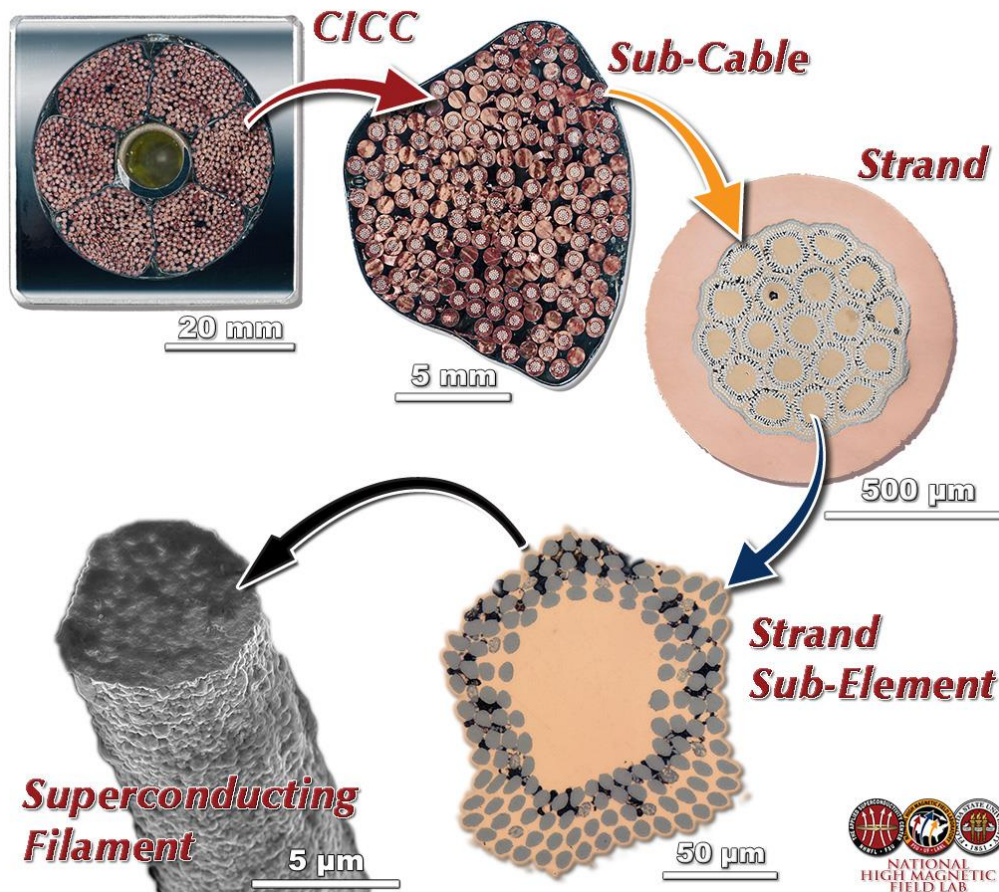


Figure 3. 5 TF CICC composition to The Nb₃Sn filaments. Figure from Florida State University.

The jacket is made of a 316LN stainless steel. The last step to manufacture the CICC is the jacketing. This process takes place in a special hangar, where the first step is to join round tubes of proper thickness and dimensions together by butt-welding, to obtain the required straight unit length of the order of few hundred meters. This process is done automatically by a welding machine. The process parameters like current, time or tension must be adapted to the specific production. Otherwise the mechanical properties cannot be guaranteed [15].

To check and control the jacketing process, it is examined with x-rays discarding possible imperfections or deformations in the structure and some tests are made to verify possible helium leak points in each weld.

The cable is inserted into the jacket by the traditional pull-through approach, using a special pulling rope connected to the head of the cable by another special tool. An insertion gap is required in a defined value to not exceed the maximum pulling force that strands can resist before suffering a deformation. It varies depending the size and length of the cable. No lubricant, which would definitely ease the insertion process, is usually admitted because it is

thought to introduce dirtiness and some of the oil components could react with the jacket during heat treatment.

After this, to fit perfectly with the conduit, the ITER TF conductor is submitted to a round-to-round compaction. The thickness of the conduit does not change but the outer diameter goes from 48 mm to 43.7 mm by compression made with a compaction machine which consists of three pairs of rollers, whose axes are on three different planes perpendicular to the conductor axis. It is possible to use more pairs of rollers but it depends on small changes in the final dimensions. The cable is slightly compressed and achieves the requested void fraction. After jacketing the CICC is insulated with a layer of glass fabric for electric insulation.

3.1.2 Topical issues

Two topical issues are present in the CICC for TF coils, one is the irreversible degradation in Nb_3Sn CICC [17]. Transverse mechanic load due to the Lorentz forces produce a stress in the cable inside the jacket. After cyclic load experiments in CICC and tests in extracted strands from the loaded cables, a degradation in the superconductor performance was revealed. Micrographic investigations indicate that this irreversible degradation is produced by the filaments damage (radical cracks). Only by filling the free space inside the cable with solder, avoiding strand bending, can be prevented the irreversible degradation. However, that is not feasible because that space is necessary for the coolant flow.

The second issue is the change of length upon the heat treatment for Nb_3Sn CICC. The TF coils conductors are wound to fit in the D-shape pancake (*Figure 3.6*), and then are placed in a furnace for the heat treatment of the superconductor.



Figure 3. 6 ITER TF pancake from ASC (La Spezia, IT).

This process produces changes in the CICC length. In a TF coil conductor with about 10 m in straight section, the change of length can be close to 10mm and must be predicted with precision and considering the geometry of the winding. The wide range of change of length

does not affect the conductor performance but is a serious issue for the assembly of the TF windings in the radial plates disposed along the coil.

3.1.3 World production

Several countries have been manufacturing different parts of the CICC around the world. The quality and the technical properties of the materials and processes are essential to produce the superconductors for ITER. The conductors have already achieved some standards after several experiments testing the conductor's performance. Some coils are already available for their installation in the ITER tokamak.

For the strands, there are many suppliers around the world but only two main models. Two examples of suppliers in the two kinds of process are Bruker EAS (Germany) for the bronze route and OST (USA) for the internal tin diffusion. Both have a slow process that takes years for the correct production and manufacturing. After the strands are produced and tested by the suppliers, strands are delivered to the cabling companies which are in the ITER project [15].

ITER TF cables are assembled and manufactured in points distributed around the world, *Table 3.1* have a list of the manufacturers over the world.

Company	Country	Parts
TRATOS	Cavi, Italy	TF and PF coils
Nexans Korea	Korea	TF coils
New England Wire Technologies	New Hampshire, USA	TF coils
Boasheng	China	TF coils
Hitachi Cable	Japan	TF coils
VNIKP	Podolsk, Russia	TF and PF coils

Table 3. 1 Different ITER TF cable suppliers [12].

The ITER organization tries to distribute the manufacturing of the pieces among its participants and for that reason the production is very varied and the conductors are manufactured by different companies for each stage of the fabrication in different locations. For the jacketing process, the manufacture is distributed among Japan at NSE, where also CS coils are jacketed, China at ASSIP, Russia at IHEP, USA at HPM and Europe at Criotec, where some work is subcontracted to Korea [12].

3.2 Rectangular conductors for fusion magnets

The round cross-section cables from ITER TF conductors are easier to manufacture but the winding of CICC in a coil is a very complex process. Between these conductors there cannot be any gap or void region due to the enormous magnetic Lorentz forces. The space between conductors must be filled. In case of ITER TF coils, steel radial plates maintain the conductors at their position. Radial plates are show in *Figure 3.7*.

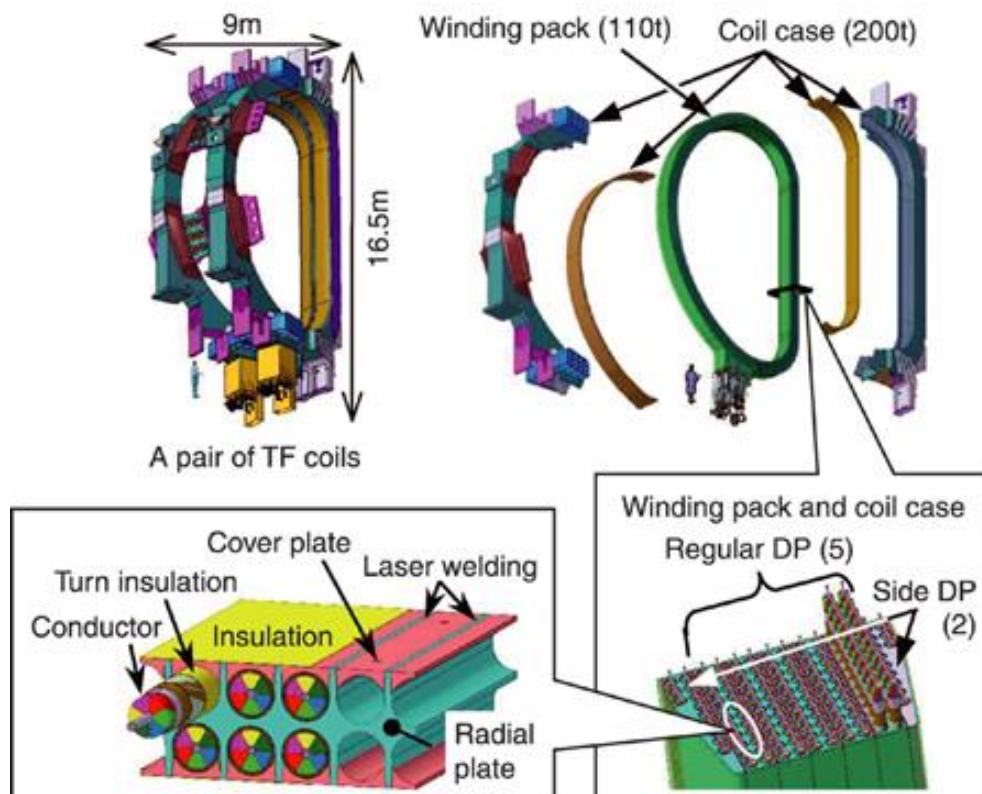


Figure 3. 7 TF coil structure in ITER. Japan Atomic Energy Agency (JAEA).

Rectangular conductors are more demanding from the point of view of the manufacturing process, but they are relatively easy to wind in coils without radial plates. Another advantage is that rectangular conductors tested for DEMO are less prone to “cyclic load degradation” than circular ITER TF conductors. The main criteria for DEMO is to maintain the temperature margin between the operating temperature and the T_{cs} at a value of at least 1.5K, and the hot spot temperature below 150K. This hot spot is the point where the temperature tends to be higher due to the higher external magnetic field.

3.2.1 SPC conductors

First rectangular conductors that are going to be described are the SPC conductors for DEMO (DEMONstration Power Station). This is a future project, which will be based on experience

gained with ITER. It would be the first fusion power station generating electricity similar to what a commercial power plant would do.

The Swiss Plasma Center (SPC) has designed, manufactured and tested prototype sections of Nb₃Sn conductors for DEMO TF coils. The conductor designed has a rectangular cross-section based on a double layer of Nb₃Sn winding [18]. The cable has six Nb₃Sn conductor grades, which provide a homogeneous temperature margin over the winding-pack cross-section and minimize the production costs.

These conductors are designed to work at 82kA of current and 13T of magnetic field. Conductors are composed by 17 sub-cables, where each sub-cable is constituted by one copper core wire surrounded of 18 superconductor strands. The cable is surrounded by 48 Cr plated copper wires at its perimeter. It has a steel jacket to minimize the thermal strain [18]. The SPC conductor scheme is illustrated in *Figure 3.8*.

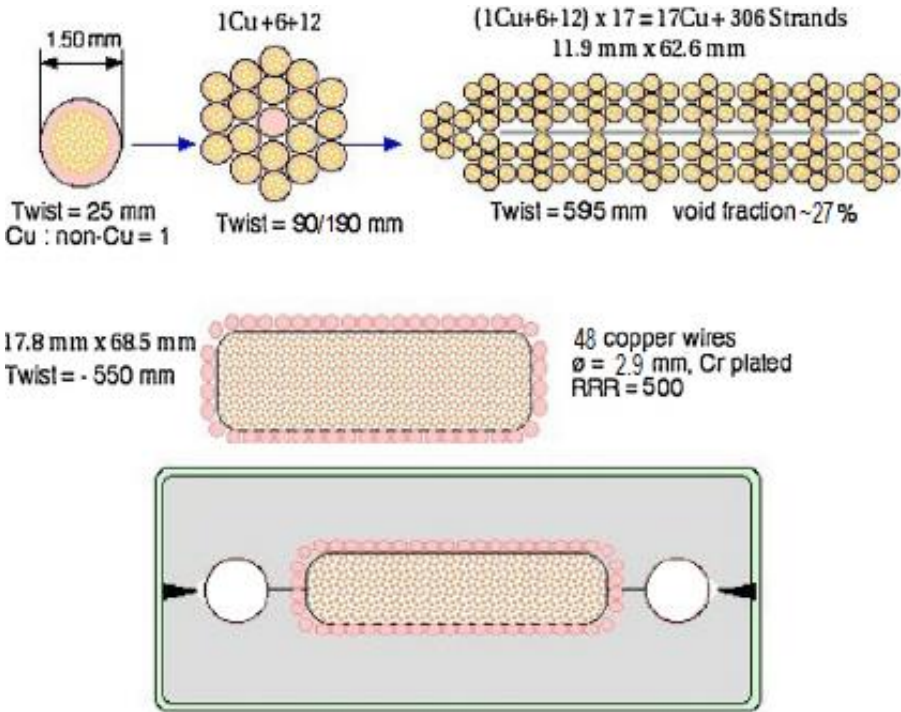


Figure 3. 8 SPC conductor specifications [18].

The SPC DEMO conductors are manufactured with a react-and-wind technique, in which the conductor is heat-treated before winding into a coil. The react-and-wind technology is not suitable for coils with small bending diameters, as the fragile superconducting filaments might break during the coil winding process, and consequently the superconducting properties of the coil would be degraded. In DEMO TF coils, this should not be a big problem, as the coils are very large and only small bending of conductors is necessary. The big advantage of the react-and-wind technology is lower strain in the Nb₃Sn strands, which leads to higher critical current for the same amount of superconductor compared to the wind-and-react technology chosen by ITER.

The cabling manufacture of the conductor prototype was produced in TRATOS (Cavi, Italy). The process has two stranders in series, the first one for the superconducting flat cable and the second one for the external copper wires revolved in the opposite direction. The compaction is obtained by passive rollers. A smaller number of copper wires in the manufacturing process compared to the conductor design led to gaps in the external layer between the wires.

The steel sections used for jacketing of the flat conductor were manufactured by milling. They were used to set up the longitudinal laser welding of the jacket (conduit) around the cable. The geometry of the side channels was optimised to allow an ultra-sound quality control of the welding. Two stationary fibre optic laser sources were used simultaneously for the longitudinal welding at Montanstahl, Switzerland.

3.2.2 ENEA conductors

ENEA is an Italian agency which is involved in development of new technologies. ENEA conductor layout is based on the same winding pack as SPC conductors. The dimensions of the cable are 69.4x25.8, its strands have diameter of 1 mm, and the cable void fraction is 25%. This design has a CICC structure with one or two central channels. It is another conductor design that could be used in the DEMO TF coils [19].

In the one channel design, the strand bundle is assembled as a five-stage cable around a perforated tube. The jacketing process is similar to the CICC for ITER layout by pull through technique into a circular conduit, with subsequent rolling of the conductor to a rectangular shape during the compaction. A layer of soft copper wires surrounds the superconductor strands to smooth the loads during the manufacturing process. Conduit thickness is 8.7 mm with rounded corners. An example of ENEA two-channel conductor is shown in *Figure 3.9*.

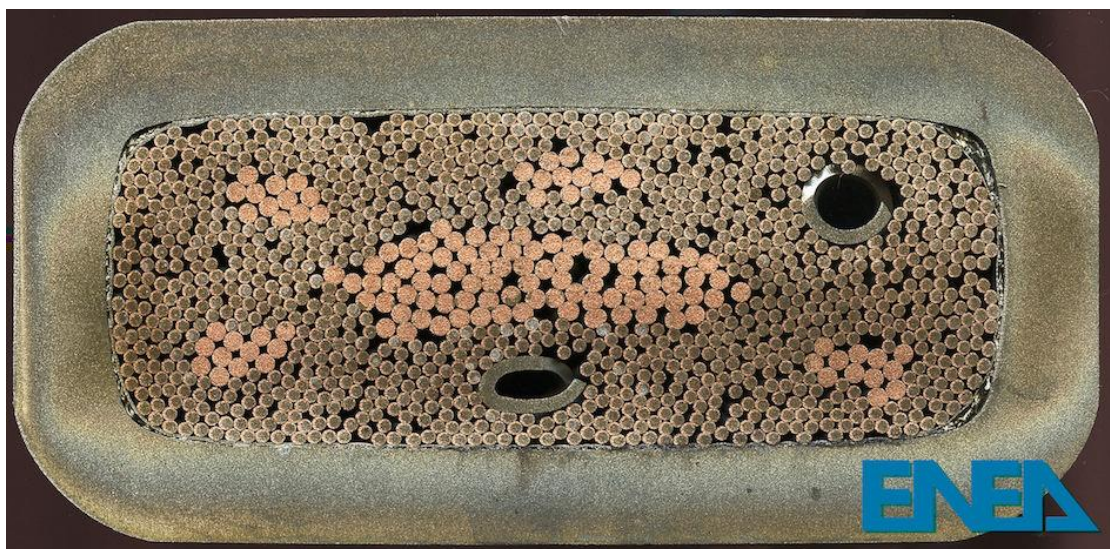


Figure 3.9 ENEA DEMO conductor cross-section. ENEA.

This type of conductors maintains the ITER approach of wind-and-react method, but it has the same coil winding as the SPC prototype, namely the double layer disposition. It is assumed

that the thermal strain in the React & Wind (RW) design is $\epsilon_{th}=-0.3\%$, and in the wind-and-react $\epsilon_{th}=-0.5\%$.

The winding pack in the WR method has less steel compared to RW due to the larger superconductor cross-section and the larger helium cross-section for the Nb₃Sn Double Layers as it is shown in *Table 3.2*. These design characteristics are due to the higher thermal strain and higher void fractions. The void fraction in ENEA conductors is by 8% larger than SPC [19].

Parameter	RW CRPP	WR ENEA
No. of turns	24	28
Superc. (mm ²)	275.9	353.4
Steel (mm ²)	3271	1802

Table 3. 2 steel and superconductor section in the Double Layer 1 of DEMO designs [20].

The new rectangular conductors are already in prototype state and one of the most important tests to analyse the performance of magnetic conductors for fusion is the thermal-hydraulic analysis which includes three studies.

The first one is the hydraulic analysis, which calculates the mass flow rates at the expected value of pressure drop in the coil. The second one is the heat removal analysis, which studies the helium temperature profiles in each conductor by means of heat deposition rate. The last one is the calculation of the temperature and pressure evolution during a quench. This one has two scenarios to be analysed: the extreme one for maximum pressure and the more realistic one to predict the maximum temperature (the so-called “hot-spot” temperature) [21].

3.2.3 CEA conductors

The French Alternative Energies and Atomic Energy Commission (CEA) develops another possible DEMO conductor. The CEA proposal design is based on ITER experience. The conductor has a central steel channel for cooling the superconductors with the same structure as the ITER CICC.

CEA conductors, as ITER layout, has a Cable-In-Conduit structure. CEA also keeps the pancake winding employed at ITER, but the main difference is that this conductor design has a square cross-section with 1392 Nb₃Sn superconductor strands and 294 pure copper strands [22]. The conductor has a nominal current of 95.5kA providing an effective magnetic field of 13.09T. It has a *T_c* of 6.25K with a 29% void fraction. The structure of CEA conductor is shown in *Figure 3.10*.

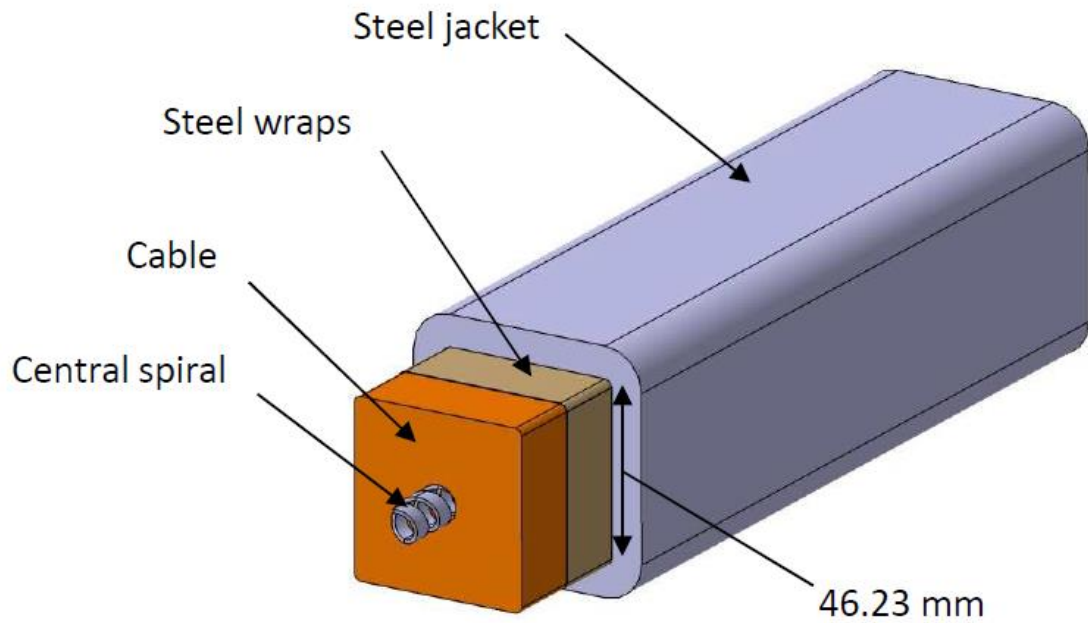


Figure 3. 10 CEA conductor proposal [22].

The temperature margin predicted for the CEA conductors is 1.5K in the weakest point for the case of uncooled coil casing. If cooling channels embedded into the coil casing are considered, the temperature margin grows up to 1.60K at the end of the high magnetic field location. For a quench analysis considering one of the most realistic scenarios the hot spot temperature reaches 148K, which complies with the requirement to stay under the 150K limit.

CHAPTER 4

Conductors assessment



ITER TF CICC, ITER Newslines 284.

Jose Manuel Trueba Cutillas

4.1 Magnetic field assessment in round and rectangular conductors

To estimate the magnetic field in fusion conductors, one has to add up two field components – the self-field of the given conductor and the external magnetic field induced by other conductors in the winding pack and by the other coils.

4.1.1 Magnetic field in circular conductor

In the calculation of the self magnetic field for conductors with round cross-section, the first step is to define the equations which allows us to calculate the field distribution in the conductor. I use Ampere's law to find the field inside a long straight wire of radius R carrying a current I . Assuming that the wire has a uniform current per unit area, we define the J (current density) as:

$$J = I/\pi R^2 \quad (15)$$

We have to distinguish two zones of magnetic field - inside the conductor and outside. The variable describing position inside of the wire is denoted as r , and can vary between 0 and R . The magnetic field is constant along circular loops of r radius, just as it does outside of the wire. By applying Ampere's law, we get:

$$\int B \cdot ds = 2\pi r B = \mu_0 I_{enclosed} \quad (16)$$

The current enclosed in the circular loop is the current per unit area multiplied by the area of the loop:

$$I_{enc} = J\pi r^2 = I \frac{r^2}{R^2} \quad (17)$$

Therefore, we find a new equation for the magnetic field in a circular loop:

$$2\pi r B = \mu_0 I \frac{r^2}{R^2} \quad (18)$$

From the last equation, we obtain the final equation for the magnetic field at radius r inside of the wire of total radius R :

$$B = \mu_0 I \frac{r}{2\pi R^2} \quad (19)$$

Inside the wire the magnetic field is proportional to r , while outside it's proportional to $1/r$.

When the formula is defined, the next step is to implement the equations and input parameters in a program to calculate the magnetic field. The first values to introduce are the constants. The first of them is the vacuum permeability:

$$\mu_0 = 4\pi 10^{-7} \text{ V} \cdot \text{s} / \text{A} \cdot \text{m} \quad (20)$$

Another parameter is the radius of the conductor. For this simulation, we only count with the superconducting area, where the current is passing through, and the corresponding radius is 2 cm, in the case of ITER conductors. The calculation of the field is later done over the cable cross-section using the Cartesian coordinates x and y to calculate the magnetic field in the transverse section. In this first part, the program only accepts values inside the cable.

The total current which pass through the cable is defined as a variable input. ITER TF conductor, which has the same cable cross section as assumed here, is designed for the operating current of 68 kA.

The next step is to calculate the x and y components of the magnetic self-field as each x and y components has a different module. In the selected point, the components are obtained substituting in the magnetic field formula the radius r by x in B_x component and by y in the B_y component.

Depending of the current direction we have to put the current in positive or negative value to obtain the gradient components in the point. When the current I has a negative value the direction of the vectors also changes to its opposite direction. For example, with an input values of $x=13\text{mm}$, $y=-7\text{mm}$ and $I=68\text{kA}$ we obtain a final self-field of $[0.238\text{T}, 0.442\text{T}]$ in x and y components.

In the next step, the average magnetic field over the area of the cable cross section has to be calculated. We integrate the magnetic field over the cable area, and then divide it by the cable area. The area of interest is a square shape; to enclose the full cable, the limits go from -20 mm to 20 mm in x and y axis. For illustration, the self-field in a quarter of the cable from 0 to 20 mm in x and from 0 to 20 mm in y is plotted in *Figure 4.1*. In this case the average magnetic field is 0.4533 T for 68 kA currents.

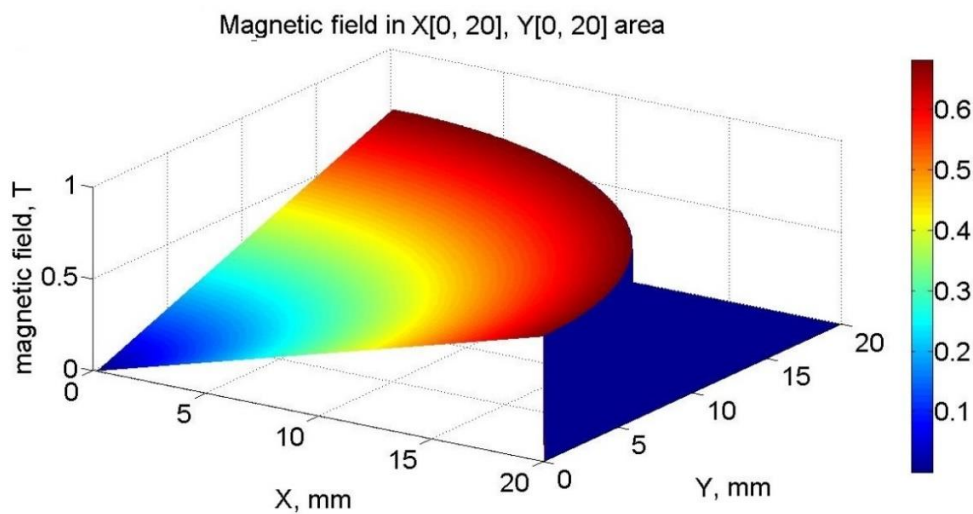


Figure 4. 1 Area plot of the magnetic self-field in a portion of the conductor.

Once the area is defined, the first step is make two vectors with the x and y lengths divided in several points from the minimum x and y values to the maximum ones. In our case we define values every 0.0404 mm.

When the x and y vectors are defined with all the points for x and y lengths, it is converted to meters and the size of the vectors is measured in order to generate one matrix for the radius values and another for the final magnetic field.

The matrix generated with x and y dimensions of the x and y sizes is composed by ones (as seed value) at the beginning, after it is generated each row of the matrix is substituted by the result of adding the entire squared x vector by the corresponding squared value of y for each row in a loop until all the squared radius are defined in the matrix. Finally, to obtain the radius values, the matrix is operated into a square root in all its values.

Once we have the matrix composed by the different radius to the centre of the cable in the origin of the axis, it is possible calculate the magnetic field operating each matrix radius value in the magnetic field equation (19).

All the values are checked to ensure that the radius is not larger than the limit of the cable for two centimetres, only when the radius is lower it will be operated and substituted in their corresponding magnetic field matrix position to consider only the values for the round conductor.

The magnetic field matrix has the same dimensions of the radius matrix but it is generated as a zeros matrix which will be filled only with the magnetic field values. To make the average of the field only the points inside the cable are accounted neglecting the zero values. The complete magnetic shelf-field for round conductor with 68kA current is plot in *Figure 4.2*.

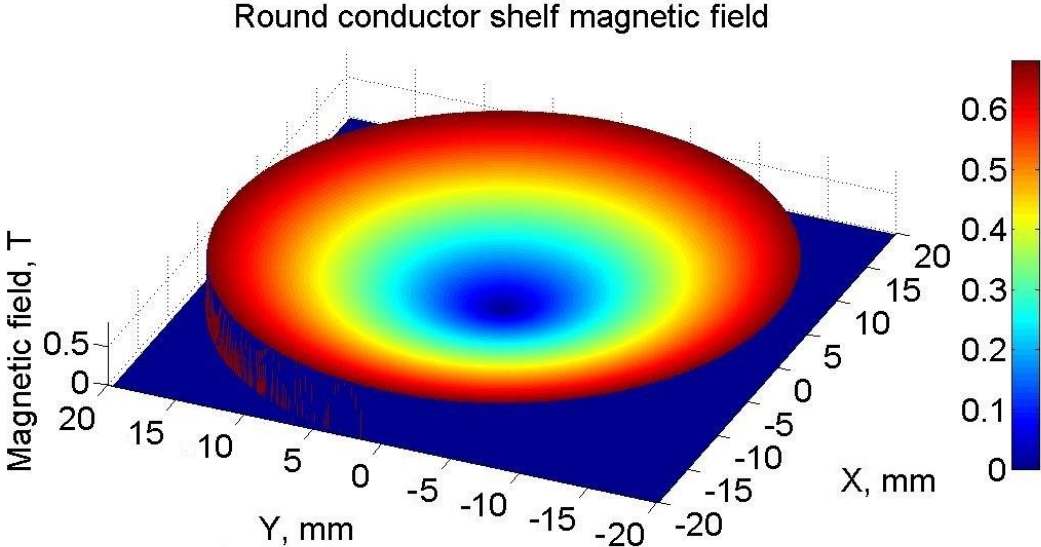


Figure 4. 2 Round conductor shelf-field.

For the simulation of the self-magnetic field in the whole conductor we use the radius of 20mm with a current of 68kA. The obtained average field value is 0.4533 T. The average field has been calculated among 192,433 points, always inside the cable cross-section.

When the conductors are transporting current in the coils of ITER or any other tokamak, the magnetic field generated by every conductor affects the other conductors. This process generates a background magnetic field sensed by individual cables. A 10 T background field is a typical value present in the ITER TF coil. We add the external background field to the y component in transversal direction to the cable.

This means that on the cable axis, where self-field is zero, only the external field is present, and equals to 10 T. The gradient of the self-field describes circles in counter clockwise when the current has a positive sense. In this graphics, the positive sense of the current respect to the surface plane is the positive direction of the z axis. This means that when the background field is added together with the self-field, in one half of the conductor the total field is larger than the background field, and in the other half it is smaller than the background field. The external field in the conductor cross section is shown in *Figure 4.3*.

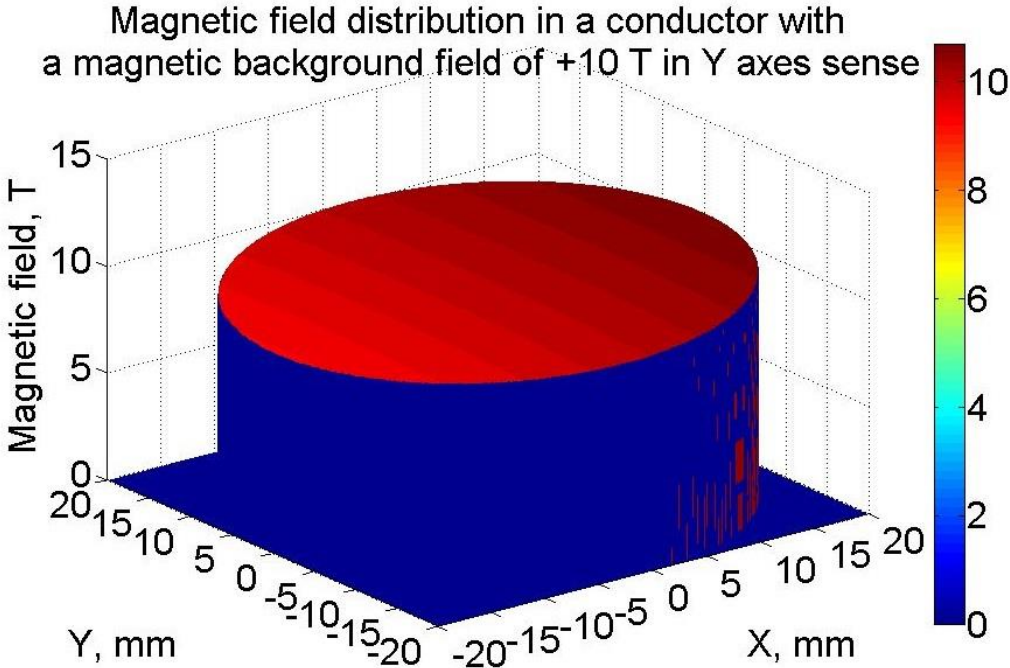


Figure 4. 3 Magnetic field in round conductor with background field plus its self-field.

The average magnetic field calculated among 769,853 points is 10.0058 T. The maximum value of 10.68 T is observed at $x=20\text{mm}$ and $y=0$, while the minimum value of 9.32 T is observed at $x=-20\text{mm}$ and $y=0$. These values correspond to the 68kA current flowing through the conductor.

It can be observed that the half of conductor with higher magnetic field compensates the other half, where the self-field has the opposite orientation that the external background field. However, the average field is not exactly 10 T and that is because at totally perpendicular

vectors of SF with BF the final result in a vector module higher than 10 T, in the border point $x=0, y=-20$, the B_x and B_y are 0.68 T and 10 T respectively. This means a module of 10.0231 in that point, and in the opposite edge of the conductor the B_x component is negative but the module is exactly the same value. That is one clear reason because the average field is slightly higher than the BF.

4.1.2 Magnetic field in rectangular conductor

Later in the thesis we will compare circular and rectangular conductors. For the sake of comparison, we will consider rectangular conductors with the same area as the round conductors. The equations used to calculate the magnetic field of rectangular conductor is more sophisticated than the equation for the round conductor.

For a current I in the rectangular bar, the current density is $I/4ab$, where “ a ” is the distance from centre of the rectangle to the middle point of one side, and “ b ” is the distance from the centre to the middle point of the contiguous side of the rectangle. With this definition, the lengths of the rectangle sides are $2a$ and $2b$.

The first step to calculate the magnetic field in two dimensions x and y with a finite cross-section is to define the vector potential of line current. Beginning with the complex potential function [23], the vector function is identical with the real part of flux function component of the complex function, i.e. for the line current i :

$$A = \frac{\mu_0}{2\pi} i \log r \quad (21)$$

where r is the distance from the conductor to the point and A , the dimensional field. A for the line current is identical with A outside the conductor with finite round cross-section:

$$A = \frac{\mu_0}{2} J a^2 \log r \quad (22)$$

here J is the current density and a is the radius of the conductor. When the rectangular cross-section is examined and the current density is considered for the rectangular case and the equation is integrated over the rectangular cross section, the following equation is obtained:

$$A = \frac{I\mu_0}{8\pi ab} \int_{-a}^a \int_{-b}^b \log r \, dx' dy' \quad (23)$$

here the vector potential is calculated at any point (x, y) , distance r from a filament is represented by coordinates (x', y') . Expressing r in x and y coordinates we have:

$$A = \frac{I\mu_0}{16\pi ab} \int_{-a}^a \int_{-b}^b \frac{1}{2} \log[(x' - x)^2 + (y' - y)^2] \, dx' dy' \quad (24)$$

The field components H_x and H_y in function of the flux values represented by A are given by:

$$H_x = \frac{1}{\mu_0} \frac{\partial A}{\partial y} \quad H_y = -\frac{1}{\mu_0} \frac{\partial A}{\partial x} \quad (25)(26)$$

The resulting expressions can be simplified by expressing them in terms of the distances from a point in the field to the four corners of the section, where these distances are r_1 , r_2 , r_3 and r_4 , and using the angles ϑ_1 , ϑ_2 , ϑ_3 and ϑ_4 defined as angles between the lines to the corners and lines parallel to the x-axis, see Figure 5.4. This gives:

$$H_x = \frac{I}{8\pi ab} \left[(y+b)(\theta_1 - \theta_2) - (y-b)(\theta_4 - \theta_3) + (x+a) \log \frac{r_2}{r_3} - (x-a) \log \frac{r_1}{r_4} \right] \quad (27)$$

$$H_y = \frac{I}{8\pi ab} \left[(x+a)(\theta_2 - \theta_3) - (x-a)(\theta_1 - \theta_4) + (y+b) \log \frac{r_2}{r_1} - (y-b) \log \frac{r_3}{r_4} \right] \quad (28)$$

The integration of the equation 24 to determine this results is described in annex [C]. To illustrate the distances and angles I made a schematic representation of these variables in Figure 4.4:

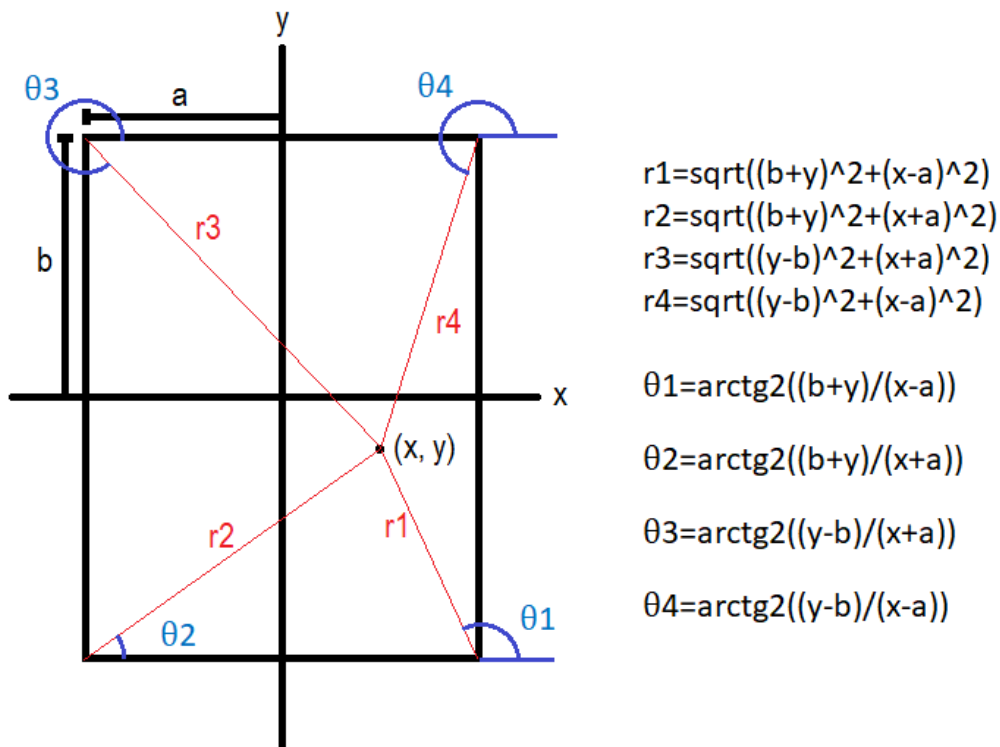


Figure 4. 4 Rectangular scheme about distances and angles.

Through the magnetic field general formula which relates H with B using the vacuum permeability we find that:

$$B_x = \mu_0 H_x \quad B_y = \mu_0 H_y \quad (29)(30)$$

With these parameters defined, the magnetic field inside the conductor can be calculated by a program with the two dimension components. If we set a given x length, the y length of the conductor is automatically calculated such that the area of the rectangular conductor is equal to the area of the round cable with 20 mm radius. For example, if we set $x=60$ mm, the y is computed to be $y=20.944$ mm and the values of x and y range between $[-30, 30]$ and $[-10.472, 10.472]$ respectively.

The program identifies a and b as half of the sides lengths, and it calculates the self-magnetic field at any requested coordinate using the equations described above. For the previous example the B_x and B_y components for $x=30$ mm and $y=0$ mm are 0 and 0.6235 T, respectively.

Following the same approach to calculate the magnetic field at one point I developed a program which generates a matrix of zeros with dimensions from $-a$ to a in the x dimension and $-b$ to b in the y dimension. Each point coordinates are introduced in a loop which calculates all the radius and angles for each point and calculate the modular magnetic field in the corresponding point of the cross-section to finally substitute it in the same position of the zeros matrix previously generated. The self-field plot is displayed in *Figure 4.5* for the described dimensions with an effective current of 68kA.

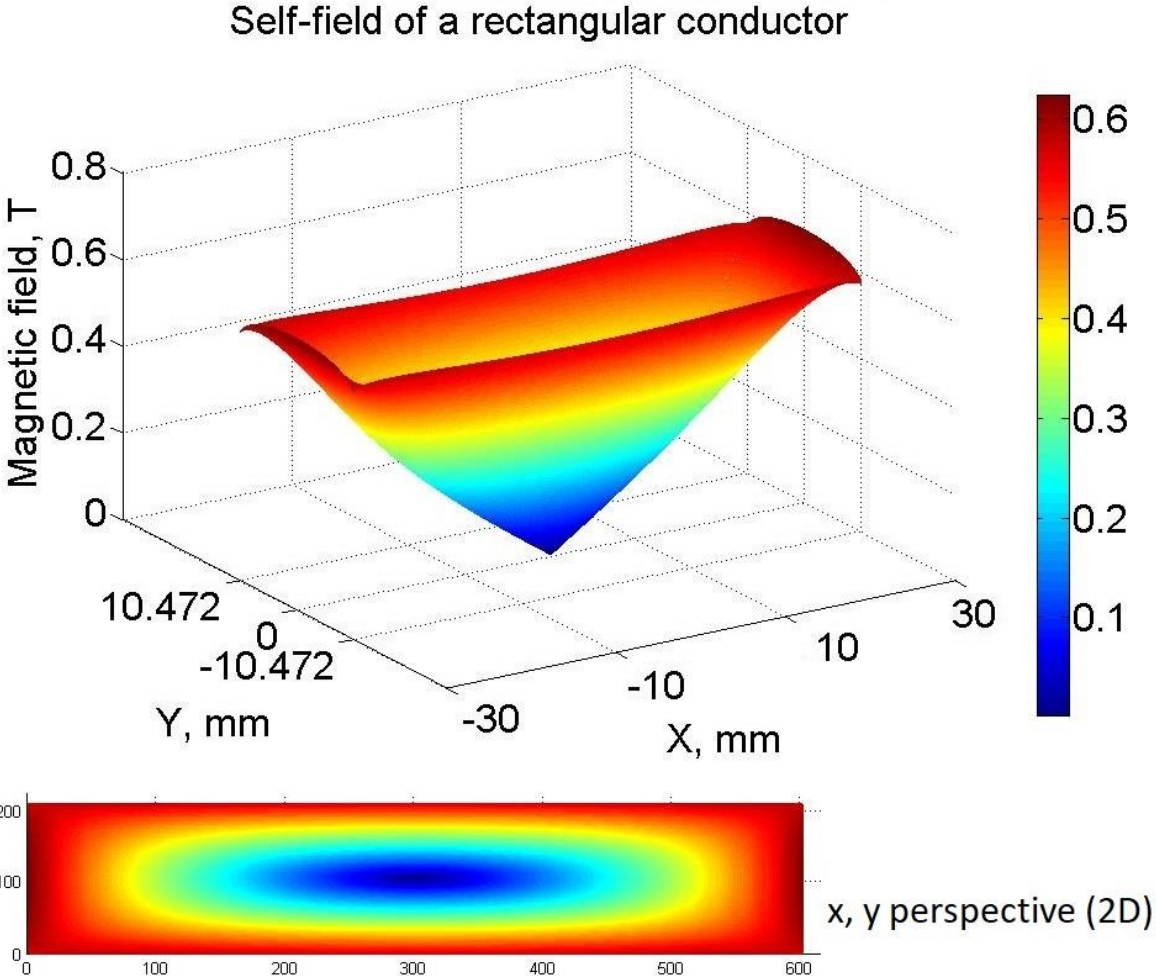


Figure 4. 5 Self magnetic field in rectangular conductor 60mmx20.944mm and 2D perspective in x, y plane.

In this case, the calculated average magnetic field is 0.3898 T. The averaging was done over 126,210 points in the rectangular area. The maximum field value is reached in the middle of both y edges, and its value is 0.6235 T, while the minimum value of 0 T is found in the centre of the rectangular cross-section, the blue peak of *Figure 4.5*.

In case of an external background field, the program sums up background field and self-field. As an example, for the background magnetic field of 10 T introduced in the y direction is graphically illustrated in *Figure 4.6*.

In this case, the average magnetic field is 10.0043 T, the maximum field of 10.6235 T is found in the middle of the y edge, while at the other side of the conductor the field gets down to the minimum of 9.3765 T.

As in the case of the round conductor, the self-field in the conductor centre is zero, and only the external background field is present.

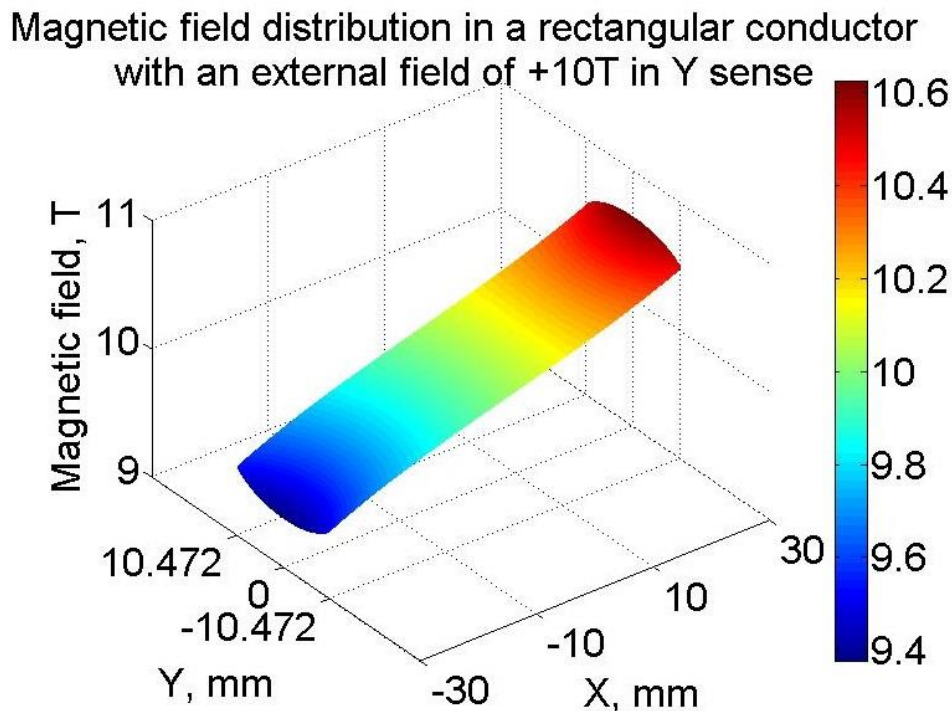


Figure 4. 6 Magnetic field distribution in a rectangular conductor with a 10 T external field pointing in the Y direction.

Comparing self-field with self-field + background field we can observe how the distribution completely changes. The self-field vectors which share the sense of the external field produce a high concentration in the magnetic field distribution while those which are in opposite direction cause the lower fields in the distribution.

4.2 Critical current density, J_c for a known magnetic field in superconductors

When the magnetic field is calculated for a given position within the superconductor defined by the x and y coordinates, we can calculate the local critical current density at that point for the superconductor cable. The equations to calculate J_c were defined previously in Chapter 2. The EUTF4 constants (Table 2.2) are used to calculate the critical current density in the examples of round and rectangular conductor. Once the matrix for the magnetic self-field values is obtained we can calculate the values in the critical current density equation with the help of MATLAB.

4.2.1 Critical current density in round conductor

The program written in MATLAB calculates the matrix of the J_c values over the cross section of the round conductor according to the parameters requested by the user. The nominal radius of the round conductor is 20 mm, following the ITER TF conductor.

The program inputs are the x and y components of the background field, the operating current in the cable, the temperature of the conductor and the strain.

In the following examples, we consider the following common values for this conductor similar to ITER TF conductor. These values are 0 T for B_x , 0 T for B_y , 68 kA for I , 4.2 K as the temperature in the conductor and -0.5 % for the strain due to the difference in the thermal contraction of the superconducting cable and steel jacket.

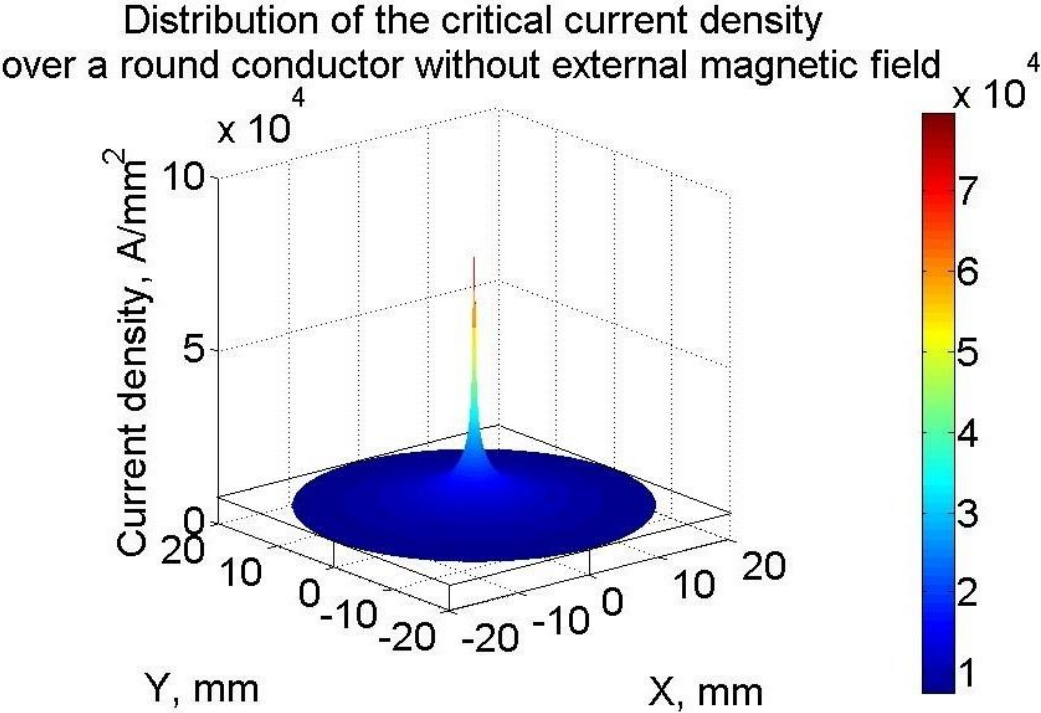


Figure 4. 7 J_c distribution in a round superconductor in magnetic self-field.

The first simulation is plotted for the same magnetic self-field as in the section 4.1. When we have all the input parameters defined, the first step is to calculate the values which are constant for the whole superconductor cross section, those that do not depend on the magnetic field as the critical temperature, the critical magnetic field, the strain function and the reduced temperature.

After we have these constant values calculated with the inputs as temperature or strain, we calculate the reduced magnetic field with a MATLAB function which allows to compute a matrix point by point. Then we calculate the current density at each point of the reduced field matrix, obtaining the matrix for J_c distribution over the cable cross-section, as shown in *Figure 4.7*.

It can be observed that for very low values of magnetic field the critical current density increases steeply. When there is no magnetic field, as is the case in the central point, the critical current density cannot be calculated. Because the scaling law described in Chapter 1 (equation 6) show an infinite value for J_c when B is zero.

The average critical current density, if there is zero external magnetic field in the conductor, is $9,425.1 \text{ A/mm}^2$. Internally in the program, the integration is performed over 785,346 points distributed homogeneously over the conductor cross-section. The maximum value at the point closest to the centre is $79,464 \text{ A/mm}^2$, while the lowest value at the edge of the section is $7,504.8 \text{ A/mm}^2$.

Despite the pronounced rise of the J_c in the central points, the average remains close to the lower value at the border of the conductor.

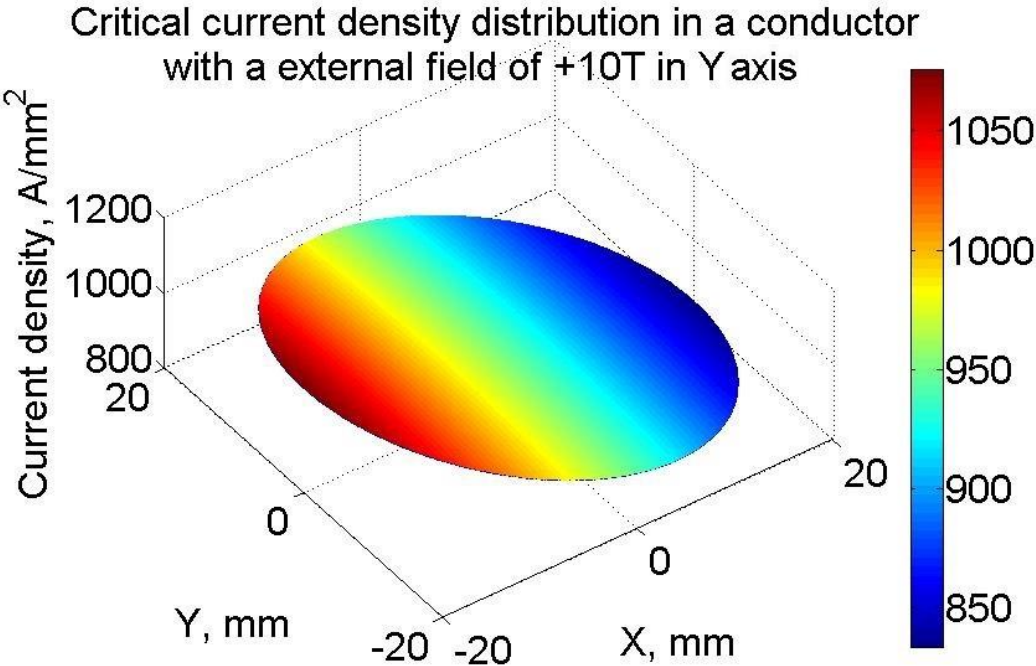


Figure 4. 8 J_c distribution when a background field of 10 T is present.

When the background field is considered, the J_c decreases. Its distribution over the section is shown in *Figure 4.8*.

We find an average current density of 948.6 A/mm^2 , which is significantly lower than in the case of the self-field. Here we find a uniform change of J_c in the inverse sense than the magnetic field. That means that where the field is minimum the J_c has its maximum value of 1075.4 A/mm^2 , while where the magnetic field is maximal the critical current density is minimal and equal to 833.4 A/mm^2 .

The critical current density is an important parameter characterising a superconductor in fusion magnets.

4.2.2 Critical current density in rectangular conductor

J_c for the rectangular conductor expresses the same behaviour in the central point of the conductor as the round cable. That is normal because the magnetic field distribution is similar in both conductors. We can observe the J_c distribution in self-field in *Figure 4.9*.

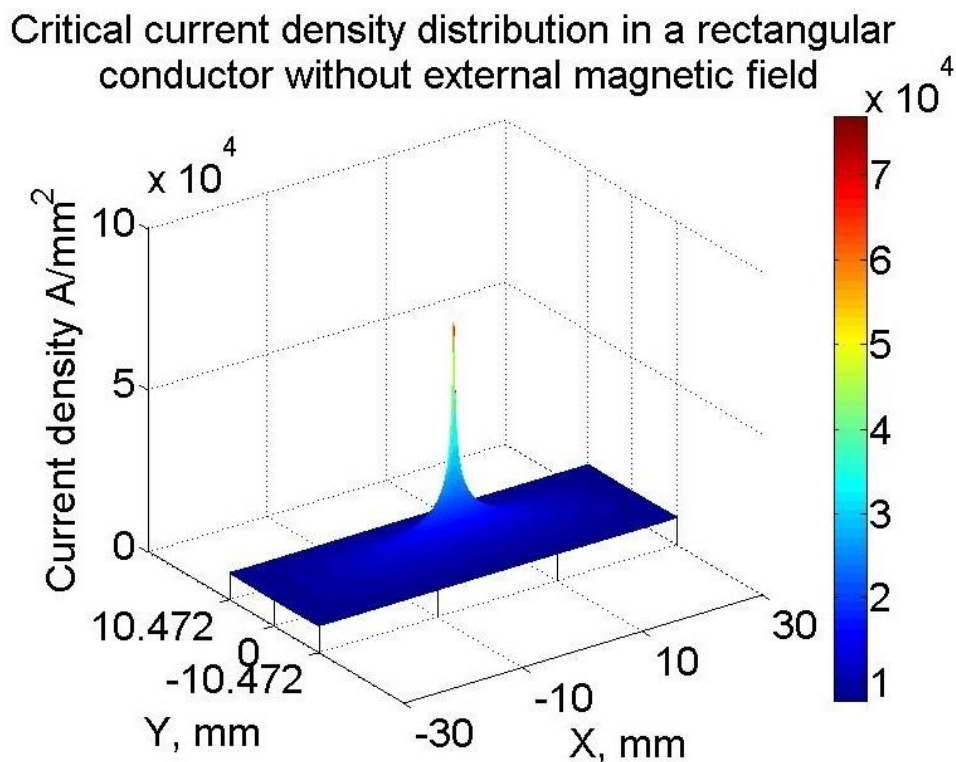


Figure 4. 9 J_c distribution in a rectangular conductor without background field.

Here we also find a huge different between the maximum J_c value of $76,667 \text{ A/mm}^2$ and the minimum of $7,789 \text{ A/mm}^2$ in the point of highest magnetic field. The average J_c in this conductor is $10,057 \text{ A/mm}^2$, which is higher than the average J_c in the round conductor in the same conditions.

It is interesting to see the J_c values without external field to compare it with the realistic conditions, where the conductor senses an external magnetic field produced by the other conductors. As we can see, the background field has an important influence in the critical current over the conductor. This is true not only for the final average J_c , but also for the smooth change of J_c across the cable cross section. In *Figure 4.10* we can observe a similar variation in the J_c distribution as for the round conductor when the external field is applied to the rectangular one.

Critical current density distribution in a rectangular conductor with an external field of +10T in the Y axis

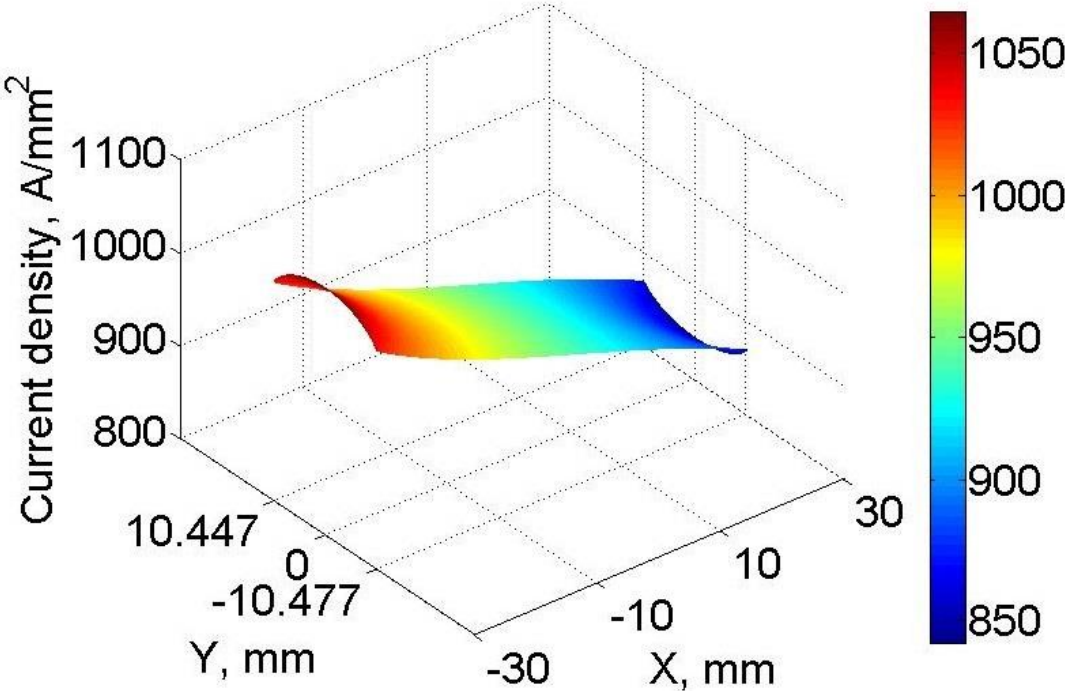


Figure 4. 10 J_c distribution in rectangular conductor with a background field of +10T in Y direction.

Here we can note that the surface does not have the flat form that was shown in *Figure 4.8* for the round conductor. This undulations in the distribution surface are produced by the magnetic field distribution for rectangular conductors in the same conditions. In *Figure 4.6* we find similar waves in the sides of the conductor but it was not so pronounced as in J_c because the values vary to a greater extent for the critical current distribution in relation with the magnetic field.

The critical current density, maximum, minimum and average values are respectively 1,064.3, 842.3 and 948.5 A/mm². This example shows a slightly minor average J_c than the round conductor, which is normal because both conductors have the same area and the same conditions of current, strain and temperature. Furthermore, the difference between the maximum and the minimum critical current density is much smaller for the rectangular conductor case.

4.3 Electric field distribution in round and rectangular superconductors

Electric field in the superconductors is described by the following equation:

$$\frac{E}{E_c} = \left(\frac{J}{J_c}\right)^n \quad (31)$$

Where E_c is the critical electric field in low temperature superconductors. This value is set as a constant in our analysis for all the points in the conductor and its value is:

$$E_c = 10\mu V/m \quad (32)$$

Electric field locally at any position of the superconductor can be calculated as:

$$E = E_c \left(\frac{J}{J_c}\right)^n \quad (33)$$

where the critical current density J_c was presented in the previous section, and the n-index defines how steeply the electric field increases with the current density. The typical n-index of individual strands are 20-50, the n-index of the whole conductor is typically reduced down to 6-20. The n-index usually slightly depends on J_c [24].

The other parameter present in this formula is J . This is the current density in the conductor that we assume constant over the conductor cross-section. This assumption is not strictly true, because there is a relatively low resistance between the strands, and therefore the current could in principle pass from one region with a higher electric field, through the copper, to a different region with a lower electric field.

However, due to the cable twisting, the current rebalancing is limited, and in the first approximation the assumption of homogenous current density is valid. We can calculate the current density by:

$$J = I/A \quad (34)$$

The units of J must be the same as the critical current density in this relation. J_c is calculated in A/mm^2 so for J we have an area of $237.6 mm^2$ for all conductors, and current of 68 kA. This area belongs only to the superconductors area because in normal operation, current only flows through the superconductors material. The corresponding resulting current density is $286.19 A/mm^2$.

We are going to employ the same values for strain, temperature, current, dimensions and background field as used in the previous sections with the new E_c constant. The n-index of 10 will be assumed for circular and rectangular conductors. This value belongs into the usual range of Nb_3Sn conductors.

4.3.1 Electric field in round conductor

In the first plot, the electric field over the round conductor is calculated by the relation described in the E field formula operating the J_c mesh point by point obtaining the *Figure 4.11*.

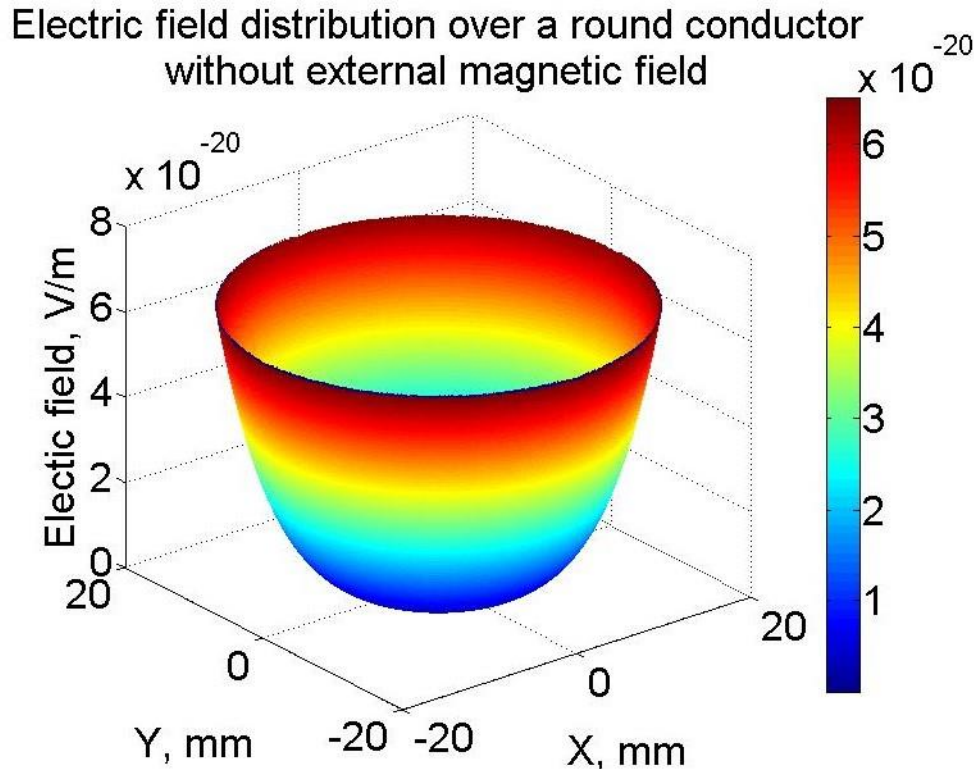


Figure 4. 11 E field distribution over a round conductor without an external magnetic field.

The average electric field for this plot is 2.089×10^{-20} V/m and the maximum and minimum values are respectively, 6.5×10^{-20} V/m and 3.67×10^{-30} V/m. As we can observe, electric field rises exponentially from the centre to the edge of the conductor when only the self-magnetic field is present.

In the central point where the magnetic field is zero, the electric field cannot be estimated as the J_c cannot be calculated for that particular point, nevertheless in the real round conductor this is not a problem because in that point the cooling channel is present.

When the background field is present the electric field increases in the same direction as the magnetic field over the conductor but with an exponential curve while in the magnetic field the increase is practically linear. This is shown in *Figure 4.12*.

We should note that for the electric field calculation over the round conductor, the superconductor characteristics as E_c , n -index or J_c are present while in the magnetic field distribution none of these factors take part in the calculation.

The average electric field when the 10 T background field is present rises to 7.76×10^{-11} V/m. For the same scenario, the maximum electric field is 2.8×10^{-10} V/m while the minimum field is situated in 1.78×10^{-11} V/m.

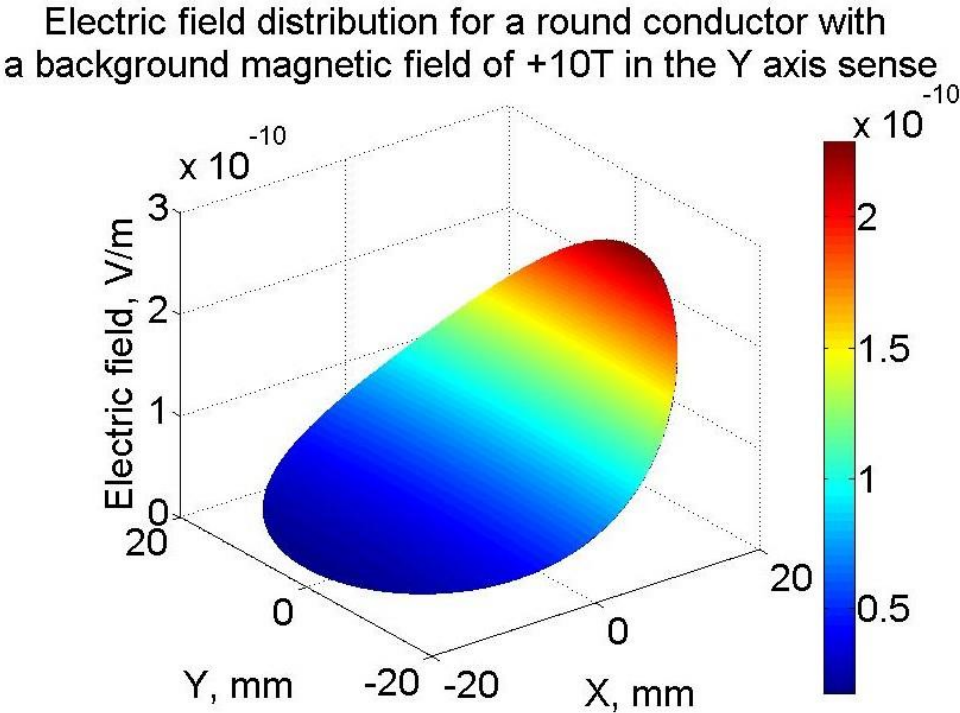


Figure 4. 12 Electric field distribution over a round conductor cross-section when an external magnetic field of 10T is present.

4.3.2 Electric field in rectangular conductor

The electric field for rectangular conductors is calculated through the same equation used in the round conductor. The only factor which changes from the round conductor equation to the rectangular cross-section is the J_c . Provided the operating current has the same value, otherwise the critical current could change, but in our analysis, we are using always the same operating current to find out the influence of the cable shape on the conductor performance.

We can observe in *Figure 4.13* that the distribution of the electric field when the background field is not present is very similar to the round conductor one. The electric field in rectangular conductors increases especially at the edges of the rectangle.

For the case when the background field oriented along the Y axis is included, the difference of electric field between both sides will be larger than it is in the case when background field is oriented along the X axis. This effect is produced because the orientation in these distant sides for the magnetic self-field vectors is practically parallel to the Y axis and as we can observe in the *Figure 4.13* for that sides the module of the electric field values is larger than for the sides closer to the centre.

The interesting values of the electric field in *Figure 4.13*, as we are giving for all the plots, are the average field which is 1.1488×10^{-20} V/m, the maximum field in a point, which is

4.484×10^{-20} V/m, and the minimum value of the field in the closest to the centre point who is 5.2544×10^{-30} V/m.

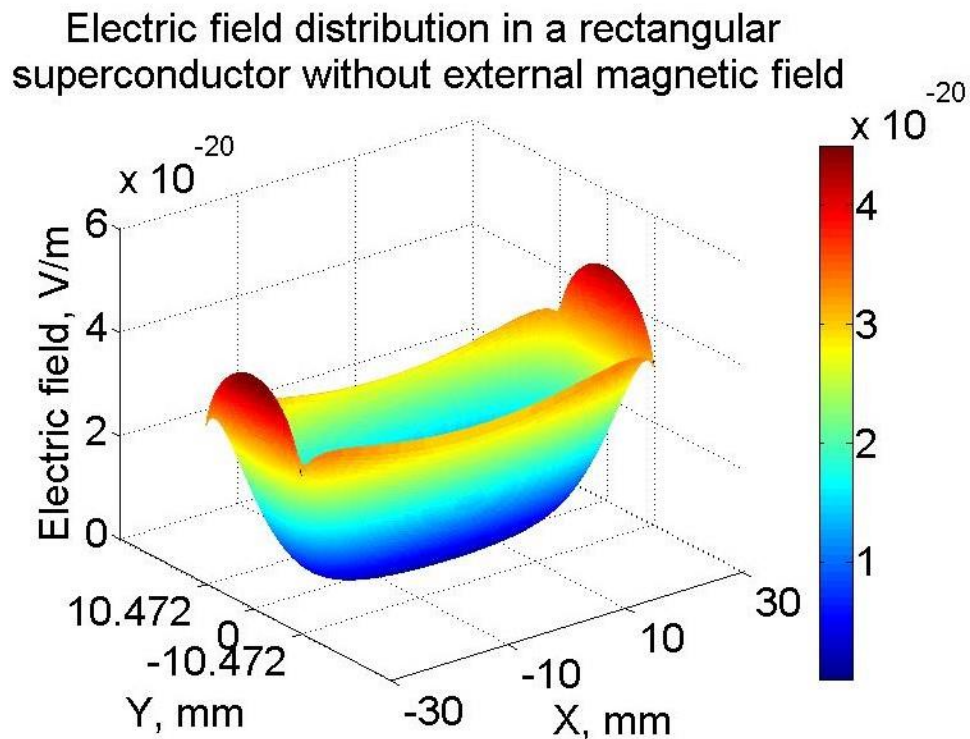


Figure 4. 13 Electric field distribution in a rectangular conductor without external magnetic field.

In Figure 4.14 is plotted the distribution when the background field is present.

When the external field is oriented along the Y axis, we can observe an exponential increase of the electric field along the X axis. In the side with higher field values we find also higher field values in the middle of the side.

The average, maximum and minimum values are respectively, 7.365×10^{-11} V/m, 2.05×10^{-10} V/m, and 1.976×10^{-11} V/m. Despite the high difference between the maximum and minimum points, the average electric field remains low.

If we compare the electric fields for the round and rectangular conductors when the background field is present, we note that the electric field is higher in the case of round conductor. This is the consequence of the shape of the conductor, which is the only thing that is different. Consequently, also the magnetic field distribution is different, as well as the E field, which is however very small.

Electric field distribution in a rectangular superconductor with an external magnetic field +10T in Y axis

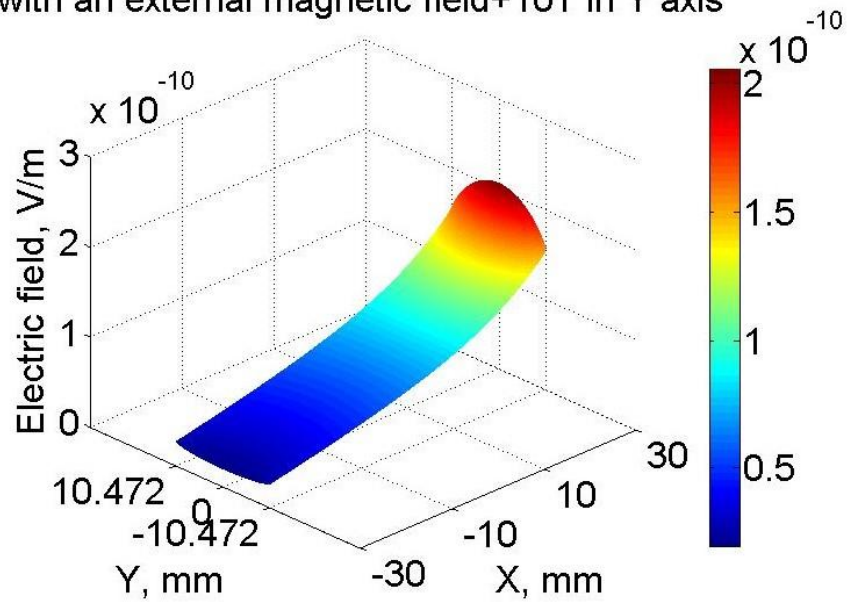
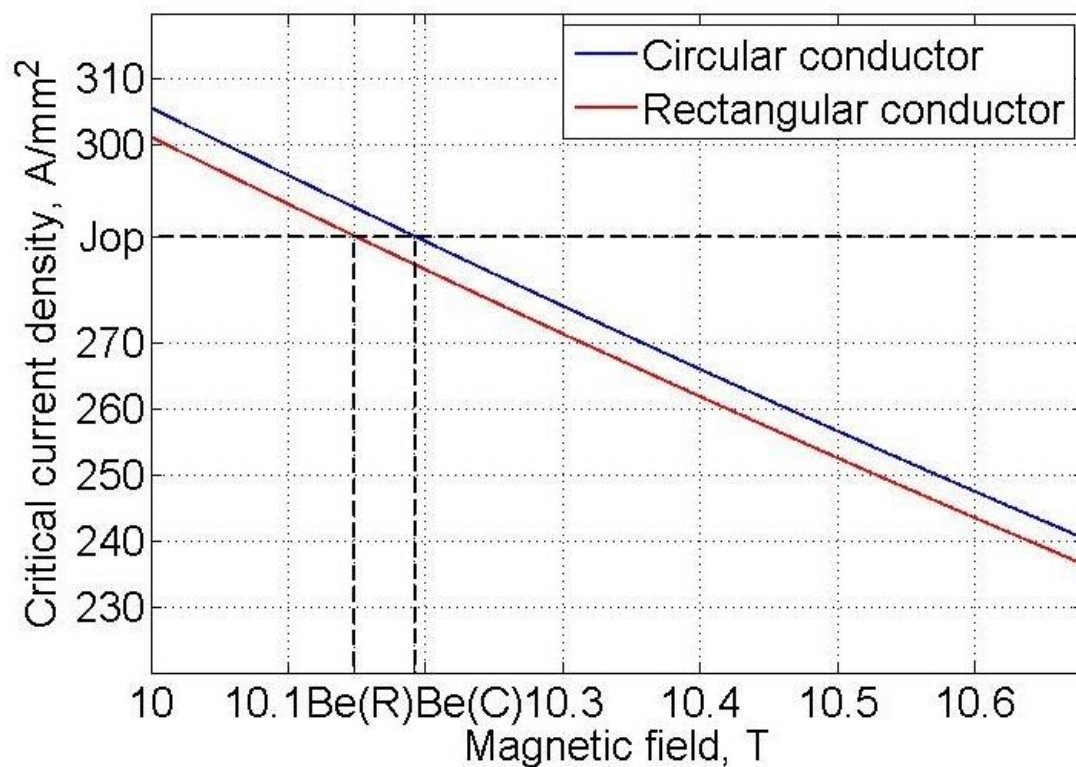


Figure 4. 14 Electric field distribution when an external magnetic field is present in a rectangular conductor.

CHAPTER 5

Results and conclusions

Critical current density with T_{cs} and 10T external magnetic field in function of total magnetic field



Effective magnetic fields from circular and rectangular conductors.

5.1 Electric field distribution as function of temperature

The electric field along the superconductor has zero value in normal operating conditions. When the temperature increases close to the current sharing temperature, the electric field starts to develop. The increase is not a problem until the electric field reaches the critical electric field (E_c).

When E_c is reached, the respective temperature at that moment is defined as the current sharing temperature (T_{cs}). This is the experimental definition of T_{cs} , and depends on the exact value of E_c . Usually, E_c in low temperature superconductors is set to $10 \mu\text{V/m}$. Once E_c is exceeded, the electric field rises very quickly, in fact exponentially, with the temperature increase.

As T_{cs} is one of the most important parameters characterizing superconductors, one of the main aims of this thesis is to find out, how the current sharing temperature depends on the shape of the cable cross section.

It was explained that T_{cs} is the temperature at which the current starts to flow through the copper section of strands, and if that temperature increases too much, a quench could develop. For this reason, T_{cs} should be as high as possible.

In *Figure 5.1* we can observe the function of electric field $E(T)$ as function of temperature, with illustration of T_{cs} corresponding to E_c . This example has been calculated for the electric field in a round conductor, where the variable factors as current, strain, external field or n-index are the same as in the previous examples.

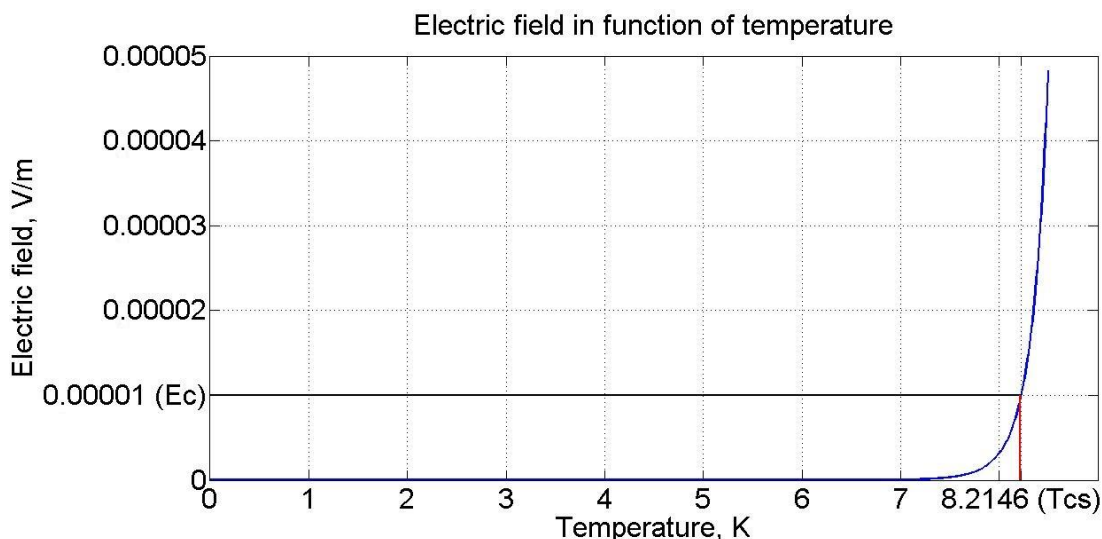


Figure 5. 1 Average electric field in a round conductor as function of temperature.

In the following we will assume that electric field in the superconductor is not homogeneous across the conductor section. Consequently, the process employed to calculate T_{cs} is

numerical, contains integration to calculate electric field for a given temperature, and T_{cs} is found using a bisection method. To find the T_{cs} temperature, the first step is to set a minimum and a maximal temperature as a boundary, for example $T_{min}=0$ K and $T_{max}=T_c$. After that, the temperature is set to the middle between T_{min} and T_{max} . Average electric field E is calculated for this middle temperature value; if E is lower than E_c the middle temperature will be set as the new E_{min} , and if on the contrary E is higher than E_c the respective temperature will be set as T_{max} . This process is iteratively repeated in a loop until the absolute value of E minus E_c will be less than a required tolerance parameter, in our case $1 \times 10^{-10} \mu V/m$.

If we have a look in *Figure 5.2* we find that the T_{cs} in the rectangular conductor of 60x21mm, used as example in previous sections, is slightly higher than for the round conductor of the same cross section area. This is a good sign and one of the reasons why the rectangular conductor has been employed in the prototype designs for DEMO.

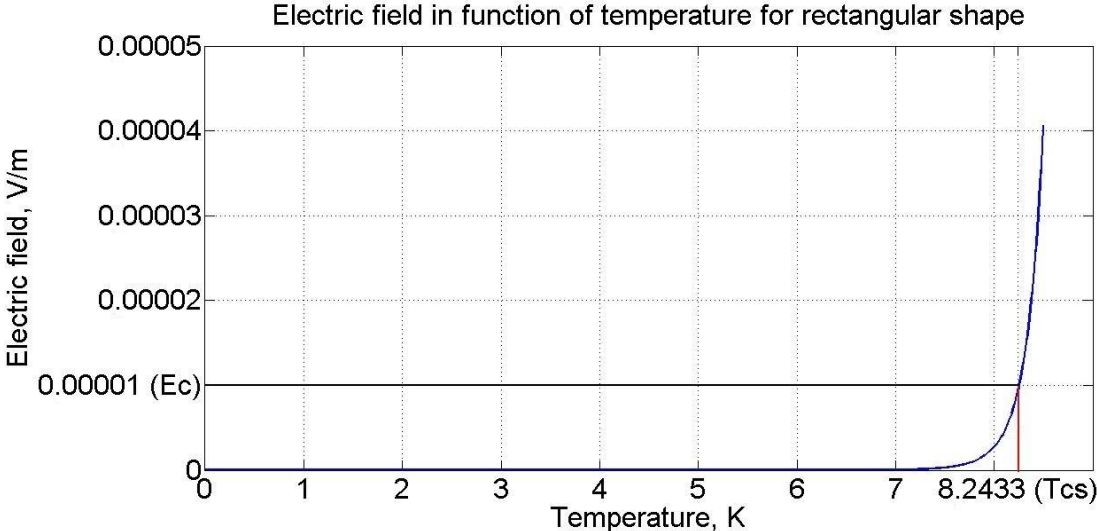


Figure 5. 2 E field average in rectangular conductor in function of temperature.

The dimensions of the rectangular conductor used for *Figure 5.2* are the same as those introduced in the previous examples. The dimension variations of the rectangular conductors affect directly the final T_{cs} . For this reason, this example is not a general statement and it is important to investigate the full spectrum of possible rectangular conductors and the differences compared to the round conductor used in ITER.

5.2 Effective magnetic field

Once we have defined the current sharing temperature, we can calculate the effective magnetic field, B_{eff} . This quantity represents the magnetic field, at which the usual scaling law predicts the same J_c as obtained by the complex procedure for numerical calculation of J_c using the magnetic and electric field distribution across the cable cross-section described in the previous section.

To calculate B_{eff} first of all we have to determine J_c at some required temperature. The temperature of interest can be either the operating temperature, the operating temperature plus some design temperature margin, or T_{cs} . In our case, we have chosen T_{cs} as the temperature of interest. The method to calculate B_{eff} is again iterative and bisectional. Namely, J_c is calculated using the simple scaling law for a guessed B value through equation (6), until the calculated J_c value is equal to the J_c value obtain by the complex procedure. B_{eff} slightly depends on the temperature at which it is calculated. B_{eff} is larger than the background field, but lower than the peak field (peak field is the maximum field found anywhere over the cable cross-section).

In *Figure 5.3* is illustrated the critical current density in magnetic field function with the critical temperature fitted for the round and rectangular conductors.

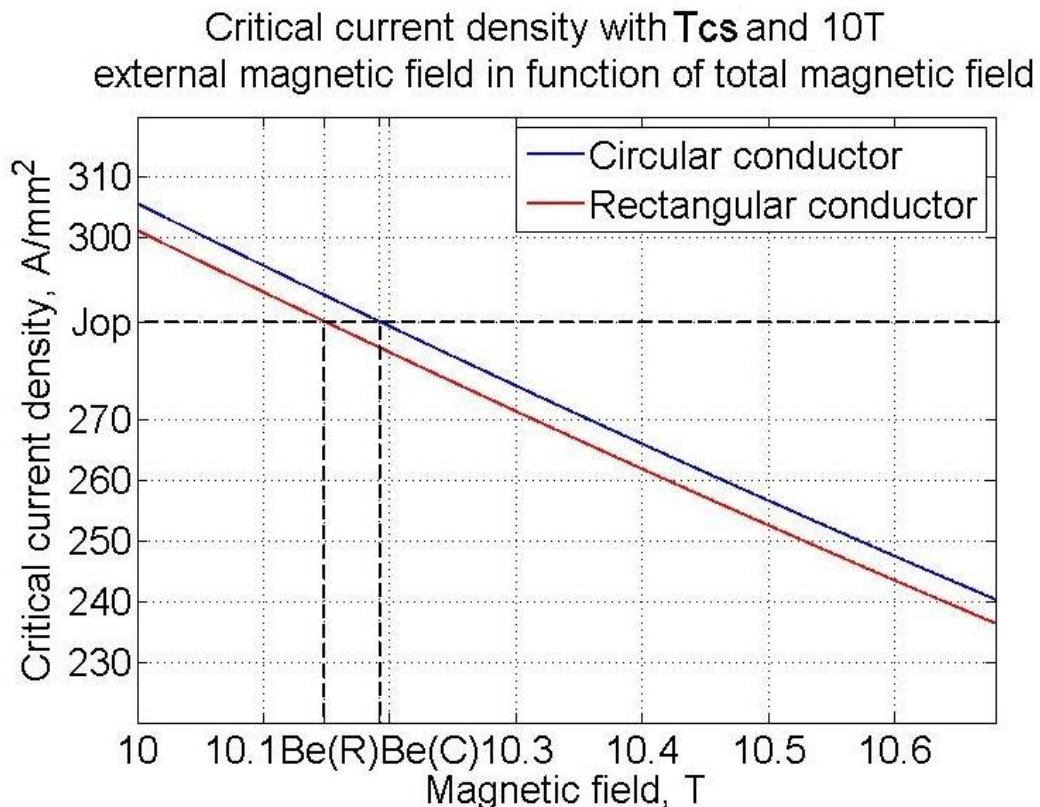


Figure 5. 3 J_c as function of external magnetic field B .

Except for the temperature, the other values are the same of the previous examples.

The J_{op} with the cross-section superconducting area of the round conductor and a current of 68kA is equal to 286.1953 A/mm² and the B_{eff} for round and rectangular conductors is respectively 10.192 T and 10.142 T.

As we can see, the assumed rectangular conductor has a lower effective magnetic field, which means that the rectangular conductor is effectively exposed to a lower magnetic field, and therefore it has higher margin to remain superconducting. On the contrary, the round conductor with the same area is effectively exposed to a higher magnetic field.

The rectangular conductor, in comparison with the Circular conductor, has a larger margin for the magnetic fields which are higher than the effective magnetic field up to the peak field of the conductor. As we can observe in *Figure 5.3*, the current density is lower when the magnetic field is higher. For this reason, is more interesting to have a low B_{eff} , which means that there are more points over the cross-section with a J_c lower than the J_c value obtain by the complex procedure, which makes the conductor more effective.

5.3 Current share temperature and effective field for different aspect ratio in rectangular conductors

The rectangular conductors are characterized by “*aspect ratio*”, which is the ratio of the two side lengths, x/y . The aspect ratio 1 corresponds to a square section conductor. Let’s consider conductors of the same cross section area, with the same operating current, strain, background field and n-index as defined previously. This means also that all conductors have the same amount of superconductor material.

5.3.1 Current share temperature in function of geometry

Figure 5.4 illustrates different current sharing temperatures for different aspect ratio varying from 1/10 ratio to 10/1.

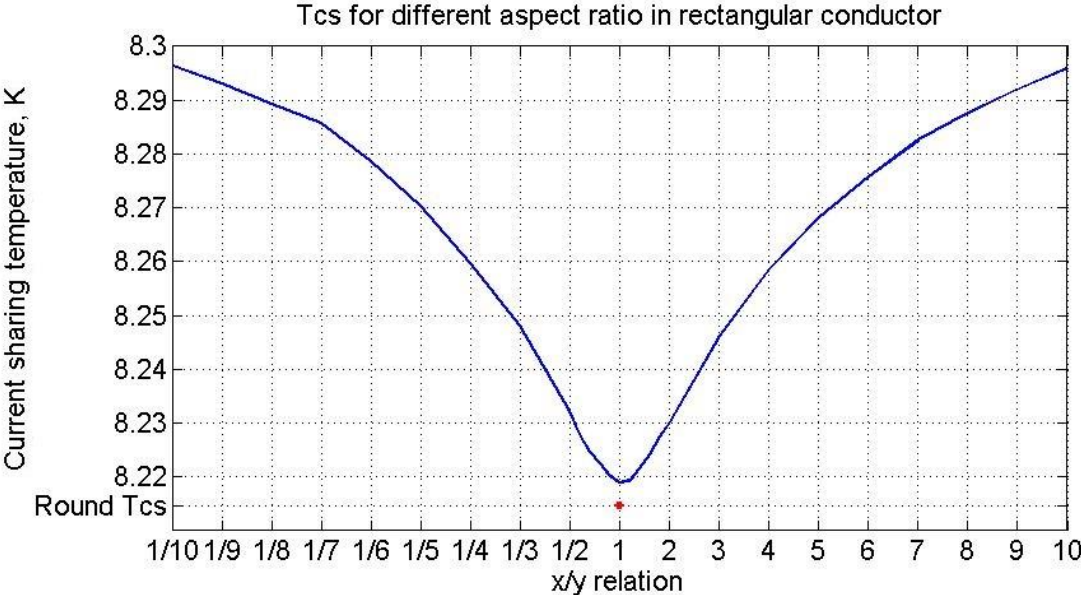


Figure 5. 4 Tcs for aspect ratio from 1/10 to 10/1. The red point indicates Tcs of a round cable with the same cross section area.

The current sharing temperature in the circular conductor is represented by a red point for 8.215 K while, at the minimum point corresponding to the square, the Tcs of the rectangular conductor is 8.219 K. The corresponding length of the conductor side is 35.45 mm.

We find the lowest Tcs in the rectangular conductor when it has a square shape as the CEA conductor. This can be explained by the fact, that the strands in a conductor, where other strands are located nearby, feel strongly the magnetic field of the neighbouring strands, which reduces their critical current density. In the cable, in which strands are further apart, i.e. the cable with large aspect ratio, the strands located further apart from each other act weaker on the other strands.

We can observe how T_{cs} increases when the difference between x and y is larger. The increment describes a curve which shows a positive evolution for the ratios closed to the square point. However, this increase of T_{cs} saturates at large imbalance between the sides.

In *Figure 5.5* it is illustrated how T_{cs} saturates for the extreme aspect ratios close to the aspect ratio of one hundred to one.

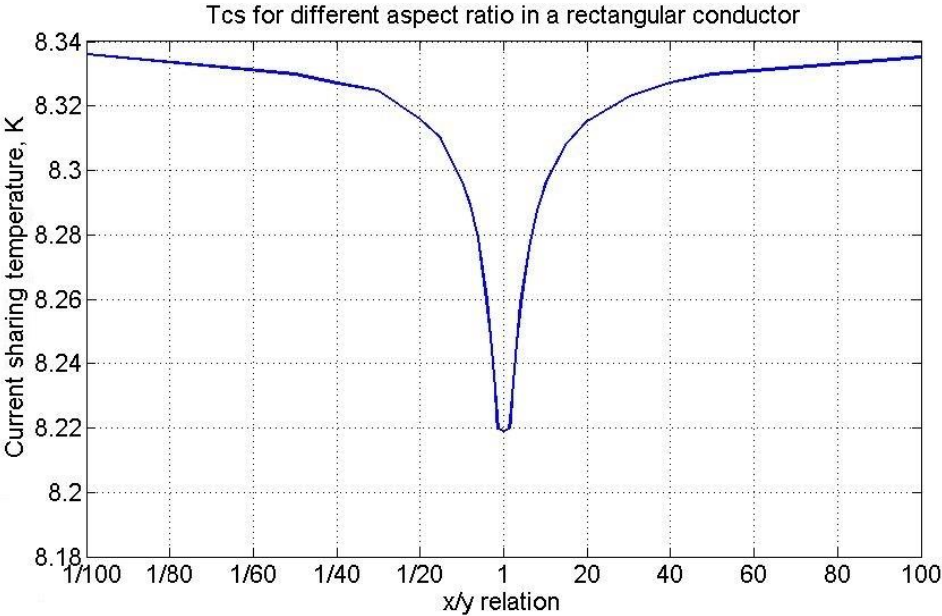


Figure 5. 5 T_{cs} for aspect ratio from 1/100 to 100/1.

We can note that the high increase happens for 1/10 and 10/1 ratios. Above these values the temperature does not increase very much. Other question is the difference between the two extreme relations, as the background field is applied in the y axis direction, the T_{cs} for aspect ratio 1/2 is not the same as T_{cs} at 2/1 ratio.

To visualize graphically which option is better, for the case that the external field is oriented along the y axis, *Figure 5.6* shows that for a larger y side the T_{cs} is higher. This means that it is slightly better if the longer side of the rectangular conductor is perpendicular to the external magnetic field. One has to add that the difference in T_{cs} is tiny, and in reality, there are other design requirements and limitations that determine the optimal orientation of the conductor with respect to the background magnetic field. Probably the most important one is the Lorentz force, which should ideally push on the long side of the cable in order to avoid large strain of the strands and possibly also the superconducting performance degradation with the electromagnetic cycling.

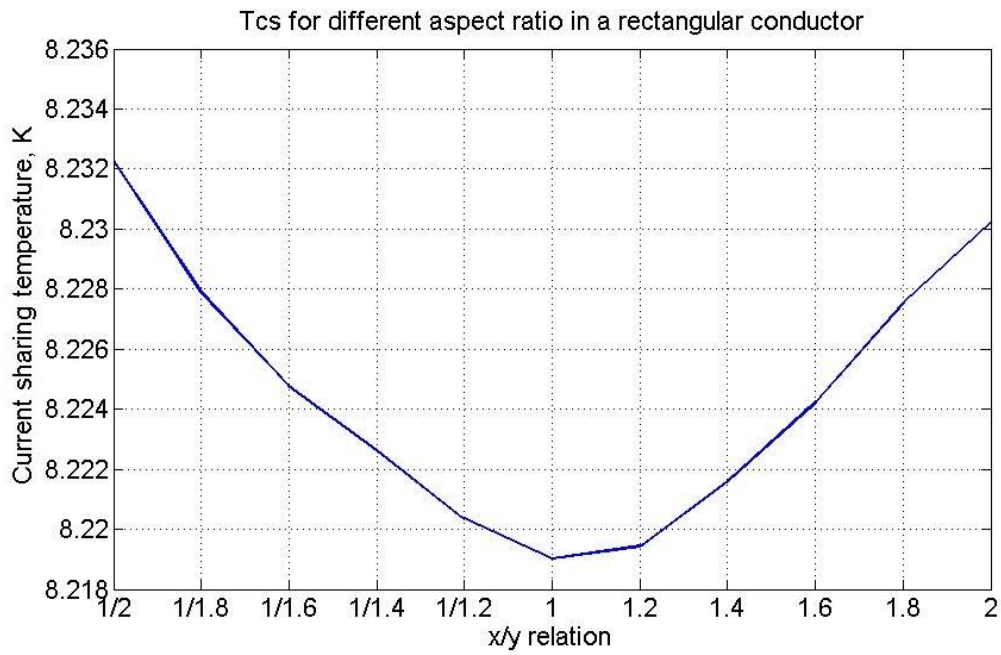


Figure 5. 6 Tcs for aspect ratio from 1/2 to 2/1.

5.3.2 Effective magnetic field in function of geometry

The effective magnetic field has the opposite trend compared to the current sharing temperature. For the square shape of aspect ratio one it reaches its maximum at 10.185 T. The round B_{eff} is higher reaching 10.192 T, as we can see in Figure 5.7.

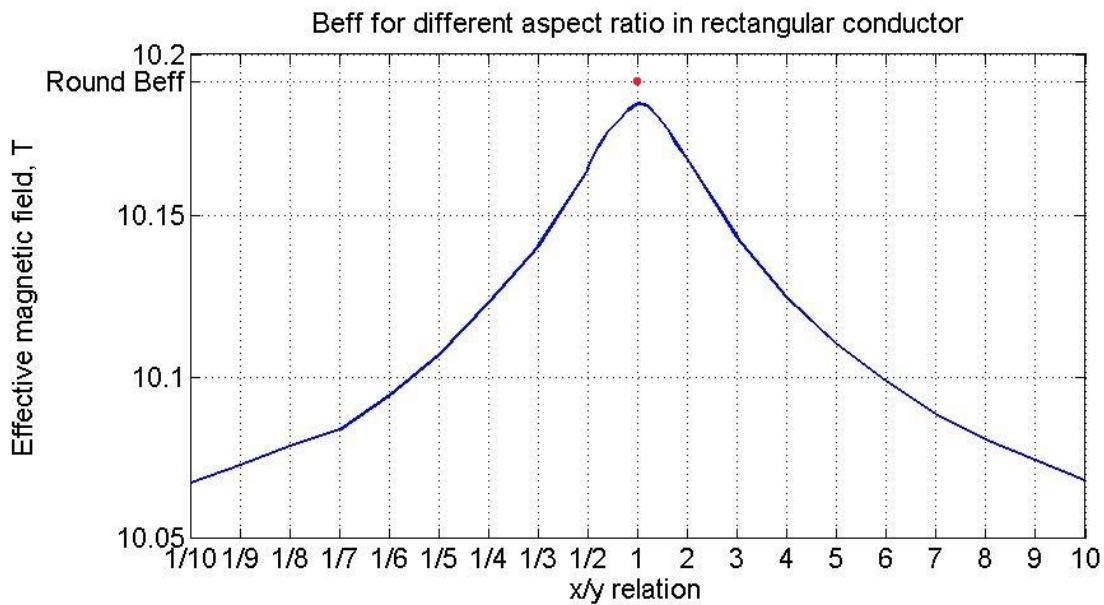


Figure 5. 7 Beff for different aspect ratio in rectangular conductor.

As it can be observed, the effective magnetic field is higher than the background field, which due to the self-field is only present in the centre of the conductor, and lower than the peak field, which is 10.662 T in the square conductor.

These results make clear the advantage of the rectangular conductor with respect to the circular one in terms of current sharing temperature and effective magnetic field. For both cases, the rectangular shapes with large aspect ratio have better performance.

Any rectangular shape has lower effective magnetic field than a circular one, which means that rectangular superconductors are effectively exposed to lower magnetic fields. This provides an extra margin to remain superconducting at slightly higher temperature, or to achieve the same performance as circular conductor with slightly lower amount of expensive superconducting material.

We can observe an inverse trend of B_{eff} with respect to T_{cs} for the lower and higher aspect ratios in *Figure 5.8* where the aspect ratio has a wider range of aspect ratios as in *Figure 5.4*. We can also note the same strong dependence on aspect ratio between 1/10 and 10/1 ratios, but in the opposite sense to T_{cs} .

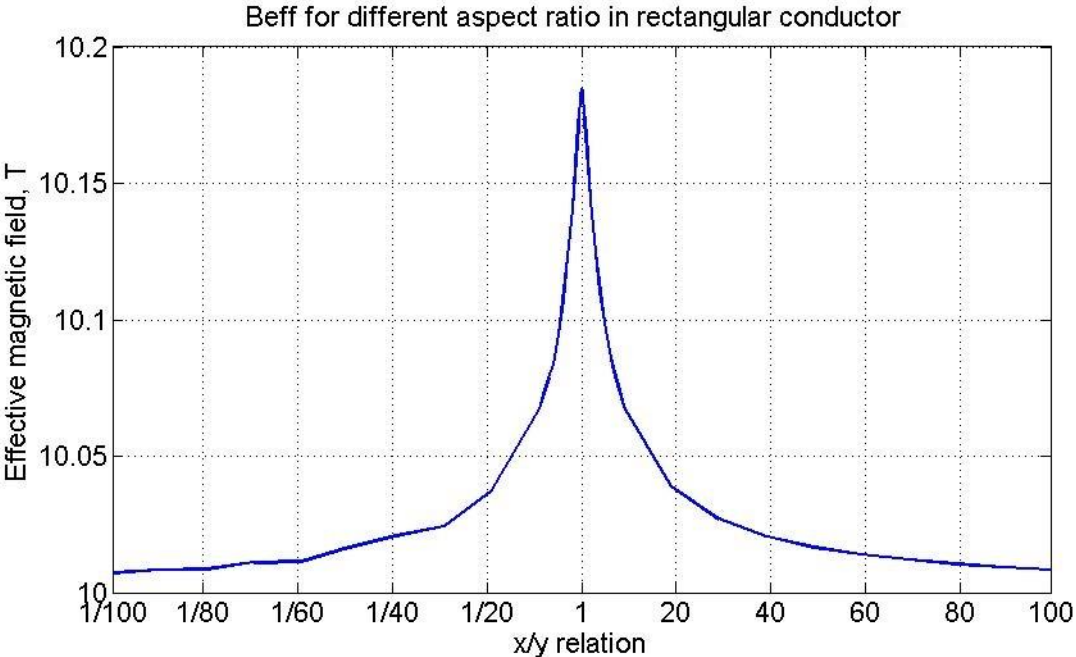


Figure 5. 8 B_{eff} for aspect ratio from 1/100 to 100/1.

As in the current sharing temperature in *Figure 5.6* we can see in *Figure 5.9* how the values for longest y side have lower effective magnetic field values.

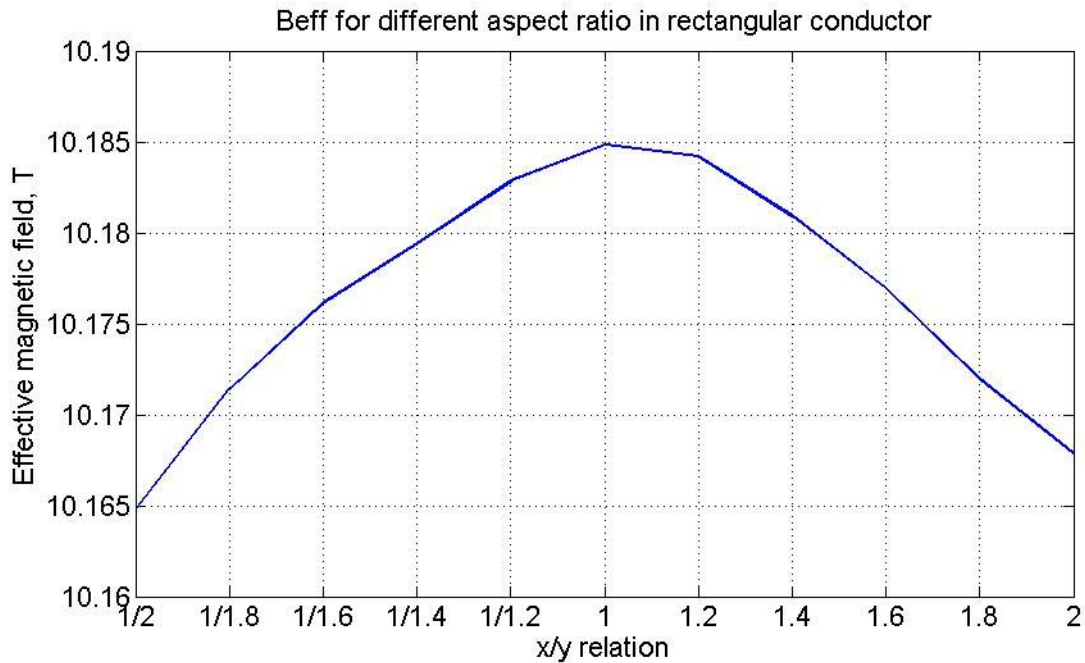


Figure 5.9 B_{eff} for aspect ratio from 1/2 to 2/1.

5.3.3 Conclusion

In conclusion, a rectangular shaped conductor with the same cross-section area and other conditions as the round conductor, has slightly better performance in terms of T_{cs} and B_{eff} . Concerning the aspect ratio, it is very clear that the rectangular shapes are slightly more efficient than the square shape. Most of the improvement is realised for aspect ratios from 1 to 1/20 and 1 to 20/1. We can also observe a tiny improvement when the longer side is oriented perpendicular to the background field. For example, only with background field along the positive Y axis the better performance occurs for larger y side as in 1/20 for B_{eff} and T_{cs} .

Of course, there are more aspects that need to be taken in account when designing a big magnet for fusion. For example, some important aspects are the convenience of manufacturability, conductor stability with respect to the cyclic loading or AC losses. The most recent designs of superconductors for fusion are based on the rectangular or square shape, where the main motivation for this choice are smaller superconducting performance degradation along the cyclic loading compared to round conductors, and easier winding of the coil. The rectangular conductors are likely to become the successors of the round conductors from ITER. The fact that rectangular conductors have slightly higher T_{cs} than the round conductors is a small additional benefit in favour of the rectangular cables.

Results Table

Parameter	Round conductor [without Background field]	Rectangular conductor [without Background field]
Average magnetic field (B_{av})	10.0058 T [0.4533 T]	10.0043 T [0.3898 T]
Max. magnetic field (B_{max})	10.68 T [0.68]	10.6235 T [0.6235 T]
Min. magnetic field (B_{min})	9.32 T [0 T]	9.3765 T [0 T]
Average critical current density (J_c)	948.6475 A/mm ² [9,425.1 A/mm ²]	948.5 A/mm ² [10,057 A/mm ²]
Max. critical current density (J_{cmax})	1075.4 A/mm ² [79,464 A/mm ²]	1,064.3 A/mm ² [76,667 A/mm ²]
Min critical current density (J_{cmin})	833.4 A/mm ² [7,504.8 A/mm ²]	842.3 A/mm ² [7,789 A/mm ²]
Average electrical field (E_{av})	7.76x10 ⁻¹¹ V/m [2.089x10 ⁻²⁰ V/m]	7.365x10 ⁻¹¹ V/m [1.1488x10 ⁻²⁰ V/m]
Max electrical field (E_{max})	2.8x10 ⁻¹⁰ V/m [6.5x10 ⁻²⁰ V/m]	2.05x10 ⁻¹⁰ V/m [4.484x10 ⁻²⁰ V/m]
Min electrical field (E_{min})	1.78x10 ⁻¹¹ V/m [3.67x10 ⁻³⁰ V/m]	1.976x10 ⁻¹¹ V/m [5.2544x10 ⁻³⁰ V/m]
Current share temperature (T_{cs})	8.2146 K	8.2433 K
Effective magnetic field (B_{eff})	10.1916 T	10.1418 T

Table 5. 1 Results calculated through MATLAB.

Bibliography

- [1] C. Day, "Design progress for the ITER torus and neutral beam cryopumps," *Fusion Engineering and Design*, vol. 86, 2011.
- [2] T.Hirai, "ITER tungsten divertor design development and qualification program," *Fusion Engineering and Design*, vol. 88, 2013.
- [3] ITER, "ITER-The way to new energy," 2017. [Online]. Available: www.iter.org. [Accessed 3 Aug 2017].
- [4] J. v. Nugteren, High Temperature Superconductor Accelerator Magnets, Twente: PhD Thesis, 2016.
- [5] C. Calzolaio, Irreversible degradation in Nb₃Sn CICC, Lausanne: École Polytechnique Fédérale de Lausanne, 2013.
- [6] L. Bottura, "J_c (B,T,epsilon) Parametrization for the ITER Nb₃Sn production," CERN-ITER Collaboration report, 2008.
- [7] D. Taylor, "The Scaling Law for the Strain Dependence of the Critical Current Density in Nb₃Sn Superconducting Wires," *Superconductor Science and Technology*, vol. 18, pp. 241-252, 2005.
- [8] A. Godeke, "A General Scaling Relation for the Critical Current Density in Nb₃Sn," *Superconductor*, vol. 19, pp. R100-R116, 2006.
- [9] K. Sedlak, "Common operating values for DEMO magnets design for 2016," EUROfusion, 2016.
- [10] J. Ekin, "Experimental Techniques for Low-Temperature," *Oxford University Press, New York*, Reprinted 2007.
- [11] W. W. W.A. Fietz, "Hysteresis in Superconducting Alloys - Temperature and Field Dependence of Dislocation Pinning in Niobium Alloys," *Phys. Rev.*, vol. 178, pp. 657-667, 1969.
- [12] P. Bruzzone, "ITER Conductors from Design, through Specification, Qualification, Production and Test," FCC, Whasingtong, 2015.
- [13] Y. Nabrar, "Performance Analysis of Mass-Produced Nb₃Sn Conductor for Central Solenoid in ITER," *IEEE TRANSACTIONS ON APPLIED SUPERCONDUCTIVITY*, vol. 26, no. 4, 2016 June.
- [14] K. Dulon, "3,000 sensors for detecting the quench," *ITER Newslines*, vol. 278, 2013.

- [15] L. Muzzi, "Cable-in-conduit conductors: lessons from the recent past for future developments with low and high temperature superconductors," *Supercond. Sci. Technol.*, vol. 28, 2015.
- [16] T. Boutboul, "European Nb₃Sn Superconducting Strand Production and Characterization for ITER TF Coil Conductor," *IEEE TRANSACTIONS ON APPLIED SUPERCONDUCTIVITY*, vol. 26, no. 4, 2016.
- [17] P. Bruzzone, "Superconductors for fusion: Achievements, open issues, roadmap to future," *Physica C*, vol. 470, pp. 1734-1739, 2010.
- [18] P. Bruzzone, "Design, Manufacture and Test of a 82 kA React&Wind TF Conductor for DEMO," *IEEE TRANSACTIONS ON APPLIED SUPERCONDUCTIVITY*, vol. 26, no. 4, 2016.
- [19] P. Bruzzone, "LTS and HTS high current conductor development for DEMO," *Fusion Engineering and Design*, 2015.
- [20] L. Muzzi, "Assessment Studies and Manufacturing Trials for the Conductors of DEMO TF Coils," *TRANSACTIONS ON APPLIED SUPERCONDUCTIVITY*, vol. 25, no. 3, 2015.
- [21] M. LEWANDOWSKA, "Thermal-hydraulic analysis of the improved LTS conductor design concepts for the DEMO TF coil," *PRZEGLĄD ELEKTROTECHNICZNY*, pp. 23-28, 2016.
- [22] R. Vallcorba, "Thermo-Hydraulic Analyses Associated With a CEA Design Proposal for a DEMO TF Conductor," *Cryogenics*.
- [23] K. J. Binns, *The analytical and numerical solution of electric and magnetic fields*, JOHN WILEY & SONS.
- [24] R. Wesche, "DC performance, AC loss and transient field stability of five medium size NbTi cable-in-conduit conductors with parametric variations," *Cryogenics*, vol. 45, pp. 755-779, 2005.

Annexes

[A]

The choice of specific models, critical field and temperature are given by the parametrization of Durham [7] and Godeke [8]. The Ginzburg-Landau (GL) parameter and strain functions are as proposed by Godeke [8], as they are simple and sufficiently accurate in the range of interest. The GL parameter is temperature and strain dependent, $k(T, \varepsilon)$ and is assumed at zero temperature and strain in the normalised version. The type of superconductor in terms of materials, shape and behaviour of the Nb₃Sn at superconducting conditions was studied in previous experiments in the PSI (Paul Scherrer Institute) and helps to the realization of this thesis. The model for the normalised pinning force vs. reduced field is kept as in the parametrization of Durham [7]. specially a strain ranges from -1 % to 0.5 % is propitious in these scaling laws. However, below -0.8 and above 0.2, strain can lead to permanent damages through filament breakages, even smallest ranges in practise. To this purpose the strain function of Godeke [8], is appropriate.

[B]

To explain the strain phenome, it starts by the deviatoric strain invariant, which is defined as:

$$\varepsilon_{dev} = \frac{2}{3} \sqrt{(\varepsilon_x - \varepsilon_y)^2 + (\varepsilon_y - \varepsilon_z)^2 + (\varepsilon_z - \varepsilon_x)^2}$$

where ε_x , ε_y and ε_z are the principal strain components. Experiments proved a linear dependence of the extrapolated upper critical field B_{c2} on the deviatoric strain and taking into account that a plastic deformation can occur in a composite conductor, considering the non-axial strain components and including the thermal prestrain (δ), which is close to the axial thermal pre-compression (ε_m), in the Nb₃Sn: $\varepsilon_z = \varepsilon_a + \delta$.

According with the previous factors B_{c2} becomes:

$$B_{c2}(\varepsilon_{dev}) \approx B_{0,d} - C_a' \sqrt{(\varepsilon_a + \delta)^2 + \varepsilon_{0,a}^2}$$

Where the $B_{0,d}$ value comes from the extrapolated upper critical field and C_a' is a constant, the $\varepsilon_{0,a}$ is an initial strain. Taking the minimum value for ε_{dev} and dividing by $B_{0,a}$ this strain function is obtained:

$$s(\varepsilon_a) = \frac{B_{c2}(\varepsilon_a)}{B_{c2min}} = \frac{1 - C_a' \sqrt{(\varepsilon_a + \delta)^2 + \varepsilon_{0,a}^2}}{1 - C_a' \varepsilon_{0,a}}$$

The strain function $s(\varepsilon)$ is based on the equation above, including the effect of the third strain invariant responsible of the asymmetry of the $s(\varepsilon)$ function.

[C]

The equation:

$$A = \frac{I\mu_0}{16\pi ab} \int_{-a}^a \int_{-b}^b \frac{1}{2} \log[(x' - x)^2 + (y' - y)^2] dx' dy'$$

Is expressed for r in terms of coordinates and this can be integrated in terms of simple functions. The result, in form given by Strutt simplification, becomes:

$$\begin{aligned} A = \frac{I\mu_0}{16\pi ab} \{ & (a-x)(b-y) \log[(a-x)^2 + (b-y)^2] \\ & + (a+x)(b-y) \log[(a+x)^2 + (b-y)^2] \\ & + (a-x)(b+y) \log[(a-x)^2 + (b+y)^2] \\ & + (a+x)(b+y) \log[(a+x)^2 + (b+y)^2] \\ & + (a-x)^2 \left[\tan^{-1} \frac{b-y}{a-x} + \tan^{-1} \frac{b+y}{a-x} \right] \\ & + (a+x)^2 \left[\tan^{-1} \frac{b-y}{a+x} + \tan^{-1} \frac{b+y}{a+x} \right] \\ & + (b-y)^2 \left[\tan^{-1} \frac{a-x}{b+y} + \tan^{-1} \frac{a+x}{b-y} \right] \\ & + (b+y)^2 \left[\tan^{-1} \frac{a-x}{b-y} + \tan^{-1} \frac{a+x}{b+y} \right] \} \end{aligned}$$

The final expression for equations 27 and 28 through this extended A are simplified using terms of distances r1, r2, r3 and r4 from a point in the field to the corners and the angles which the lines to the corners make with lines parallel to the x-axis. Resulting in 27 and 28:

$$H_x = \frac{I}{8\pi ab} \left[(y+b)(\theta_1 - \theta_2) - (y-b)(\theta_4 - \theta_3) + (x+a) \log \frac{r_2}{r_3} - (x-a) \log \frac{r_1}{r_4} \right]$$

$$H_y = \frac{I}{8\pi ab} \left[(x+a)(\theta_2 - \theta_3) - (x-a)(\theta_1 - \theta_4) + (y+b) \log \frac{r_2}{r_1} - (y-b) \log \frac{r_3}{r_4} \right]$$

Effective field in large size superconducting cables for fusion

Jose Manuel Trueba Cutillas

Supervisors: Prof. dr. ir. Jean-Marie Noterdaeme, Prof. Carlos Torre Ferrero (Universidad de Cantabria)

Counsellors: Dr. Pierluigi Bruzzone (EPFL), Dr. Sedlak Kamil (EPFL)

Master's dissertation submitted in order to obtain the academic degree of Master of Science in Industrial Engineering and Operations Research

Department of Applied Physics
Chair: Prof. dr. ir. Christophe Leys
Faculty of Engineering and Architecture
Academic year 2016-2017

